Controlling Tissue Matrix Assembly of Human Mesenchymal Stem Cells toward Engineering Native-like Bone, Cartilage, and Osteochondral Grafts

by

Sarindr Bhumiratana

Submitted in partial fulfillment of the
Requirements for the degree of
Doctor of Philosophy
in the Graduate School of Arts and Sciences

Columbia University

2012

ABSTRACT

Controlling Tissue Matrix Assembly of Human Mesenchymal Stem Cells toward Engineering Native-like Bone, Cartilage, and Osteochondral Grafts

Sarindr Bhumiratana

Medical complications caused by bone, cartilage, and osteochoondral defects present special challenges to tissue engineers. An ability to fabricate these tissues *in vitro* will eliminate clinical complications caused by current techniques used in graft reconstruction. These complications include long-term failure of synthetic grafts, inferior success of allografts, and complications from harvesting autografts. The successfully engineered grafts must exhibit biological and structural function similar to that of native tissue in order to withstand physiological conditions and integrate into surrounding tissues. In this dissertation, the ability to control tissue matrix assembly from a clinically relevant cell source, human mesenchymal stem cells, towards generating native-like tissue properties has been demonstrated. The investigational approach was crafted around three specific aims: controlling the matrix assembly of bone mineral (Aim 1), articular cartilage (Aim 2), and osteochondral tissue (Aim 3). As a result, the assembly of bone mineral structure was accomplished by regulating nucleation, mineral-binding protein deposition sites, and affinity for mineral binding. Native-like articular cartilage with physiologic form and function was created using a cell pellet compression technique, a process mimicking the native developmental mesenchymal cell condensation process. In addition, the key requirements to engineer osteochondral tissue with undifferentiated mesenchymal stem cells were established. A radically novel, imaging-compatible perfusion bioreactor was designed to enhance tissue integration and spatial regulation of supplements to direct stem cell differentiation into chondrogenic and osteogenic lineages and the formation of complete osteochondral constructs. Proof-of-concept experimentation was conducted in a large animal (pig) model of temporomandibular condyle reconstruction. Engineered bone demonstrated markedly better

regeneration and remodeling of the TMJ and its integration with the surrounding tissues (bone and muscle) compared to the implantation of acellular scaffolds. The tissue engineering approaches developed in this dissertation form a basis for promising therapeutic approaches for treating bone, cartilage, and osteochondral defects.

Table of Contents

CHAPTER III

CHAPTER IV

CHAPTER V

List of Tables

List of Figures

CHAPTER I

Introduction

CLINICAL POTENTIAL OF BONE, CARTILAGE, AND OSTEOCHONDRAL TISSUE ENGINEERING

Engineering of functional tissue grafts offers a promising alternative method for treating large defects and replacement of failing tissues. In order to produce a successful graft, engineers, scientists, and clinicians need to consider the clinical requirements of the defect, the structural and functional necessities at the time of implantation, the approach to providing integration with the host tissue, immediate survival and long-term function. These general requirements translate into the specific set of design considerations that are typically addressed in a highly interdisciplinary manner. In all cases, the design requirements need to take into account the biology of tissue development, repair and (if applicable) disease conditions, the implantation route, and the necessary properties of engineered tissue grafts. For instance, bone, cartilage, and osteochondral tissue have unique mechanical function, which must be adequately addressed. Successful tissue grafts should re-establish the cellular and mechanical function of the native tissue while matching the size and shape of the defect.

Autologous grafts are considered to be a gold standard for bone, cartilage, and osteochondral reconstruction due to their bioactivity, mechanical competence, and immediate cellular function. Nevertheless, alternative methods would eliminate the following disadvantages with the implementation of autologous grafts: the restricted volume of the tissue available for harvest, donor site morbidity, the lack of precision in size and shape, and the unmatched structural and biomechanical properties of tissues harvested. Allografts and graft substitutes may fulfill some of these obstacles but lack sufficient tissue healing responses, which leads to failure. Mimicking physiologic form and function of engineered bone, cartilage, and osteochondral tissue are important criteria for graft success which would offer a promising alternative method for treating

skeletal defects. This dissertation aimed to generate native-like bone, articular cartilage, and osteochondral tissue *in vitro* from human stem cells.

HYPOTHESIS

The proposed hypothesis is that mesenchymal stem cells (MSC), when differentiated, can assemble native-like bone, articular cartilage, and osteochondral tissues by emulating the physiologic tissue developmental process. Based on the progress in bone, cartilage, and osteochondral tissue engineering (Chapter III), this dissertation aims at engineering native-like bone, articular cartilage, and osteochondral structures from MSC by regulating bone and cartilage tissue matrix assembly.

SPECIFIC AIMS

Bone, cartilage, and osteochondral tissue engineering have tremendously progressed over the past decade; however, engineering clinically relevant grafts from human mesenchymal stem cells (hMSC) is still far from fruition. Understanding mechanisms and developmental processes of *in vitro* tissue formation are beneficial for developing techniques and culture systems to successfully engineer functional grafts. This dissertation aims at investigating and solving unmet challenges in regard to the formation of bone, cartilage, and osteochondral tissue from hMSC *in vitro*. The focus is on controlling tissue matrix assembly in *vitro* by controlling the local hMSC environment as well as innovating novel fabrication of functional tissue constructs. The dissertation is divided into three specific aims focused on the techniques to regulate and control the matrix assembly of (i) bone, (ii) articular cartilage, and (iii) osteochondral construct.

Aim 1 Engineering mineral architecture by directing mineral deposition of hMSCs through chemical and structural features of scaffolds

Bone mineral architecture defines bone strength, stiffness, and durability. Previous bone tissue engineering techniques focused on chemically or structurally stimulating hMSC osteogenic differentiation to enhance osteogenic expression and production of bone matrix. However, the matrix deposited by hMSC in previous studies did not form native-like structures. This motivates the studies in regulating deposition of bone mineral and protein matrix onto defined locations resulting in controlled bone structural formation. The approach was designed to mimic the mechanism to form mineralized collagen fibrils, the native bone building block. As a result, the bone mineral and protein matrix deposition could be modulated, resulting in engineered bone with native-like structure and enhancement in mechanical function.

Aim 2 Engineering articular cartilage with integration to subchondral bone from hMSC using novel cell pellet compression technique

Cartilage constructs were successfully engineered from young primary animal chondrocytes, but not from hMSCs. All previous studies of cartilage tissue engineering using hMSCs reported poor compressive stiffness due to inferior assembly of cartilage matrix. Based on the developmental process of mesenchymal cell condensation that leads to the formation of cartilage during normal development, we proposed a novel technique that is based on hMSC pellets interfaced with subchondral bone. This innovative method was optimized to successfully engineer, for the first time, articular cartilage with physiological mechanical properties.

Aim 3 Determining the requirements of tissue engineering osteochondral grafts

Controlling spatial bone and cartilage formation from a single cell source within a construct is a difficult task, which requires substantial regulation of growth factors and stimuli. Understanding the requirements of successfully generating osteochondral grafts from a single stem cell source would facilitate the translation of tissue engineering approaches. This aim investigated the importance of MSC predifferentiation, the use of soluble factors, and bioreactors in the formation of stratified cartilage/bone (osteochondral constructs). The results provide insight into the necessary criteria for designing systems to engineer complete osteochondral grafts from hMSC *in vitro*.

A bioreactor was designed for culturing anatomically-shaped osteochondral grafts from a single cell source. This system allows spatial control of bone and cartilage development as well as the enhancement of osteochondral integration. The temporomandibular joint (TMJ) condyle was selected as a model for the bioreactor design due to its size, anatomical complexity, and clinical need. The pre-clinical proof of concept in a large animal model was conducted to determine the efficacy of both bioreactor and the tissue-engineered anatomical autologous bone graft in regenerating tissue. More importantly, the outcomes of this study point to the practicality and promise of employing tissue engineering technology for the production of personalized autologous grafts for skeletal reconstruction.

CHAPTER II

Bone and Cartilage Biology, Medical Complications, and Current Treatments

Mimicking physiologic form and function of engineered bone, cartilage, and osteochondral tissue is important for graft success and represents the main focus of this dissertation. Nature builds and repairs tissue through a complex process involving multiple biochemical factors and various cellular players that precisely interact in a well-controlled environments. Each tissue type undergoes unique developmental steps, and as a result, exhibits unique tissue architecture and function. Advances in bone and cartilage biology have determined the fundamental direction towards engineering tissue structure *in vitro*. Furthermore, understanding medical complications and current treatment modalities is essential for determining the success of tissue engineered bone, cartilage, and osteochondral grafts.

BONE BIOLOGY AND STRUCTURE

Bone is a hard connective tissue that provides mechanical and metabolic functions vital to survival and health; these functions include supporting the body's framework, supplying blood cells to the entire body, and maintaining mineral and fat reserves. Bone varies in geometry, cellularity, mechanical properties, and developmental pathways. Flat bone and the outer regions of long bone are comprised of compact (cortical) bone that contains ~80-90% mineralized tissue. This high density of mineralized tissue provides mechanical strength. The ends of long bone are made primarily of trabecular (cancellous) bone, which contains ~15-25% mineralized tissue. Compared to cancellous bone, cortical bone has a much higher compressive stiffness (12-20 GPa vs 0.2-0.8 GPa) and strength (100-230 MPa vs 2-12 MPa) [1]. The mechanical properties of bone generally depend on its structure and orientation. A successful bone graft should ideally match the physiologic structure and mechanics of native bone being replaced. Therefore, understanding

bone developmental biology will help tissue engineers to apply basic scientific knowledge to the engineering of functional bone grafts.

Bone development

Bone formation begins within the first month of development through two different processes: intramembranous ossification and endochondral ossification. Intramembranous ossification leads to flat bone formation when fibrous membranes are replaced by bone tissue. Examples of flat bones include the cranium (skull), illium (pelvis), and rib cage. Intramembranous ossification involves direct differentiation of mesenchymal cells into pre-osteoblasts and osteoblasts [2], while endochondral ossification involves the replacement of cartilage by bone tissue to form long bone. The two processes result in distinctly different compositions and structures of the bone matrix [3], although recent studies have identified several shared molecular regulators [4]. In both processes, the major events in bone development are the formation and infiltration of vasculature and the differentiation of stem cells into bone-forming cells. The key angiogenic regulators include members of the fibroblast growth factor (FGF), insulin-like growth factor (IGF), transforming growth factor-β (TGF-β), and vascular endothelial growth factor (VEGF) families [5, 6]. In addition, factors which play essential roles in bone development include growth hormones such as Indian Hedgehog (Ihh) and parathyroid hormone related peptide (PTHrP) [7, 8], FGF-2 [9, 10], and TFG-β family cytokines [11-13], especially BMPs [14, 15].

Bone remodeling

Bone remodeling is a continual, lifelong process that stimulates bone regeneration, maintenance, and homeostatsis [16]. Remodeling is the bone's response to signals associated with bone growth, micro-damage and mechanical loading. In the process, existing bone is resorbed by osteoclasts and new bone tissue is formed by osteoblasts. Signaling pathways include the action

of several hormones, such as PTHrP and vitamin D, and cytokines such as BMPs, FGF, IGF, TGF-β, PDGF (in bone formation) and GM-CSF, ILs, and M-Csf (in bone resorption) [16-18].

Bone healing

Unlike soft tissue, healing of bone does not lead to scar formation and, if the defect is below a critical size, results in the reestablishment of native bone anatomy and function. Fracture repair is usually complete by 6-8 weeks after the initial injury and is characterized by the inflammatory phase, reparative phase (which includes intramembranous ossification), chondrogenesis followed by endochondral ossification, and remodeling [19, 20]. Examples of growth factors and extracellular matrix proteins involved in bone repair processes include TGF-β, FGF (I and II), PDGF, BMP (2, 4, and 7), osteonectin, osteocalcin, and collagens [21].

BONE MEDICAL COMPLICATIONS AND TREATMENTS

Due to the multiple functions of bone in locomotion, mechanical support, and physical protection of various organs and metabolism, bone injury can cause significant pain, discomfort, and physical disability. Treatment options most commonly utilize a graft, which is a routine option for conditions following tumor resections and large fractures. Bone fracture is commonly caused by accident, high force impact or stress, or trivial injuries resulting from osteoporosis. Some fractures can lead to serious complications such as non-union fracture where the fractured bone fails to heal, mal-union where the fractured bone heals in a deformed manner, and compartment syndrome that may result in amputation of the affected limb. Most fractures require immediate treatment by securing the fracture in place to facilitate self-healing. Surgically-implanted bone grafts can enhance healing by filling in the gap of a nonunion and thereby facilitate bone integration and regeneration. After implantation, the graft needs to biologically and functionally integrate with the existing skeletal system. The three most clinically used bone grafts are autografts, allografts, and grafts substitutes, with each having its own advantages and

disadvantages. The treatment of choice depends on the patient's general condition and the specific fracture or symptom

Autografts, which are grafts taken from the patient's own skeletal system, represent the gold standard in bone grafting. The bone graft is harvested from non-essential bone such as the illiac crest and cut into the shape and size needed. Therefore, this method requires an additional surgical site and may introduce additional post-operative pain and complications. Furthermore, the size and total amount that can be harvested is limited. Despite these drawbacks, autografts are often preferred because they alleviate the risks of graft rejection and disease transmission. A special type of structural autograft is the vascularized fibular graft, which requires a microsurgical approach to connect the nutrient fibular vessel to a vascular bundle adjacent to the site of the defect. The operation causes high morbidity at the donor site, and its usage is generally limited to tumor reconstructions [22, 23].

Allografts are bone grafts harvested from human donors. Bone allografts include fresh or fresh-frozen bone, freeze-dried bone grafts, and demineralized freeze-dried bone grafts. As compared to autografts, allografts offer a better supply of bone in suitable shapes and sizes, and help avoid the donor site morbidity. However, allografts pose a risk of immune rejection and infection since the tissue is harvested from another individual and contains foreign immunogenic material. These risks are reduced when the cellular materials are removed during the graft processing and storage, such as in decellularized and demineralized bone allografts.

Graft substitutes include natural or synthetic materials, which can be organic, inorganic, or combinatorial products. Graft substitutes are available in unlimited supply, and can be fabricated in any desired size and shape. The materials used as graft substitutes include collagen sponge, calcium phosphates (e.g. hydroxyapatite and tricalcium phosphate), bioactive glass, and metals such as titanium and its alloys. These materials provide osteoconductivity for bone healing formation and some of them are resorbed with time *in vivo*. Graft substitutes provide less risk of

infection and graft immune rejection in comparison to allografts. However, stress shielding, which may cause bone atrophy, is a concern when applying this type of graft. Although graft substitutes offer great benefits, they are still inferior to autografts and allografts in terms of enhancing bone healing through biological response.

CARTILAGE BIOLOGY AND STRUCTURE

Articular cartilage, a white, dense connective tissue, serves as the load-bearing material of joints and is characterized by its excellent lubrication, and wear properties [24]. Ranging from 1 to 7 mm thick, cartilage is composed primarily of two phases; a solid matrix (collagen fibrils and proteoglycan (PG) macromolecules) [25-27] and a mobile interstitial fluid phase (mostly water) [28, 29]. The polyanionic nature of the glycosaminoglycan (GAG) chains of PG draw water into the tissue [29], resulting in a large osmotic pressure that expands against the constraining collagen network. The interplay between swelling pressure and tension in the collagen fibers results in a highly specialized tissue that is well suited to bear compressive loads within the joint. To maintain the necessary matrix composition, chondrocytes, which make up less than 10% of the tissue volume [30], balance extracellular degradation and matrix turnover by synthesizing and secreting extracellular matrix (ECM).

The composition, structure, and material properties of articular cartilage are known to vary across the tissue's depth [31] and can be divided into four discrete zones: the superficial, middle, deep, and calcified cartilage zones [32, 33]. The superficial zone is a thin region at the articulating surface marked by collagen fibers that have the highest concentrations of water and collagen compared to the other zones, but the lowest level of proteoglycans. Additionally, chondrocytes in this zone are flattened. In contrast, the middle zone is rich in randomly oriented collagen, contains the highest concentration of proteoglycans, and is randomly dispersed with cellular bodies. In the deep zone, which has the lowest levels of collagen, the chondrocytes are

oriented perpendicularly to the surface and arranged in a columnar structure. Finally, the calcified cartilage zone separates the uncalcified layers of cartilage from the subchondral bone.

CARTILAGE MEDICAL COMPLICATIONS AND TREATMENTS

In most cases, damage to articular cartilage is a consequence of clinical osteoarthritis and is marked by disability and pain [34]. Affecting nine percent of the United States population aged 30 and older, osteoarthritis has total direct costs estimated at $28.6 billion dollars annually [35]. Due to its avascular nature, articular cartilage exhibits a poor intrinsic healing response [36]. The hallmarks of this debilitating disease are the loss of mechanical properties, increased collagen degradation, reduced proteoglycan synthesis, and decreased cellularity [37, 38].

Alternatively, damage to cartilage can be caused by physical injury of the articular surface. While physical injury to cartilage primarily occurs with traumatic loading of the joint (traumatic injury), it can also be a consequence of surgical procedures that include graft harvesting (iatrogenic injury). In native cartilage, the mechanotransduction resulting from injury can induce chondrocyte death as early as within a few hours, and up to 7 days post-injury [39]. The subsequent downstream effects are frequently marked by changes similar to those seen in osteoarthritis.

When damage to the tissue is widespread, a total joint replacement is often the only solution, artificially replacing the articulating surface and underlying bone. Such invasive repairs, however, often require revision surgeries due to wear, subsidence and loosening of the implant in the bony union [40-43]. For the repair of focal lesions and damage to the articular surface, more conservative approaches may be used. Clinical options include tissue adhesives [44, 45], enzymatic treatments [46], laser solder welding [47], autograft cell/tissue transfer via periosteal grafts [48], autologous osteochondral grafting such as mosaicplasty [49] or costcochondral graft [50, 51] and the Carticel method [52]. While these options offer temporary relief of symptoms,

they also introduce long-term problems. Primarily, the availability of healthy cartilage from which to harvest cells is limited for cell-based therapies or osteochondral graft harvesting. Furthermore, autologous osteochondral grafts are usually harvested from non-load bearing regions which may provide tissue of sub-optimal material properties for use in contact regions [53]. This procedure itself can induce significant cell death in the surrounding region [54, 55], leading to further structural and biochemical breakdown of the donor site tissue.

CHAPTER III

Progress in Bone, Cartilage, and Osteochondral Tissue Engineering

An "ideal" process for engineering functional bone, cartilage, and osteochondral grafts that would be tailored to a patient's and specific defect is illustrated (**Fig.III**) The personalization of tailored grafts provides an exact match to the defects being reconstructed. The process utilizes computer-assisted imaging and preoperative planning to guide manufacturing of patient-specific implants. Using a computer program, the 3-dimensional contour, size, and shape of the graft is designed, and the anatomically shaped scaffold is fabricated. Cells are then seeded into the scaffold and cultured in a specially designed "anatomical" bioreactor to support the development of engineered bone grafts. The graft is then implanted into the patient and allowed to integrate with the native tissue. The personalizing process and the capability of creating anatomical and functional tissue grafts would greatly facilitate the surgical procedure as well as improve the aesthetics of bone repair. Successful tissue engineering of functional bone, cartilage, and osteochondral grafts requires specific and careful consideration of the three major players of tissue engineering: cells, scaffolds, and environmental factors provided by the bioreactor.

CELL SOURCE

Cells play an important role in bone, cartilage, and osteochondral tissue engineering by forming and remodeling the tissue-specific extracellular matrix. Primary cells extracted from adult tissue (osteoblasts and chondrocytes in this case) have been used extensively to validate the feasibility of tissue engineering approaches because these cells exhibit native cellular functions. Primary osteoblasts and chondrocytes harvested from bone and cartilage, respectively, maintain genetic expression and produce tissue matrix similar to that found in the native tissue when cultured in vitro [56-60]. However, these cells are not clinically favorable due to the complications associated with their harvest and expansion: these include donor site morbidity, the difficulty of

the cell isolation process, and the challenge of obtaining adequate cell quantities for therapeutic purposes.

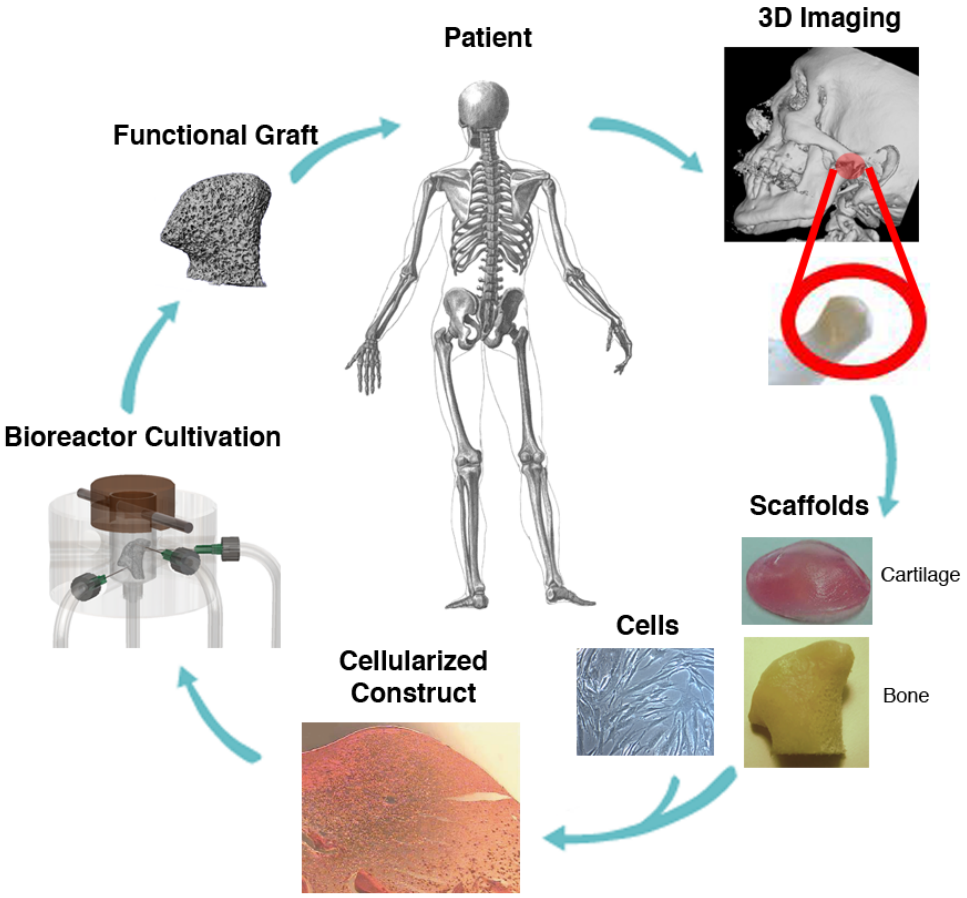

Figure III: Engineering of cartilage/bone grafts. The process begins with 3D imaging of the defects for manufacturing an anatomically-shaped scaffold consisting of strong mineralized region for the formation of bone, and hydrogel region for the formation of cartilage. Both regions are seeded with cells and cultured in a bioreactor (also manufactured with the aid of imaging) that provides environmental control and physical stimulation. After cultivation, the functional graft can be implanted at the defect site.

Adult stem cells, particularly mesenchymal stem cells (MSCs), have demonstrated high clinical potential for bone, cartilage, and osteochondral tissue engineering. Although these cells also need to be harvested from the body, the process is much less invasive and much simpler than

obtaining primary cells. Bone marrow mesenchymal stem cells (BMSCs) and adipose-derived mesenchymal stem cells (ASCs) can simply be isolated from aspirates of bone marrow and fat, respectively. BMSCs are the most extensively investigated and utilized therapeutic cells for orthopedic regeneration and reconstructive therapies [30]. ASCs have similar immunophenotype, morphology, and multilineage potential to BMSCs. Because ASCs are more abundant and more accessible than BMSCs, causing very little donor site morbidity, these cells are being actively investigated as an alternative to BMSCs [61, 62].

Other MSC sources which are less investigated yet potentially beneficial include dental pulp stem cells (DPSCs) and umbilical cord-derived stem cells (UCSCs). DPSCs can be extracted from dental pulp at the time of tooth extraction [63]. Harvesting UCSCs is also not invasive, however, they must be isolated and stored at birth limiting potential clinical use for a large fraction of the current population [64]. Similar to BMSCs and ASCs, DPSCs can be differentiated into osteoblasts which are able to form mineralized bone tissue *in vitro* [65]. UCSCs also exhibit potential for orthopeadic cell-based therapy with even greater proliferative capability than BMSCs [64]. Tissue engineering processes to generate bone grafts require isolation, purification, and *in vitro* expansion in order to obtain adequate numbers of high-quality cells. The ease of isolation, *in vitro* proliferative capability, and pluripotency make stem cells suitable for therapeutic purposes and a more attractive cell source than primary cells.

Despite the pluripotency of embryonic and fetal stem cells, these cell sources have not yet shown advantages over adult stem cells in tissue forming capability. Futher, they are not autologous, and related ethical controversies persist. Nevertheless, the technique of manipulating embryonic stem cells for engineering bone has been established and has demonstrated success in bone formation both *in vitro* and *in vivo [66]*.

Human induced pluripotent stem cells (iPSC) offer the potential for engineering a wide range of tissues, as these cells are both autologous and pluripotent [67]. Osteogenic potential of iPSC has

been demonstrated through direct differentiation and derivation of MSC-like cells [68]. However, the clinical applicability of iPSC is still far from fruition. iPSCs evolve very slowly in culture, and yields can be rather low [67]. In addition, the iPSC used for therapeutic purposes must be free of genomic insertions of transgene sequences [68]. Novel techniques must be developed to overcome these obstacles prior to clinical use.

To date, adult MSCs have demonstrated the highest clinical potential in the application of bone, cartilage, and osteochondral tissue engineering; therefore, this cell source was selected for the present studies. In order to successfully form osteochondral tissue *in vitro*, suitable scaffolds and environmental factors must be applied to direct adult MSCs differentiation. The cells must develop into osteogenic and chondrogenic lineages and assemble tissues at the defined locations i.e. form bone in the subchondral bone region and cartilage matrix in the articular surface region. In addition, the structure and quality of the tissue formed should match the native tissue for functional purposes. Numerous efforts have been attempted to engineer bone, cartilage, and osteochondral tissue, with current approaches reviewed below.

BONE TISSUE ENGINEERING

A successful bone graft should ideally match the physiological properties of the implant location in addition to providing a platform for healing. Scaffolds used in bone tissue engineering need to resemble the extracellular matrix of bone tissue, and thereby provide infrastructure for the cells to reside, proliferate, differentiate, and assemble mechanically functional bone [69]. In addition, scaffolds should be biocompatible, degradable into non-toxic products, osteoconductive (to recruit bone cells from the recipient), osteoinductive (to differentiate stem cells into bone-forming cells), osteointegrative (to provide permanent and functional attachment to native bone), and exhibit mechanical properties similar to those of native bone. Scaffolds composed of natural substances, protein- or organic-based polymers, ceramics, metals, as well as their combinations, have been extensively investigated for application in bone tissue engineering. Each material has

advantages and disadvantages. For example, organic polymers such as silk and poly-lactic-glycolic acid are much less stiff than native bone, and are easily fabricated into desired size, shape and porosity [70, 71]. In contrast, ceramics such as hydroxyapatite have mechanical properties similar to native bone but has limited structural flexibility [72, 73]. Optimization of materials for bone tissue engineering is still in progress [74-76].

Engineering clinically-sized autologous bone grafts requires the availability of large numbers of cells and advanced cultivation systems for seeding and cultivation of anatomically shaped scaffolds, sufficient nutrient delivery to the cells within scaffolds, and regulatory signals for cell differentiation and functional assembly [77]. In a suitable environment and with adequate stimulation, MSCs differentiate into osteogenic cells, and produce bone proteins and minerals [78, 79]. Biological and chemical factors such as dexamethasone [80] and BMP-2 [81, 82] have been shown to play significant roles in stimulating MSC osteogenic differentiation.

Mechanical signaling is also essential for bone formation. Physiologically, two types of mechanical cues that can affect bone formation are mechanical compression and shear stress [83]. Various technologies have been developed for engineering human bone grafts by utilizing scaffolds and bioreactors [77, 84, 85]. Specially designed bioreactors have been used, including spinner flasks, rotating wall vessels, and perfusion bioreactors [86-88] to maintain cell viability and achieve homogenous tissue development inside large constructs. Perfusion bioreactors have exhibited the most promising results in terms of controllability and bone tissue formation.

A typical bone bioreactor with medium perfusion consists of a medium reservoir, a culture chamber, and a perfusion loop with a pump and gas exchanger. The pump draws media from the reservoir through the cell-seeded scaffold, which resides in the culture chamber. Medium flow serves two purposes: provision of convective nutrient supply to the cells inside the porous construct, and mechanical stimulation through fluid shear load. Tissue engineered bones via perfusion bioreactors have been shown to be superior over those engineered by static culture [89]

and spinner flasks [90]. The effect of fluid shear stress enhances progressive deposition of mineralized matrix throughout the 3D engineered tissue constructs [79]. Perfusion bioreactors have shown an enhancement of bone-like tissue development in terms of production of bone matrix, (i.e., collagen type I, osteocalcin, osteopontin, and bone sialoprotein) in hMSC-seeded decellularized bovine trabecular bone [87]. Cellular content similar to native bone was achieved under optimal conditions in perfusion bioreactors [78]. More importantly, tissue engineered bone grafts were superior to either scaffold alone or cell-seeded scaffold in terms of graft incorporation into the critical size mouse calvarial bone defects [91].

CARTILAGE TISSUE ENGINEERING

Successfully engineered cartilage must mimic native-like tissue mechanics as well as cellular activity. Hydrogels have become the scaffold material of choice for cartilage tissue engineering due to their intrinsic hydrophilic nature and high water content, which similar to native soft hydrated tissues [92]. Investigated hydrogels include polyethylene(glycol) [93], hyaluronic acid [94], silk [95], collagen [96], and agarose [97-103].

Chondrocyte-seeded agarose constructs have been shown to successfully repair articular cartilage and tibial defects in animal models [104, 105]. The properties of agarose permit application of physiologic deformational loading immediately upon encapsulation such that constructs may be physically stimulated before extensive ECM development. Together, the characteristics of the agarose hydrogel system have allowed for the fabrication of the most reproducible and robust cartilage tissue growth in culture [106]. Furthermore, this system serves as an important tool to study tissue-engineering strategies. Clinically, agarose is being used as a co-polymer with alginate as a hydrogel scaffold for a commercial product, ACI (Cartipatch), used in cartilage defect repair and has demonstrated good 2-year clinical follow up [107, 108].

Focused efforts on applying a range of chemical cues such as growth factors (transforming growth factor (TGF)-β3, TGF-β1, insulin-like growth factor (IGF), fibroblast growth factor (FGF_2) [109-112]), corticosteroids [113, 114], and interleukins [115-117] have been investigated. Through paracrine signaling and direct cell-cell contact, the exchange of these chemical factors promotes extracellular matrix development. For functional tissue engineering, physiologically relevant stimuli were applied to encourage the development *in vitro* [118]. Rotating wall bioreactors have been used to provide a hydrodynamic, low-shear environment supportive of enhanced nutrient transport [119, 120] and cartilage-like tissue growth [121-123]. However, these bioreactors do not reproduce the physiologic deformational loading and hydrostatic pressure environment of the chondrocyte [124]. In comparison, applying physiologic loading through a combination of applied physiologic hydrostatic pressure and perfusion [125] or dynamic deformation loading [59, 102, 103] can achieve near-physiologic values for equilibrium modulus and GAG content. Applied deformational loading gives rise to enhanced convection of nutrients [126, 127], in a mechanism similar to how joint loading provides nutrients from the synovial fluid to avascular cartilage *in situ*. There is a growing body of literature suggesting that physical forces can be used to modulate chondrogenesis of MSCs [128-131], as reviewed by Huang and co-workers [132]. However, to date, tissue engineered cartilage from MSCs has not yet accomplished similar tissue quality as tissue engineered cartilage from primary chondrocytes.

OSTEOCHONDRAL TISSUE ENGINEERING

Osteochondral tissue engineering focuses on forming cartilage and bone in a spatially controlled manner i.e. bone formation in the subchondral region and cartilage formation on the articular surface. Strong integration between the two tissues is a neccessity for successful, tissue engineered osteochondral grafts. Integration can be attained by suturing, cell-mediated ECM formation, and the use of fibrin and other glues [133]. Since differentiating MSCs into osteogenic and chondrogenic lineages require different stimulating factors (i.e. organic

phosphate for osteogenic induction and TGF-β3 for chondrogenic induction), engineering fully developed osteochondral constructs *in vitro* is challenging. One strategy to spatially control stem cell differentiation is to pre-induce stem cells to develop into specific lineages prior to fabrication of the osteochondral constructs. MSCs were pre-differentiated with chondrogenic and osteogenic factors in 2D and 3D, prior to combining them into osteochondral constructs [134-136]. However, the constructs fabricated utilizing this system did not show strong integration or native-like bone and cartilage structure.

SUMMARY

Bone, cartilage, and osteochondral tissue engineering have progressed significantly. Successful development of these engineered tissues must exhibit biological factors and structures similar to native tissues to provide proper support and function. hMSC are the most clinically relevant cell source due to their proliferative capability and their ability to differentiate into osteogenic and chondrogenic lineages; thus, this cell source was selected for all of the studies conducted in this dissertation. The ability to control hMSC differentiation with cultivation media and growth factors allows for tissue development into specific lineages. However, there is a limited number of hMSC approaches which demonstrate the ability to control native-like tissue structure formation. This dissertation focuses on systems providing native-like control of the development of bone, cartilage, and osteochondral tissues.

CHAPTER IV

Goals, Rationale, and Investigational Approach

GOALS

The *goal* of this dissertation is to regulate *in vitro* development of bone, articular cartilage, and osteochondral tissue from hMSC into constructs with native structural and mechanical properties. hMSC demonstrates the potential of differentiation into bone and cartilage; however, controlling the tissue architecture formed with hMSC has not been successful. The difficulty in regulating tissue matrix assembly and the lack of techniques to spatially control hMSC differentiation and direct matrix deposition into native-like structures have been the major stumbling blocks to successful hMSC graft formation. The proposed *hypothesis* is that the control of hMSC differentiation in a manner consistent with physiological development can result in the *in vitro* assembly of native-like bone, cartilage, and osteochondral tissues.

The overall investigational approach was to apply physiologic tissue developmental processes towards the formation of native-like bone, cartilage, and osteochondral structures. The technique of engineering tissue from hMSC *in vitro* provides insights into the development of systems for the engineering of implantable, personalized, and functional tissue grafts. Various tissue-engineering techniques including the design of novel scaffolds and bioreactors and the manipulation of tissue fabrication process have been employed to study the hypothesis. The research in this dissertation was divided into three coordinated aims: (i) regulate bone mineral matrix assembly (Aim 1), (ii) govern articular cartilage development (Aim 2), and (iii) spatially control osteochondral tissue formation (Aim 3) by differentiating hMSC into specific lineage *in vitro*.

AIM 1: ENGINEERING MINERAL ARCHITECTURE BY DIRECTING hMSC MINERAL DEPOSITION THROUGH SCAFFOLD FEATURES

Introduction to the Problem

There have been numerous efforts to enhance and improve tissue engineered bone formation from hMSCs. hMSCs were osteogenicly induced through combinations of scaffold properties and chemical compositions, media supplements, and mechanical stimulations provided by bioreactors. The osteogenic differentiation of hMSCs is a suitable indication of successful tissue engineered bone formation. However, the genetic expression and the matrix production provided by the differentiated hMSC have not been translatable. Inside tissue-engineered bones, the entire tissue does not exhibit the form and function of native bone, and instead shows particulate mineral formation within the pore space of the scaffold rather than the connective mineral architecture seen in native bone [137, 138]. As a result, mechanical properties of the tissue engineered bone were significantly inferior to native bone, as the structure and architecture of bone matrix comprise bone strength and stiffness [139]. This aim investigated the mineralization process of tissue-engineered bone *in vitro* and control of the localization of deposited minerals.

Topic Background

A thorough understanding of native bone biology and the developmental process facilitates an experimental design to regulate formation of bone mineral architecture. The basic building blocks of bone are the mineralized collagen fibrils. The collagen constitutes the main component of a three-dimensional matrix in which the mineral forms. The mineral in this family of materials is dahllite, also known as carbonated apatite ($Ca_5(PO_4, CO_3)_3(OH)$) [140]. The major components are intimately associated into an ordered structure of mineralized collagen fibrils. The manner in which the building blocks are organized into higher order structures can also vary, and in fact, is the basis for differentiating between different types of bone such as cancellous, cortical,

mineralized tendon, and teeth. Seven levels of hierarchical organization of the family of mineralized collagen based materials were categorized ranging from nanoscale (mineral crystal) to macroscopic level (bone) [141]. As a result, this unique architecture of the bone contributes to its superior strength and toughness in comparison to synthetic materials.

Mineralization signaling molecules

Many organic and inorganic molecules play essential roles in bone mineralization. In addition to calcium, phosphate, and collagen, which are the components of bone mineral, many other important molecules play various roles in stimulating, and controlling mineral formation. Selected molecules are described in greater detail as follows.

Alkaline Phosphatase (ALP): During tissue mineralization, osteoblasts significantly increase the production of ALP which in turn cleaves phosphate esters to produce free inorganic phosphate. In addition to being the main component of hydroxyapatite, inorganic phosphate also acts as a signaling molecule and effects gene expression. Inorganic phosphate has been shown to induce the expression of several mineralization-involved proteins [142]. In addition, elevation of inorganic phosphate results in the upregulation of type II and III sodium-dependent phosphate transporters. These transporters facilitate the influx of inorganic phosphate into the cell, resulting in further induction of genes, including ALP [143, 144].

Pyrophosphate (PPi): PPi ($P_2O_7^{4-}$) is formed by the hydrolysis of ATP into AMP in cells. It has been shown that PPi inhibits mineralization in three ways: (i) It can prevent mineral growth by binding to the outer surface of the mineral; (ii) it induces the expression of osteopontin; and (iii) although PPi itself is a substrate for ALP, it can prevent the cleavage of the phosphate esters by inhibition of ALP in an uncompetitive way. However, PPi can also be cleaved by ALP into inorganic phosphate to facilitate mineral formation.

Non-collagenous proteins (NCPs): Bone mineralization is regulated by several extracellular proteins found in the organic matrix of bone [145-147], including a group of small integrin binding ligand N-linked glycoproteins (SIBLING) such as bone sialoprotein (BSP), and osteopontin (OPN). These proteins share some common features such as multiple phosphorylation sites, the possession of an Arg-Gly-Asp integrin binding motif and a highly acidic nature. Due to their integrin binding properties, these molecules can bind to the plasma membrane and are involved in signaling events between the cell and the ECM.

Bone sialoprotein is expressed nearly exclusively in mineralizing tissue [148]. It can specifically bind to collagen via a 20 AA long domain. Furthermore, BSP can bind hydroxyapatite through two glutamic acid-rich regions, which are both required for its functional activity as a nucleator of hydroxyapatite [149]. In addition, it has been demonstrated that after treatment with organophosphate for 4 – 8 h, bone sialoprotein localizes to the ECM in osteoblastic cultures, well before the first appearance of apatite crystals [150, 151]. This suggests that inorganic phosphate triggers BSP into the extracellular matrix where it can subsequently nucleate calcium phosphate in metastable solutions.

It has been reported that another specific bone matrix protein, bone acidic glycoprotein-75 (BAG-75), predicts the location of mineral nucleation, and possibly recruits bone sialoprotein [145, 152]. Purified BAG-75 can self-associate into supramolecular spherical complexes and sequester millimolar quantities of inorganic phosphate These properties indicate that BAG-75 generates a localized inorganic phosphate source for crystal nucleation reactions [153]. Interestingly, it has been proposed that bone sialoprotein is associated with a population of vesicle-like structures (defined as crystal ghosts), which are 500 – 800 nm in size. Bone sialoprotein does not, however, associate with the smaller 50 – 300 nm vesicle population [145].

Osteopontin is a protein with a wide distribution. It is found in mineralized tissues, in epithelial lining cells of numerous organs, and in body fluids. Many functions have been attributed to

osteopontin, including inhibition of bone mineralization and of pathologic calcification [154]. The effect of osteopontin on mineralization is dependent on its phosphorylation level, as dephosphorylated osteopontin does not inhibit mineralization while highly phosphorylated osteopontin promotes mineralization [155, 156]. On the other hand, osteopontin tends to be enriched on surfaces undergoing bone turnover and regulates adhesion and activity of osteoclasts, facilitating osteoclastic bone resorption [157].

In addition to the SIBLING protein family, a number of other proteins have been identified to be involved with and/or regulate matrix mineralization. These include acidic proteins such as osteocalcin, and SPARC (secreted protein, acidic, rich in cysteine) also known as osteonectin. Osteocalcin is the most abundant osteoblast-specific noncollagenous protein [158]. Osteocalcin binds to hydroxyapatite by means of its g-carboxyglutamic acid-rich region, and its synthesis and accumulation in bone is highly correlated to mineral deposition. Osteocalcin-null mice develop a phenotype that is marked by a higher bone mass without a change in osteoblast number, although osteoclast number is doubled. These mice do not respond to ovariectomy, indicating that bone resorption is not impaired [158]. Osteocalcin is proposed to play a role in remodeling as osteocalcin implants stimulate bone formation, osteoclast activity and early onset for remodeling [159], demonstrated by osteocalcin-null mice which are impaired in resorbing bone particles [73].

Osteonectin is a calcium-binding glycoprotein found bound to type I collagen in many tissues undergoing remodeling [154]. Osteonectin-null mice display a decreased bone formation and osteoblast and osteoclast number, resulting in a decreased bone remodeling which causes a profound osteopenia, indicating that osteonectin might also play a role in cell differentiation. Furthermore, several in-vitro studies have demonstrated that osteonectin can prevent crystal nucleation and retard crystal growth [160].

Cell-mediated mineralization

Mineralization may occur through osteoblast-driven or chondrocyte-driven ossification. However, due to the scope of this study on bone mineralization with osteogenic induced MSCs in a tissue-engineering model, only osteoblast-driven ossification is discussed. Osteoblasts express a number of genes that code for bone matrix components and enzymes that are involved in bone synthesis, including type I collagen, tissue non-specific alkaline phosphatase (ALP), bone sialoprotein, osteocalcin and osteopontin. Many of these genes are under the control of the osteoblast-specific transcription factor Runx2. As the bone matrix continues to grow, the osteoblasts get entrapped in their own matrix and terminally differentiate into osteocytes or undergo apoptosis.

Understanding detailed mineralizing mechanisms is essential for the application of engineering bone architecture with hMSCs. Bone mineralization occurs based on two mechanisms: (i) a spontaneous mineral precipitation; and (ii) an infiltration of amorphous calcium phosphate complex, which may intertwine (**Fig.IV-1**). Mineralization is subject to spontaneous precipitation from concentrated calcium and phosphate ions initiated at the site of non-collagenous proteins (NCPs). A study demonstrated that spontaneous hydroxyapatite crystal precipitation occurs with the presence of bone sialoprotein but not in the presence of osteopontin [161]. Following the initiation, the crystal then nucleates to form rigid mineral structure. To induce cell-mediated mineralization, the organism has to create an environment in which the metastable equilibrium between Ca^{2+} and PO_4^{3-} is disturbed, leading to precipitation of $Ca_x(PO_4)_y$ complexes. Disturbance of the equilibrium can be achieved by a local increase of calcium and/or inorganic phosphate, or an alteration of the molecules that inhibit or facilitate precipitation of the two ions. Physiologically, an increase in phosphate concentration is a common event in mineralization and can be found in the hypertrophic zone of the growth plate and under the mineral facing surfaces of osteoblasts [142] and odontoblasts [143].

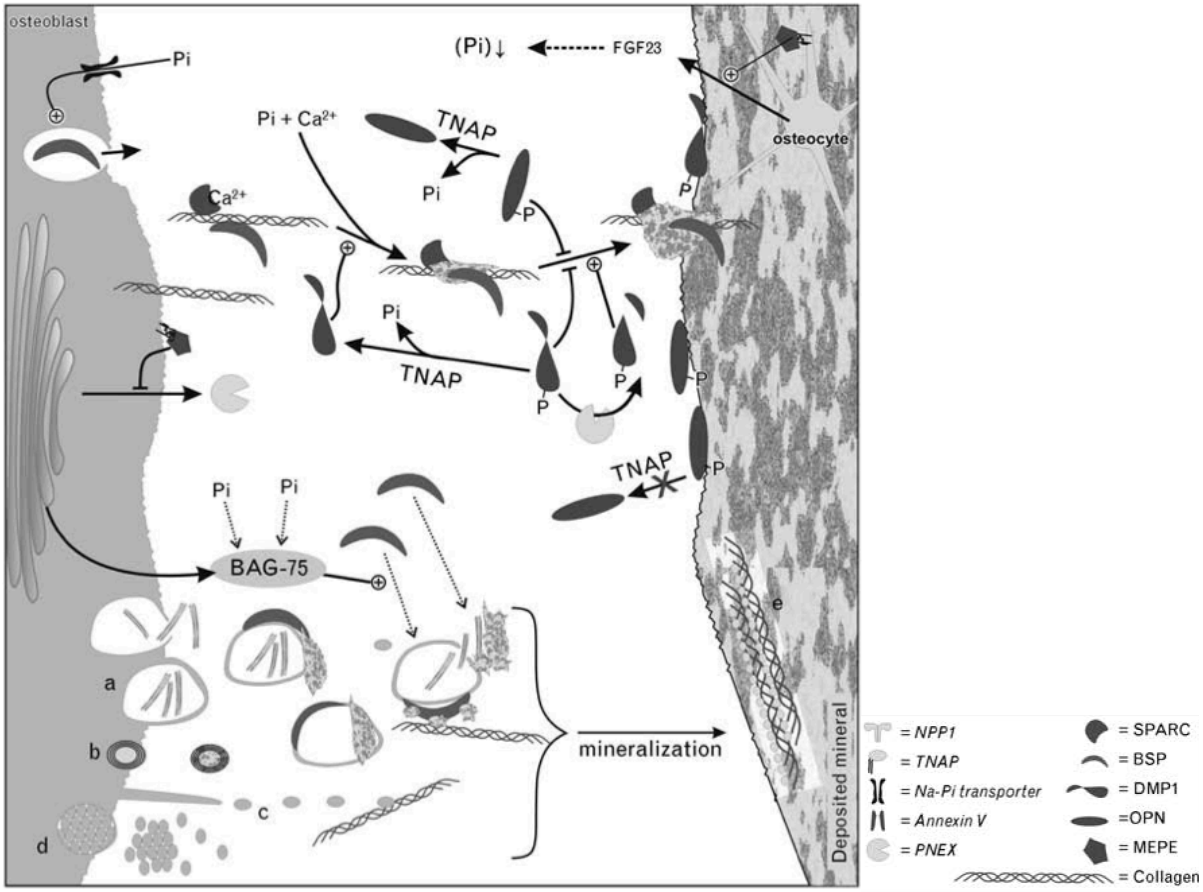

Figure IV-1: Mechanism of cell-mediated bone mineralization. In osteoblast/osteocytes matrix extracellular phosphoglycoprotein (MEPE) negatively regulates the phosphate concentration via FGF23 and phosphate-regulating gene with homologies to endopeptidases on X-chromosome (PHEX). Increasing inorganic phosphate stimulates the expression of a number of proteins, such as bone sialoprotein and SPARC (secreted protein, acidic, rich in cysteine). These proteins initiate mineralization around type I collagen fibers by binding of calcium and inorganic phosphate. Propagation of mineralization is negatively regulated by phosphorylated osteopontin and dentin matrix protein 1 (DMP1), which may be reversed by TNAP, or cleavage by PHEX. Several membrane enclosed structures (lower panel, bottom half) have been related to mineralization. (a) Formation of intracellular vacuoles containing mineral needles (or empty ghosts), which are excreted into the extracellular matrix (ECM). Bone acidic glycoprotein-75 (BAG-75) sequesters high quantities of inorganic phosphate and recruits bone sialoprotein to these structures, enabling further mineralization. (b) Multilamellar vesicles are found in vascular smooth muscle cell (VSMC)-mineralization, and (c) matrix vesicles are present in all forms of mineralization. (d) Exosomes are excreted during osteoblast- mediated mineralization. (e) These structures may associate with collagen fibers and facilitate mineralization, resulting in mineralized collagen fibers cover with lipid vesicles [162].

Another major theory of cell-mediated mineralization of bone proposes that mineralization is initiated by an intracellular origin. Rohde *et al*. described a novel model for mineralization by

osteoblasts, in which amorphous calcium/phosphate material is directly secreted via an exocytotic process from vacuoles of the osteoblast [163]. Many studies have demonstrated the presence of intracellular mineral structures inside vesicles of an osteoblastic cell [145, 150, 152]. TEM micrographs of mineralized nodules formed by osteoblasts after 28 days in culture showed matrix vesicle containing needle-like apatite crystals inside a cell [164]. In addition, BMP-2 stimulated bone marrow-derived mesenchymal stem cells develop needle-like amorphous calcium/phosphate (ACP) structures inside vacuoles [163]. These mineralization needles consist of two different phases: a mineral-containing phase and a white, hollow, presumably proteinaceous phase. It was hypothesized that the deposited crystals propagated into the collagen fibril matrix after excretion, and once there, matured to hydroxyapatite.

In vitro collagen mineralization was achieved by substituting the NCPs either with polyaspartic acid (pASP) or with fetuin, both inhibitors of hydroxyapatite crystallization [165, 166]. By employing such technique, the detailed mechanism of mineralization of collagen fibrils was recently developed [167]. The study proposed pre-nucleation calcium phosphate clusters form complexes with the functional matrix (in this case pASP) resulting in negatively charged, loosely packed, diffusive structures. The exact structure and composition of the pre-nucleation clusters are unknown at this time. Collagen fibrils, which contain positively charged regions at the border of the gap and overlap zones (close to the C-terminal), allow for pre-nucleation calcium phosphate infiltration. Pre-nucleation clusters infiltrate the nano-sized, positively charged region and bind to a distinct region on the collagen fibers. Once inside the collagen, the fluid diffuses through the interior of the fibril, solidifies into a disordered amorphous phase and, finally, becomes oriented crystalline hydroxyapatite inside the fibrils (**Fig.IV-2**).

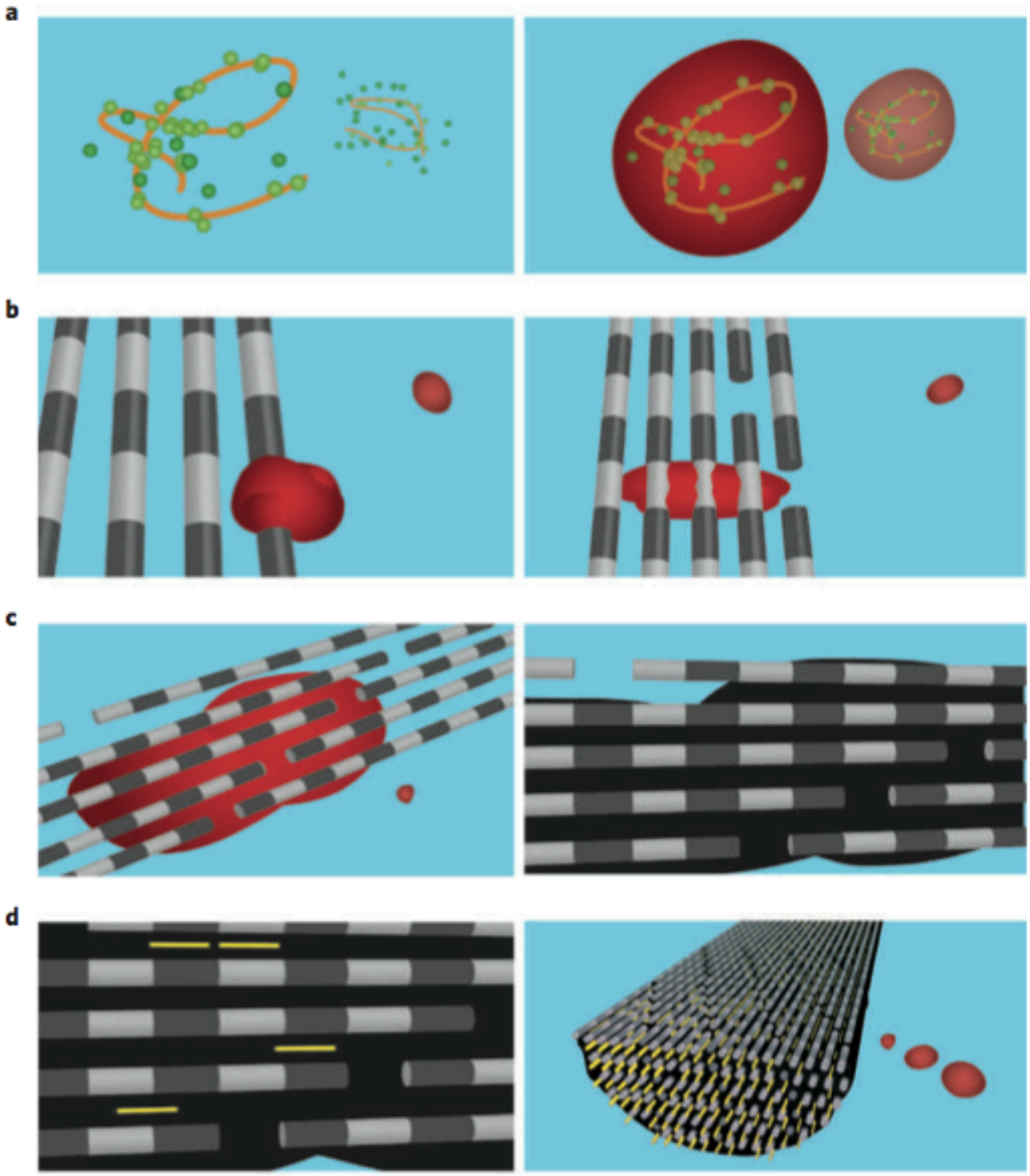

Figure IV-2: Mineralization of a collagen fibril. a, Calcium phosphate clusters (green) form complexes with the polymer (orange line), forming stable mineral droplets. **b,** Mineral droplets bind to a distinct region on the collagen fibres and enter the fibril. **c,** Once inside the collagen, the mineral in a liquid state diffuses through the interior of the fibril and solidifies into a disordered (amorphous) phase (black). **d,** Finally, directed by the collagen, the amorphous mineral transforms into oriented apatite crystals (yellow) [168].

Development of Theory and Hypothesis

In order to induce formation of bone architecture *in vitro*, it is critical to control the locale for mineral deposition. As mentioned earlier, the two mechanisms of bone mineralization currently accepted are spontaneous precipitation and formation of NCP-mineral complexes. Mineral precipitation is initiated at the site of NCPs or nucleated to form a larger structure. In contrast, the NCP-mineral complex infiltrates collagen fibrils or deposits on scaffolding platform. This aim focuses on controlling mineral deposition from hMSCs based on the two known mineralization mechanisms. hMSCs, once osteogenicly induced, produces bone matrix proteins such as collagen type I and NCPs, and deposit mineral through alteration of the calcium/phosphate environments and deposition of ACP. The strategy for engineering bone architecture is to direct mineral deposition and absorption onto the designed structure. Three distinct strategies to investigate and control *in vitro* mineralization were developed and investigated.

Aim 1.1: Nucleation and growth of mineralized bone matrix on silk-hydroxyapatite composite scaffolds (Chapter V)

This aim is motivated by the concept that bone mineral nucleates from pre-existing mineral. In addition, our preliminary data suggested that in the conventional tissue engineered bone cultivation method, hMSCs cannot produce sufficient mineral to match that of the native bone within 5 weeks of culture. We hypothesized that pre-existing minerals embedded in a silk sponge scaffold would provide a platform for mineral deposition in addition to increasing the total mineral content. The mineral thus nucleates along the pre-determined scaffold structure resulting in trabecular bone-like mineral architecture.

Aim 1.2: Effect of silk sponge scaffold stiffness and surface roughness on mineral deposition and functional bone formation (Chapter VI)

Cells have a capability of detecting the mechanical properties, surface topology, and chemistry of the substrate they are attached to. Increasing scaffold stiffness alters the environment that cells are exposed to while increasing surface roughness does not only alter the contact structure but also increases the surface area for cell attachment and protein absorption. This study altered scaffold stiffness and surface roughness of silk sponges while maintaining homogeneity of scaffold chemical composition through the incorporation of silk micro particles. The effects of scaffold stiffness and surface roughness on mineral and protein matrix deposition were investigated.

Aim 1.3: Effects of Bone Sialoprotein on Cell-Mediated Collagen Mineralization (Chapter VII)

Bone sialoprotein (BSP) can specifically bind to collagen and hydroxyapatite via functional groups. Previous studies have suggested that BSP can either act as a nucleus for the formation of the first apatite crystals on collagen fibril or associate with crystal ghosts to facilitate collagen mineralization. However, the dominant BSP mechanism under cell-mediated collagen mineralization is unknown. This aim employed tissue engineering approaches to study the effect of BSP on osteogenic-induced hMSCs in mineralizing collagen fibril.

AIM 2: ENGINEERING ARTICULAR CARTILAGES WITH INTEGRATION TO SUBCHONDRAL BONE FROM HMSC USING A NOVEL CELL PELLETS COMPRESSION TECHNIQUE

Introduction to the Problem

Primary chondrocytes have been largely used in cartilage tissue engineering. Adult chondrocytes may be obtained from a patient's own healthy, non-load bearing cartilage, however, this may

lead to donor site morbidity and further tissue degeneration [169]. Chondrocytes from the diseased cartilage may also be harvested during preliminary debridement procedures but the feasibility of the cell quality and amount of cellular content is uncertain for therapeutic purposes. Juvenile chondrocytes, bovine [170] and human [171], have been shown to be superior in term of biosynthetic capacity over their adult counterparts. Juvenile bovine chondrocytes encapsulated in hydrogel systems recreate and even surpass the properties of native bovine tissue by the temporal application of chemical [109] and/or physical factors [172], or a combination of the two [106]. However, the clinical utility of juvenile cell sources is limited due to the obvious challenges related to tissue procurement.

Nevertheless, primary cells have limited potential for clinical application. An ability to obtain sufficient cell numbers to produce constructs with sufficient mechanical properties is challenging due to the reduced biosynthetic activity of cells from patients with advanced stages of the disease [173, 174]. Alternatively, undifferentiated cartilage precursor cells, including MSCs isolated from patient bone marrow aspirate [175], from adipose tissue [176-179], or from the synovium [180-182] have been explored as alternative sources of cells. However, studies have not yet been successful in generating functional cartilage from these cell sources.

Topic Background

In theory, mesenchymal progenitor cells should have chondrogenic capability since chondrocytes originate from mesodermal cells. Cartilage tissue engineering techniques successfully used with juvenile chondrocytes were not capable of directing MSCs to form cartilage tissue at the functional level. [183]. The cartilage engineered with MSCs was inferior in gene expression, matrix production, and mechanical properties to cartilage engineered with juvenile chondrocytes.

The inability to form functional cartilage with hMSCs in hydrogel motivates reconsideration of the technique being employed. During tissue development, stem cells undergo chondrogenesis to form functional cartilage. Mesenchymal progenitor cells undergo mesenchymal condensation, in which the progenitor cells subsequently differentiate into chondroblasts and begin secreting cartilage molecules to form the cartilaginous tissue. hMSCs, which are also a type of mesenchymal progenitor cell, may require a specific form and function during chondrogenesis.

Cartilage engineered with scaffold-free fabrication techniques, demonstrated better quality than MSCs encapsulated in hydrogel. In one study, packing of MSCs was conducted by centrifuging cell suspension on transmembrane [184]. The cells proliferated and differentiated, producing cartilage matrix with an increase in construct thickness from several microns to hundreds of microns. Despite this increase, functional properties of the constructs were not reported in the study. This technique was also applied in the engineering of osteochondral constructs with a thin cartilaginous layer [185]. Another scaffold-free technique to generate an osteochondral construct is to press porous scaffolds into centrifuged cells pellets [134]. Interestingly, both scaffold-free methods resulted in cartilage matrix content approaching the value of the native tissue. However, due to the properties of the scaffold-free construct, structure and thickness could not be controlled. Furthermore, the cartilage tissue formed in the wrong locations was misshaped, or too thin.

Development of Theories and Hypothesis

Based on the technique of scaffold-free fabrication and cartilage development, this aim improved upon methods of engineered cartilage tissue formation from hMSCs; it achieved this by governing processes for tissue development in order to control formation of tissue structure. We proposed here a novel cell pellet compression technique. In order to mimic the physiological

condensation process, hMSCs were centrifuged to form dense, spherical cell pellets. Multiple pellets were packed together under compression into a decellularized bone scaffold. This technique created a construct with 3 distinguished layers: cell-only layer with precise thickness (scaffold-free cartilage region), packed cell penetration into the subchondral bone (interface region), and subchondral scaffold (bone region). The packed hMSC pellets were allowed to undergo chondrogenesis within a mold to mimic the tight space during physiologic development.

Experiment: Tissue engineer articular cartilage with cell pellet compression technique (Chapter VIII)

This study optimized the process of engineering articular cartilage from hMSCs via a novel cell pellet compression technique. After centrifuging hMSC suspension in chondrogenic media, spherical cell pellets formed overnight. The longer the cultivation, the more rigid the pellet became, likely as a result of cell packing and extracellular matrix deposition. In order to pack multiple pellets together on a subchondral bone, pellets must be rigid enough to hold their shape but flexible enough to fuse together and also penetrate the subchondral bone. The study investigated the progression of cartilage formation with different level of chondrogenic maturity of the hMSC pellets.

AIM 3: DETERMINING THE REQUIREMENTS TO TISSUE ENGINEER OSTEOCHONDRAL GRAFTS

Introduction to the Problem

Successfully engineered osteochondral grafts should be populated with autologous or non-immunogenic cells to prevent immune rejection and facilitate adaptation. In addition, the fabrication technique must result in a controlled graft size and shape to match that of the defect. Since an osteochondral graft is a complex tissue consisting of bone, cartilage, and the integrated interface, engineering clinically relevant construct *in* vitro is a challenging task. The cells must be seeded to fully occupy volume for tissue formation. Adequate factors must be supplied to

maintain cellularity and spatially differentiate stem cells into tissue-specific lineages in a defined region (i.e. chondrogenesis in the articular region, bone formation in the subchondral bone region, and an integrating interface in between the two tissues). *In vitro* cultivation of osteochondral grafts with clinically relevant sizes and anatomical shapes requires an innovative bioreactor. Although a perfusion bioreactor has been successfully employed to engineer bone constructs, there is no successful bioreactor designed for complete osteochondral tissue engineering. This aim investigated the regulation of spatially controlled hMSC development to form osteochondral tissues *in vitro*.

Topic Background

Previous attempts to spatially control cartilage and bone formation employed pre-differentiating stem cells into specific lineages prior to scaffold seeding. Tuli et al. [134] press-coated MSCs on PLA constructs and cultured them in chondrogenic media for 2 or 5 weeks prior to seeding osteogenic-induced MSCs from the same source. The constructs were then cultured in cocktail media (mixture of chondrogenic and osteogenic supplements) up to 10 weeks. The results showed distinguished chondrogenic and osteogenic development in desired regions with the presence of a cartilage-bone interface.

Augst et al. separately induced hMSC-seeded silk sponges in chondrogenic or osteogenic media for 3 weeks. The two constructs were attached together and cultured in chondrogenic or osteogenic media for an additional 3 weeks to create osteochondral grafts with integration [136]. The constructs were cultured in rotating-wall vessel bioreactors to enhance transport. Pre-differentiation regulates MSCs to develop into specific lineages and results in spatially controlled, tissue-specific behavior (i.e. cartilage and bone formation). The study demonstrated that TGF-β played an important role in integrating bone and cartilage surfaces. The pre-differentiation technique demonstrated a well-developed strategy to spatially control tissue

formation. However; the shape and size of the constructs and tissue mechanics were not comparable to native tissue [134, 185].

Development of Theory and Hypothesis

The ultimate goal for a tissue engineer is to develop a system that allows fabrication of grafts with physiologic properties. Ideally, osteochondral grafts should have anatomical shape, contain a stiff subchondral bone region with osteogenic and osteointegrative properties, a physiologically thick and functional cartilage layer, and strong integration of the two tissues. hMSCs have the capability to form bone and cartilage *in vitro* through induction of media soluble factors, mechanical cues, and bioactive scaffolding materials but are nonetheless difficult to control during this complex tissue formation. Successful engineering of osteochondral grafts from hMSC requires spatial control of hMSC differentiation and stimulation of the native tissue matrix formation and assembly. This aim was to determine the essential criteria for developing a bioreactor system for engineering osteochondral grafts.

Experiment: Spatial regulation of human mesenchymal stem cell differentiation in engineered osteochondral constructs: effects of pre-differentiation, soluble factors and medium perfusion (Chapter IX)

This study investigated the effect of pre-differentiation, soluble factors, and medium perfusion in spatially regulated osteochondral tissue formed from hMSCs. Bi-phasic constructs can be formed by pre-differentiation of hMSC or by distinctly supplying lineage-specific factors. Perfusion bioreactors have been previously shown to separately enhance cellularity and extracellular matrix formation in engineered bone and cartilage tissues. The combined effects of hMSC pre-differentiation and the perfusion bioreactor in engineering osteochondral constructs have not yet been investigated. Determining the effect of hMSC pre-differentiation, soluble factors, and

medium perfusion on osteochondral tissue development provided new insights into the essential criteria required to successfully engineer clinical-relevant size osteochondral grafts.

CHAPTER V

Aim 1.1: Nucleation and growth of mineralized bone matrix on silk-hydroxyapatite composite scaffolds

ABSTRACT

We describe a composite hydroxyapatite (HA) – silk fibroin scaffold designed to induce and support the formation of mineralized bone matrix by human mesenchymal stem cells (hMSCs) in the absence of osteogenic growth factors. Porous three-dimensional silk scaffolds were extensively used in our previous work for bone tissue engineering and showed excellent biodegradability and biocompatibility. However, silk is not an osteogenic material and has a compressive stiffness significantly lower than that of native bone. In the present study, we explored the incorporation of silk sponge matrices with HA (bone mineral) microparticles to generate highly osteogenic composite scaffolds capable of inducing the *in vitro* formation of tissue-engineered bone. Different amounts of HA were embedded in silk sponges at volume fractions of 0%, 1.6%, 3.1% and 4.6% to enhance the osteoconductive activity and mechanical properties of the scaffolds.

The cultivation of hMSCs in the silk/HA composite scaffolds under perfusion conditions resulted in the formation of bone-like structures and an increase in the equilibrium Young's modulus (up to 4-fold or 8-fold over 5 or 10 weeks of cultivation, respectively) in a manner that correlated with the initial HA content. The enhancement in mechanical properties was associated with the development of the structural connectivity of engineered bone matrix. Collectively, the data suggest two mechanisms by which the incorporated HA enhanced the formation of tissue engineered bone: (i) the increased osteoconductivity of the material led to increased bone matrix production, and (ii) nucleation sites for new mineral deposition led to the connectivity of mineral architecture.

INTRODUCTION

Bone repair procedures often require a replacement graft to restore the function of damaged or diseased tissue. These grafts are in most cases derived from tissues harvested from a second anatomic location of the same patient (autografts) or from other patients (allografts). Autografts have been considered the gold standard for bone repair. However, limited supplies of suitable bone grafts, donor site morbidity and difficulties in shaping explanted bone have posed significant problems. On the other hand, allografts have a risk of disease transmission [186]. These limitations provide incentives for finding alternative methods. Tissue engineered bone offers a promising alternative treatment for clinical use, as well as a controllable model system for studies of cell function, developmental biology and pathogenesis [187, 188].

Successfully engineered bone grafts must be biocompatible and meet certain minimal mechanical requirements to be functional. The scaffold material provides many of the mechanical properties of the engineered graft. Organic- and polymer-based scaffolds are easily fabricated into different structures but often do not have the desired compressive modulus [137, 189-191]. Alternatively, ceramic scaffolds are stiffer but are often fragile and have low porosity, resulting in loosening or fracture of implants in clinical applications [192]. Combining both types of materials to form composite scaffolds can enhance the mechanical and biochemical properties of scaffolds used for bone tissue engineering.

In this study, silk protein and hydroxyapatite (HA) ceramic were chosen because of their biocompatibility and osteoconductivity, and ease and reproducibility of fabrication. Silk sponges have been used extensively in bone tissue engineering approaches with human mesenchymal stem cells (hMSCs) and were shown to facilitate bone formation in vitro and in vivo [88, 136, 137, 193]. Silk prepared with organic solvent (hexafluoroisopropanol: HFIP) and salt leeching allows the fabrication of biocompatible scaffolds with high silk content, high porosity, and good inter-pore connectivity [137, 193, 194]. HA is biocompatible, bioactive, osteo-inductive and can

slowly be replaced by host bone after implantation [195-198]. We hypothesized that embedding HA micro-particles within the walls of silk sponges would improve scaffold stiffness and enhance hMSC differentiation resulting in the development of tissue engineered bone grafts with higher mineral content and improved compressive stiffness. We therefore examined the effects of scaffold properties on the structural and mechanical outcomes of engineered bone grafts by incorporating various amounts of HA mineral in porous silk scaffolds.

Bone-like constructs have been prepared *in vitro* by culturing hMSCs seeded into biomaterial scaffolds. HMSCs offer several advantages: they can be obtained autologously, expanded *in vitro* to provide sufficient cell numbers, differentiated into osteoblasts [199-202] and have shown promising results in clinical models [203]. In this study, silk-HA scaffolds were seeded with hMSCs and cultured in perfusion bioreactors, which improve cell distribution and bone formation inside the scaffolds [78, 89, 204]. Perfusion provides adequate nutrient and oxygen supply as well as cell stimulation through fluid shear stress, which enhances hMSCs osteogenic differentiation [89, 205-207]. Constructs were cultured for up to 10 weeks before being harvested and analyzed for bone tissue formation.

MATERIALS AND METHODS

Scaffold Fabrication

All reagents were purchased from Sigma Aldrich (St. Louis, MO) unless otherwise specified. Silk fibroin was extracted from *Bombyx mori* cocoons utilizing our previously developed methods [12]. Briefly, the sericin was removed by boiling the cocoons in a 0.02 M Na_2CO_3 solution for 30 minutes. The resulting fibers were then dissolved in 9.3 M LiBr for 4 hours at 60ºC and then subsequently dialyzed against ultrapure water for 48 hours to remove residual LiBr. The aqueous silk solutions were lyophilized and redissolved in HFIP to yield a solution of 16 w/v%. The method for fabricating HA-incorporated silk sponges is shown in **Fig.V-1A**.

Reinforcement of the scaffolds was achieved by mixing HA into the NaCl particles and pouring the silk solution over the mixture. Scaffolds were prepared with pore sizes ranging between 500 and 600 mm using granular NaCl as a porogen. Once the scaffolds solidified, they were treated with methanol for 1-2 days to induce β-sheet formation and then the salt was subsequently extracted by immersion in fresh water for 48 hrs. Scaffolds were cut and cored into cylinders of 4 mm in diameter by 4 mm thick and were sterilized in 70% ethanol overnight and incubated in culture medium over night before seeding.

Four groups of scaffolds with different content of HA-silk composition were fabricated with mixtures of Silk:HA:Salt ratios by weight of 1:0:20, 1:0.5:20, 1:1:20, and 1:1.5:20. The volume fractions of silk and HA in the porous scaffold were calculated using the amount of the materials added and their densities which are 1.4 g/ml and 3.16 g/ml, respectively. As a result, the designated group names were based on approximated HA volume fraction in the scaffolds that were 0%, 1.6%, 3.1%, and 4.6% HA, respectively.

Scanning Electron Microscopy

SEM was performed to determine pore structure and surface topography on two scaffolds of each group. In brief, scaffolds were washed in PBS and then fixed in 2% glutaraldehyde in PBS overnight. Constructs were washed in graded ethanol solution up to 70% and then freeze-dried overnight in a lyophilizer. Dried samples were coated with gold and imaged at 200x and 1000x in an SEM (JEOL, Japan).

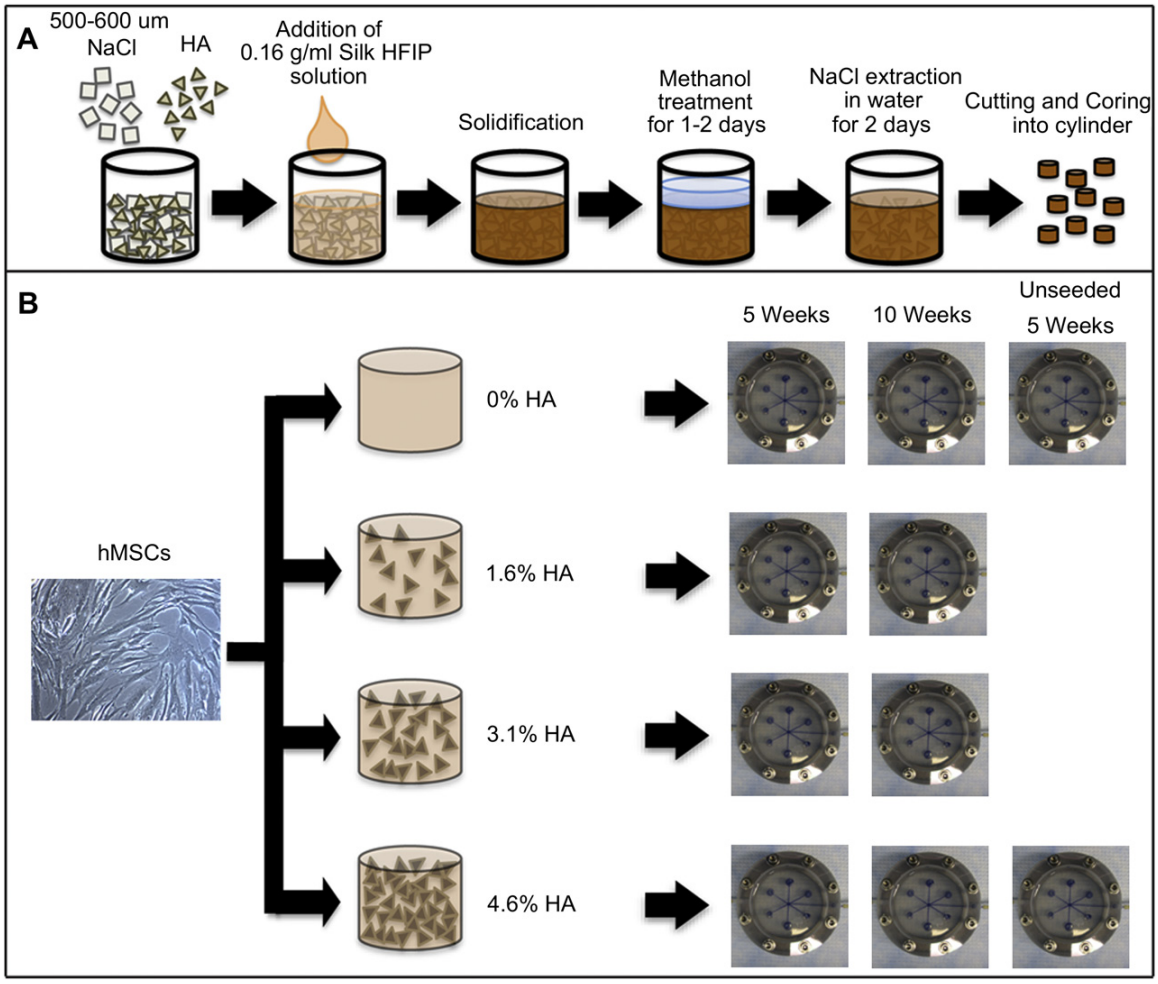

Figure V-1: Experimental design (A) Silk-HA composite scaffold fabrication process. (B) Experimental design to study the effects of embedded HA content in silk sponge in formation of tissue engineered bone constructs. Four types of scaffolds (0% HA, 1.6% HA, 3.1% HA, and 4.6% HA) were seeded with hMSCs and cultured in osteogenic media under perfusion bioreactor for 5 and 10 weeks. Unseeded 0% HA and 4.6% HA were also cultured for 5 weeks.

Human Mesenchymal Stem Cell Cultivation and Seeding

Fresh bone marrow aspirates were obtained from Cambrex Life Sciences (East Rutherford, NJ), isolated and characterized as previously described [78]. Cells were expanded in high-glucose DMEM supplemented with 10% FBS, 1% pen-strep, and 0.1 ng/mL bFGF. The hMSCs were cultured up to the third passage and then used for seeding the scaffolds. The seeding process was previously described [87, 137]. In brief, scaffolds were seeded at the concentration of 30×10^6 cells/ml scaffold volume. A 40-µl aliquot of cell suspension was pipetted onto blot-dried

scaffolds and allowed to percolate through. The scaffolds were flipped 180° every 20 minutes and 10 μl of media was added to prevent the cells from drying out. Constructs were cultured with osteogenic medium (low-glucose DMEM supplemented with 10% FBS, 10 nM dexamethasone, 10 mM sodium-β-glycerophosphate, and 0.05 mM ascorbic acid-2-phosphate) for 3 days before harvested for Day 0 sample and insertion into the bioreactor.

Bioreactor Cultivation

A perfusion bioreactor developed in our laboratory, described and used previously [87, 204], was employed in this study. In brief, 6 scaffolds were placed in each bioreactor and medium flow rate was set to provide the superficial velocity of medium through the scaffolds at 400 μm/s. One half of the medium volume was replaced twice a week and scaffolds were harvested for analysis at weeks 5 and 10 (**Fig.V-1B**). The studies were conducted twice 6 month apart with different batches of scaffolds to ensure reproducible results. Since the results of the two studies were similar, they were pooled together. Two additional experimental groups (unseeded 0% HA and 4.6% HA) were performed in the repeat experiment (**Fig.V-1B**).

Cell Viability

After harvest at day 0 and week 10, two half scaffolds per group were washed in PBS and stained with 1 mM calcein and 4 mM ethidium in PBS for 30 min. The images were taken with a confocal microscope (Leica, Germany; 20 slices at 10 μm thick).

Biochemical Assay

Constructs were cut in half in the longitudinal direction, washed in PBS and the wet weights were determined. For DNA analysis, the samples (n=8) were stored at -20°C in 1 ml of digestion buffer (10 mM Tris, 1mM EDTA and 0.1% Triton X-100) with 0.1 mg/ml of proteinase K in micro-centrifuge tubes. Samples were then thawed and maintained in this solution overnight at

56°C to extract the DNA. The DNA content was determined using a Picogreen assay (Molecular Probes, OR). For calcium content analysis, the samples (n=4) were quickly frozen in liquid nitrogen and stored at -20°C. Calcium was extracted in 500 µl of 5% TCA solution using a bead beater and analyzed with a Calcium (CPC) Liquicolor® kit (Stanbio Laboratory, USA).

Mechanical Testing

The equilibrium compressive Young's modulus (n=8 per group) was determined at day 0, week 5, and week 10 in unconfined compression at wet conditions using a modification of an established protocol [103]. An initial tare load of 0.2 N was applied and was followed by a stress-relaxation step where specimens were compressed at a ramp velocity of 1% per second up to 10% strain and maintained at the position for 1800 s. The Young's modulus was obtained from the equilibrium forces measured at 10% strain. Mechanical properties of decellularized trabecular bovine bones were also measured with the same method.

Micro Computerized Tomography

µCT imaging was performed using a modification of a previously used protocol [208] with the following settings: voltage 55kV, current 0.109 mA, slice thickness 21 µm, and inter-slice spacing 22 µm. Scaffolds were scanned prior to seeding and after cultivation. Immediately after harvesting, full constructs (n=6 per group) were aligned and stabilized along their axial direction in PBS inside microcentrifuge tubes. The tubes were placed in the specimen holder of a vivaCT 40 system (SCANCO Medical AG, Basserdorf, Switzerland). Constructs were scanned at 21 µm isotropic resolution. The bone volume was obtained using a global thresholding technique with threshold at 220. The structural parameters, which are bone volume (BV), bone volume fraction (BVF), connectivity density (Conn.D), trabecular number (Tb.N), trabecular thickness (Tb.Th), and trabecular spacing (Tb.Sp) were determined with the structural reconstruction.

Decellularized trabecular bovine bones were also scanned in parallel to compare with the cultured constructs.

Group	Silk Content (%v)	Mineral Content (%v)	SEM Image 200x	SEM Image 1000x
0% HA	7.18	0	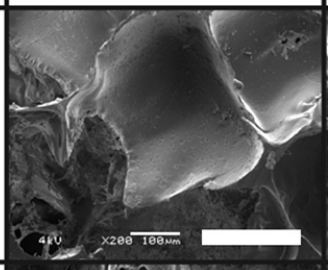	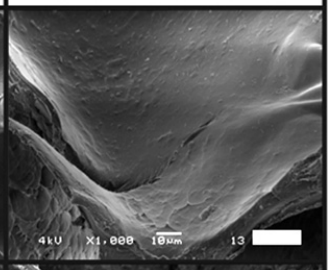
1.6% HA	7.06	1.57	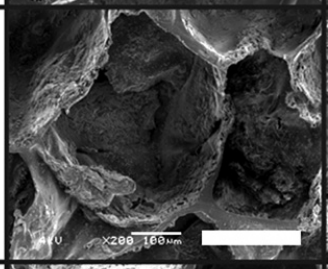	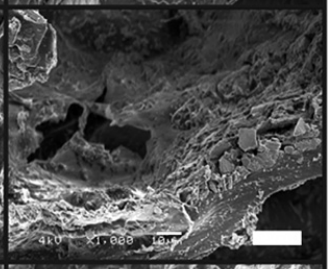
3.1% HA	6.96	3.08	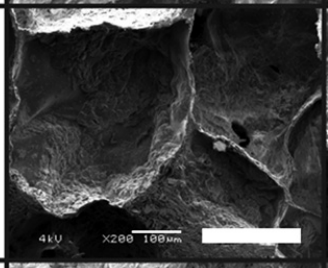	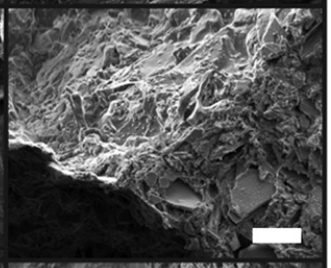
4.6% HA	6.85	4.55	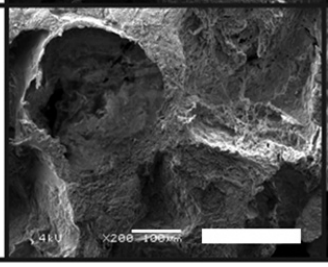	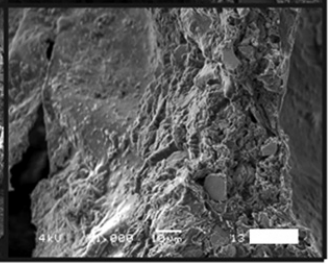

Figure V-2. Calculated volume fraction of silk and HA mineral and SEM images of 0% HA, 1.6% HA, 3.1% HA, and 4.6% HA scaffolds. 200x SEM image showed porous scaffold with interpore connectivity (bar: 200 μm). 1000x SEM image illustrated the different in surface topography of the scaffolds (bar: 20 μm).

Histology and Immunohistochemistry

Constructs were washed in PBS, fixed in 10% formalin, embedded in paraffin, sectioned into 4 μm slices and stained with haematoxylin and eosin (H&E), and Von Kossa. Immunohistochemistry staining for collagen type I, bone sialoprotein (BSP), and osteopontin was also conducted as previously described [87].

Statistical Analysis

Multiway Analysis of Variance (ANOVA) to analyze groups at the same time point and within group at different time points was carried out followed by Tukey's *post hoc* analysis using STATISTICA software, with $p<0.05$ being considered as significant.

RESULTS

Scaffold Fabrication

The inter-pore connectivity of the scaffolds was maintained with the incorporation of HA into the silk sponges, while minimally reducing the porosity as seen in low magnification SEM images (**Fig.V-2**). The pore size of the scaffolds in all groups ranged between 400-600 μm, which is equivalent to the size of the salt particles that were used in the process. High magnification SEM images showed an increase in scaffold surface roughness qualitatively as more HA was added, but with less distinct differences between 3.1% and 4.6% groups (**Fig.V-2**). The incorporated HA was trapped within the silk structure and an increase in wall thickness was observed. By converting material mass introduced into the scaffold into volume, the total material volume fraction within the 0%, 1.6%, 3.1%, and 4.6% HA groups were 7.18, 8.66, 10.04, and 11.40%, respectively; thus, a decrease in void volume was observed as more HA was incorporated. In addition, incorporation of HA gradually increased scaffold equilibrium

compressive Young's modulus measured in the hydrated state, from 120.8±48.7 kPa in 0% HA group to 251.1±116.9 kPa in 4.6% HA group (**Fig.V-5A**).

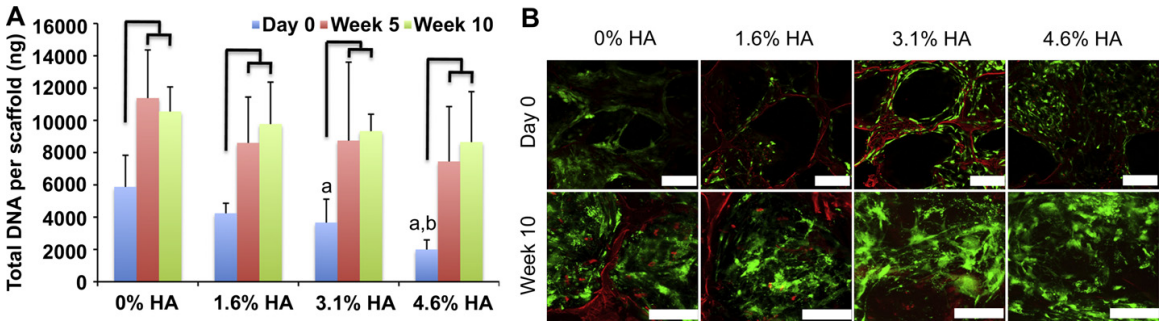

Figure V-3. (A) DNA content before and after cultivation in perfusion bioreactor for 5 and 10 weeks (Line represents a statistically significant difference between time point of the same scaffold group; [a, b] represent statistically significant differences from 0% HA and 1.6% HA, respectively, at the same time point). (B) Live/Dead image of cells inside the scaffolds before and after cultivation for 10 weeks (scale bar: 200 μm).

Cell Viability and DNA Content

After 5 and 10 weeks of culture, the DNA content significantly increased from Day 0 in all groups and as much as 4 fold in the 4.6% HA (**Fig.V-3A**). Although the average DNA content of the 0% HA was significantly higher than in the 3.1% and 4.6% HA groups at Day 0, the DNA content was not significantly different after 5 and 10 weeks of culture. Live/Dead assay showed good cell viability after seeding and after 10 weeks of culture with an increase in cell content over the culture period (**Fig.V-3B).**

Mineral Content and Micro-Structure

The structure of the tissue engineered bone developed over 5 and 10 weeks of culture (**Fig.V-4**). In the 0% HA group, the tissue engineered bone had no detectable mineral with μCT and, while over 10 weeks, the mineral deposited developed into spherical-like structures (**Fig.V-4**). Constructs from the 1.6% HA group developed into trabecular-like structures over the culture

period with some aggregates of spherical-like structures (**Fig.V-4**). In contrast, constructs in the 3.1% and 4.6% HA groups developed trabecular-like architectures with high structural connectivity (**Fig.V-4**).

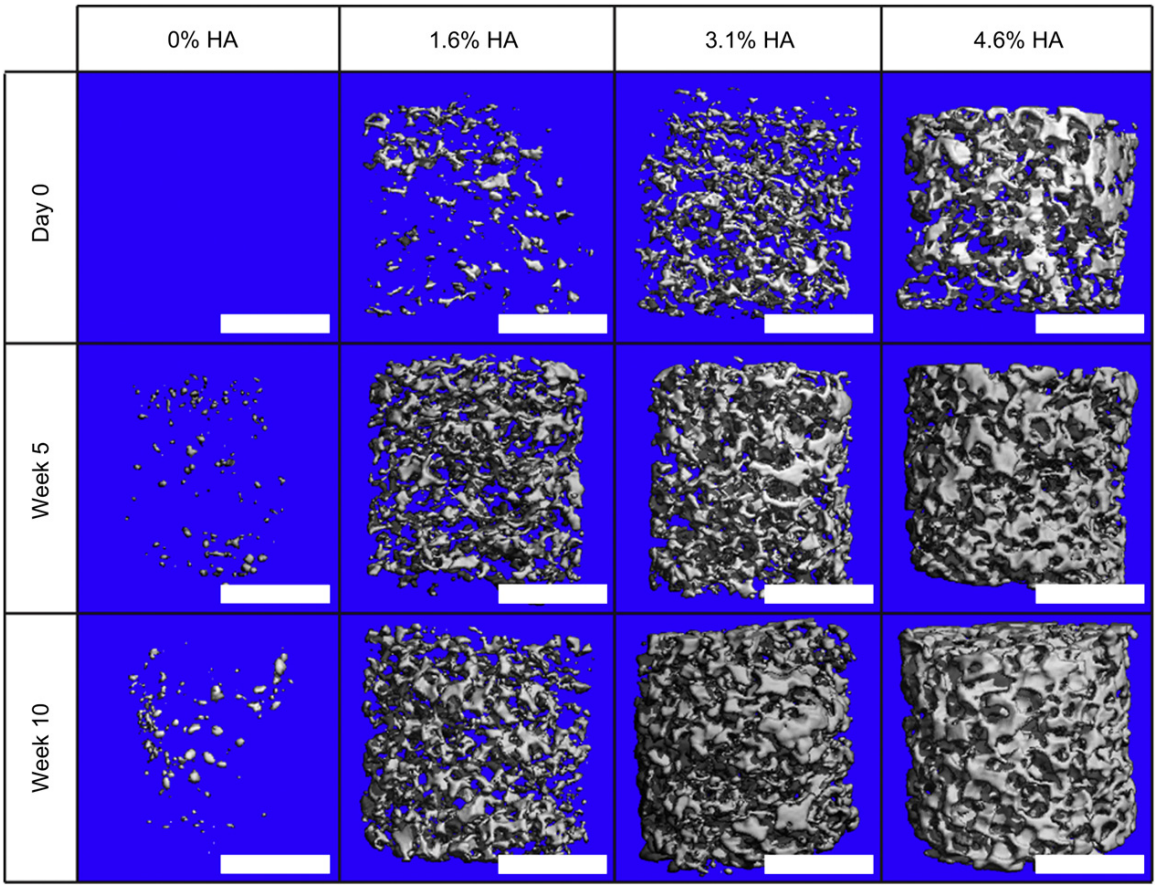

Figure V-4. Reconstructed 3D μCT images of the tissue engineered bone construct before and after cultivation for 5 and 10 weeks of all groups (scale bar: 2 μm).

Quantification of morphological parameters confirmed development of trabecular-like structures in 3.1% and 4.6% HA groups (**Fig.V-5**). BV, BVF, Conn.D, Tb.N, Tb.Th, and Tb.Sp approached the values of native bovine trabecular bone (dash lines) determined in our laboratory with the same scanning method. BV, BVF, and Conn.D significantly increased and more than doubled over 10 weeks of culture in the groups with mineral. The BVF (**Fig.V-5D**) of 3.1% and 4.6%

HA on average were 0.029±0.028 and 0.068±0.038 at day 0 and reached 0.097±0.021 and 0.126±0.019 at 5 weeks and 0.142±0.062 and 0.156±0.033 at 10 weeks, respectively. The Conn.D (**Fig.V-5E**) of 3.1% and 4.6% HA increased significantly from 0.78±1.72 and 2.34±2.57 1/mm^3 to 4.18±1.85 and 8.76±2.40 1/mm^3 at week 5 and to 9.24±8.53 and 12.83±5.43 1/mm^3 at week 10, respectively. Tb.N and Tb.Th increased over time while the Tb.Sp decreased (**Fig.V-5F-H**) in all groups except 0% HA in which Tb.Sp at day 0 could not be determined. When unseeded 0% HA and 4.6% HA were cultured for 5 weeks, all parameters remained the same as the day 0 value, indicating that changes in mineralization were cell-based (data not shown).

Mechanical Properties

The equilibrium Young's modulus gradually increased over time in all groups (**Fig.V-5A**). The moduli of scaffolds containing 0%, 1.6%, 3.1%, and 4.6% HA were 121±49, 140±70, 201±90, and 251±117 kPa, respectively, at Day 0. By 5 weeks, the moduli of scaffolds containing 0%, 1.6%, 3.1%, and 4.6% HA reached, 340±99, 594±234, 865±347, and 1005±381 kPa, respectively. The modulus of the 3.1% and 4.6% HA were significantly higher than the modulus of the 0% HA. Equilibrium Young's moduli of unseeded 0% and 4.6% HA were not significantly different from day 0. By 10 weeks, the moduli of scaffolds containing 0%, 1.6%, 3.1%, and 4.6% HA reached on average 0.532±0.180, 0.869±297, 1.600±0.577, and 1.670±0.528 MPa, respectively. The moduli of scaffolds containing 3.1% and 4.6% HA were significantly higher than the moduli of both 0% and 1.6% HA. The equilibrium Young's moduli of decellularized bovine trabecular bone determined in our laboratory with the same method ranged between 5-40 MPa. The equilibrium Young's moduli of unseeded 0% HA and 4.6% HA remained unchanged from the Day 0 value.

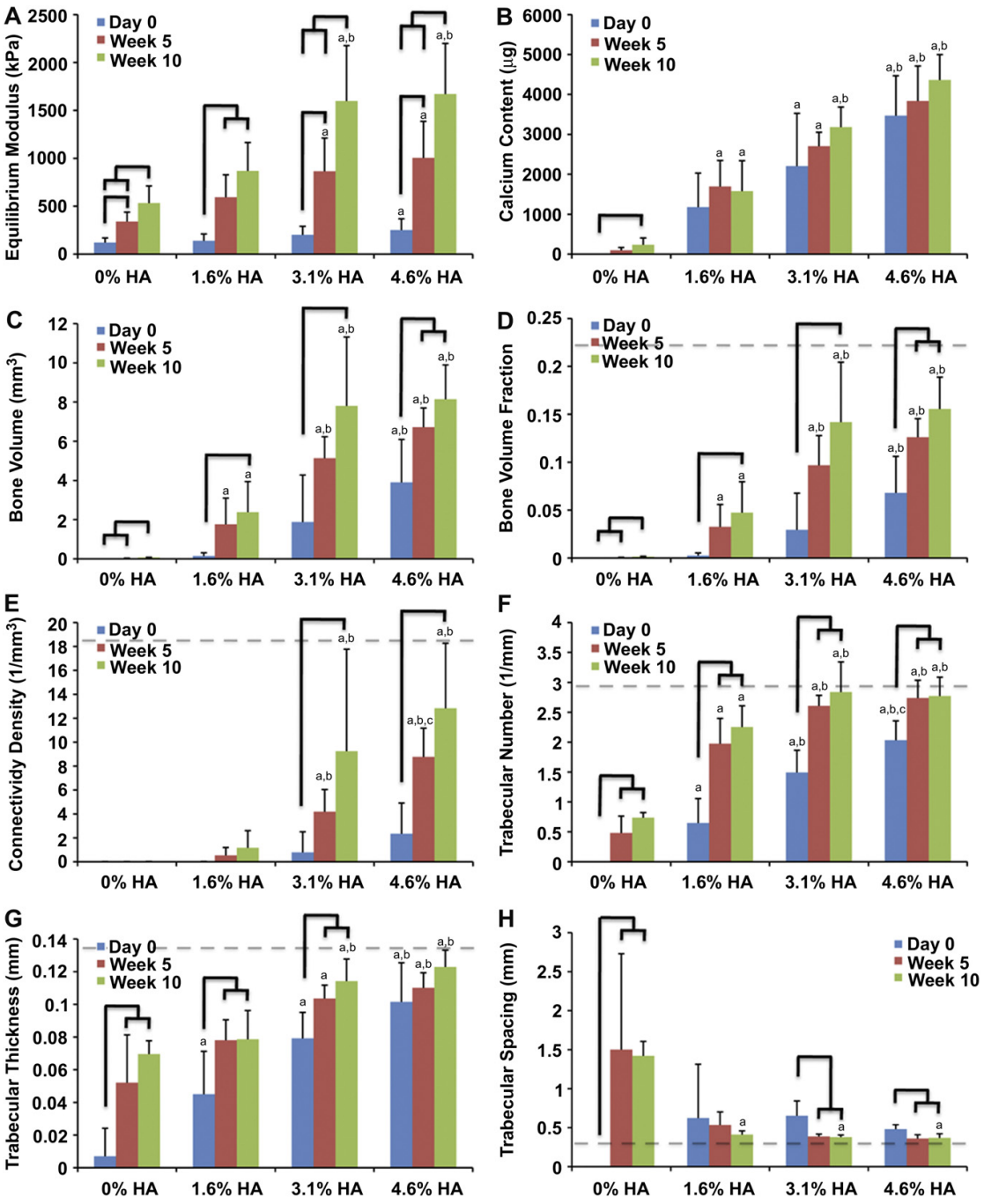

Figure V-5. Development of tissue engineered bone constructs over 5 and 10 weeks of cultivation: (A) Equilibrium Young's Modulus, (B) calcium content, and bone structural parameters determined by μCT analysis; (C) BV, (D) BVF, (E) Conn.D, (F) Tb.N, (G) Tb.Th, and (H) Tb.Sp (Dash line indicates average value of decellularized native trabecular bovine bone. Solid tree line represents a statistically significant difference between time point of the same scaffold group; [a, b, c] represent statistically significant differences from 0% HA, 1.6% HA, and 3.1% HA, respectively, at the same time point).

Calcium Content

The calcium content of scaffolds increased over time but the increases were not statistically significant within each group (**Fig.V-5B**). At Day 0, the calcium content of scaffolds containing 0%, 1.6%, 3.1%, and 4.6% HA were 0±0, 1.18±0.85, 2.21±1.32, and 3.47±1.00 mg per scaffold, respectively. Over 10 weeks, the average calcium content increased by 0.24, 0.40, 0.97, and 0.90 mg per scaffold for scaffolds containing 0%, 1.6%, 3.1%, and 4.6% HA, respectively. Both unseeded 0% and 4.6% HA did not show an increase in average calcium content (data not shown).

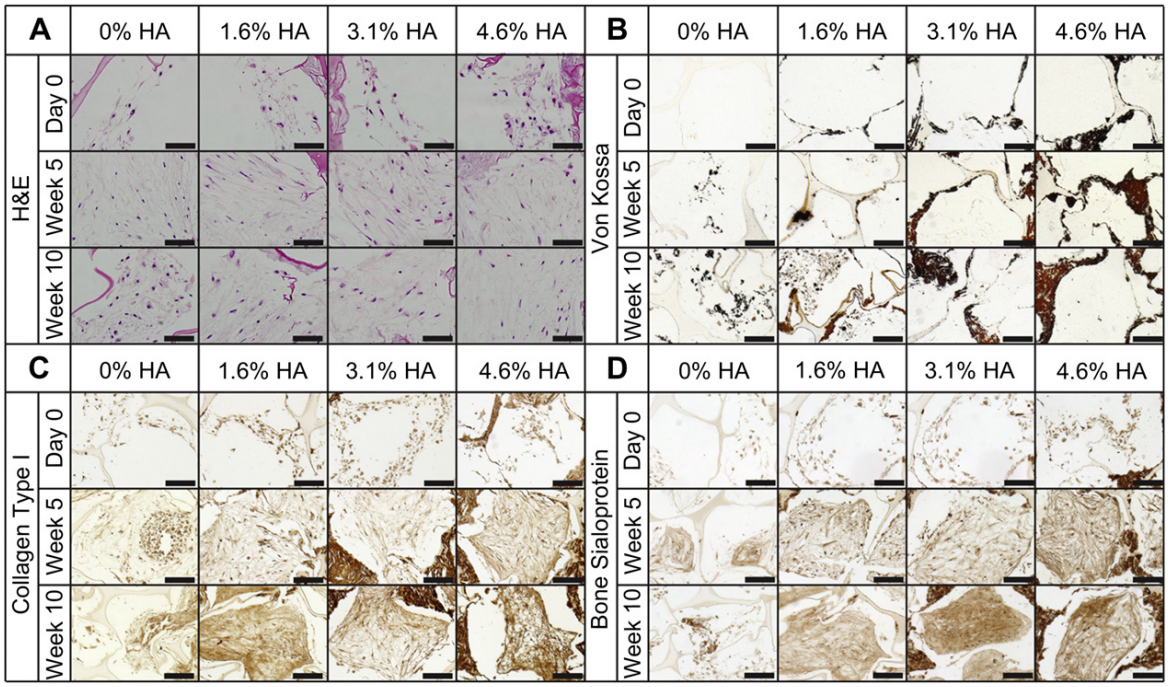

Figure V-6. Histology and immunohistochemistry of the constructs before and after cultivation: (A) H&E, (B) Von Kossa, (C) Collagen Type I, and (D) Bone sialoprotein (bar: 200 μm).

Histology and Immunohistochemistry

H&E (**Fig.V-6A**) shows increased cell content in pore spaces within the first 5 weeks of culture in accordance with DNA quantification. As seen by von Kossa staining, there was an increase in calcium content within scaffold structure as more HA was incorporated and this resulted in

thicker walls, similar to the structures seen by SEM. Over 5 and 10 weeks, the 0% and 1.6% HA exhibited a deposition of mineral in the scaffold pores while such evidence was not observed in the 3.1% and 4.6% HA. The mineral inside the pore space of 0% HA aggregated forming granular structures. Collagen type I (**Fig.V-6C**), BSP (**Fig.V-6D**), and OCN (data not shown) immunohistochemistry staining indicated an increase in bone matrix deposition over time in all group. The staining of the proteins was most intense in 3.1% and 4.6% HA at 10 weeks of culture.

DISCUSSION

Silk has shown significant promise as a biomaterial for bone tissue engineering scaffolds [189, 209, 210]. However, silk by itself is not osteogenic, and the mechanical properties of silk scaffolds are considerably lower than those of native bone (Young's moduli ~ 100 kPa vs. ~ 10 MPa for bone). In the present study, we investigated the potential of HA micro-particles to improve the osteogenic and mechanical properties of silk scaffolds, and enhance the *in vitro* formation of bone-like tissues by hMSCs without the use of osteogenic growth factors such as BMPs.

We successfully fabricated biocompatible HA-embedded silk scaffolds while maintaining pore size and interconnectivity (**Fig.V-2**). The incorporation of HA altered scaffold surface chemistry, increased surface roughness (**Fig.V-2**) and increased the stiffness of unseeded scaffolds (**Fig.V-5A**) We confirmed that HA was osteoinductive as the mineral deposition increased in a dose-dependent response to the initial amount of HA as demonstrated with μCT imaging (**Fig.V-4**). The major contribution of the HA was to guide the deposition of the newly formed bone mineral to provide significantly higher construct mechanical stiffness at the end of cultivation. Previous findings suggest that the microarchitecture (topography, orientation and connection of trabeculae), in addition to bone volume fraction, are important in governing the mechanical properties of trabecular bone [208, 211].

The compressive (Young) modulus of engineered bone constructs increased as much as 8-fold for HA scaffolds when compared to silk alone (**Fig.V-5A**), approaching that of the decellularized bovine trabecular bone measured via the same testing method. We found that 3.1% HA mineral provided sufficient bioactivity to direct hMSCs to form a trabecular-like mineral structure. Thus, the significant increase in the strength of engineered bone constructs in the present study was likely due to the combination effect of the changes in the amount of mineral (as seen from increased bone volume fractions, **Fig.V-5D**) and the improved structure (as seen from increased bone interconnectivity, **Fig.V-5E**). In contrast, an increase in the trabecular thickness of pure silk scaffolds with no concomitant change in connectivity confirmed an increase in size of spherical mineral deposits, which did not significantly improve the mechanical properties [88, 90, 136, 137]. In all cases, histological von Kossa staining confirmed the μCT data.

Calcium production by the differentiated hMSCs correlated with the amount of embedded HA in a dose dependent manner up to 3.1% HA and remained constant thereafter, which was consistent with prior reports [212-214]. With the same number of cells among the study groups, the amount of calcium deposition in the 3.1% and 4.6% HA groups was in creased by almost 4-fold as compared to the 0% HA group. However, due to the high initial values of calcium in the HA scaffolds compared to the amount of calcium produced by the cells, the increase in calcium content was steady but not statistically significant over time. Previous studies reported calcium production by hMSCs ranging from 0.25 to 8 μg/ng DNA after 5 weeks of culture in osteogenic medium supplemented with BMP-2 [90, 137, 215]. Calcium production in the present study was 0.11 μg/ng DNA over 10 weeks, a lower amount as no BMP-2 was supplemented to the cultures.

An interesting observation was that the increase in bone volume (**Fig.V-5C**) analyzed by μCT was substantially higher than the increase in calcium content (**Fig.V-5B**). It appears that since μCT employed in this study has a resolution of 21 μm and the largest HA particles observed by SEM imaging was approximately 20 μm, not mineral was detected by μCT. Therefore, the change in bone volume measured by μCT included both the initially undetected HA

microparticles that grew larger and the new mineral produced by cells. These HA microparticles therefore played a role of nucleation sites that facilitated the formation of a highly connected mineral structure. In addition to the production of mineral, the production of bone matrix proteins was also dependent on HA concentration, as seen with collagen type I and BSP (**Fig.V-6C&D**), and consistent with the effect of HA mineral on gene expression previously reported [58, 216]. The unseeded scaffolds of the 0% and 4.6% HA groups did not demonstrate changes in mineral structure, calcium content, bone matrix production or mechanical strength, indicating that these changes were cell-mediated.

It is also possible that the enhanced outcomes in the HA scaffolds may be explained in part due to the changes in the initial stiffness and surface roughness, both of which may influence cellular responses. However, initial scaffold stiffness was not significantly altered among the groups and other forms of modifying silk scaffolds have provided considerably higher initial compressive moduli but did not elicit such significant cell-mediated improvements [193]. Therefore, it is unlikely that the surface roughness of the scaffolds was the main reason for large improvement in mechanical properties, as a previous attempt to mineralize silk scaffolds through surface coating with HA did not elicit the same response [216]. By incorporating HA into the walls of the silk scaffolds, we provided the hMSCs with a more osteoinductive surface, but more crucially, the data suggests that the HA microparticles served as nucleation sites that directed mineral deposition, leading to an enhanced trabecular structure, increased connectivity and superior mechanical properties of the resulting tissue grafts. This is shown schematically in **Figure V-7**. Such a mechanism suggests that the spatial proximity of HA microparticles to each other is an important parameter and may also explain why the increase from 3.1% to 4.6% HA did not elicit a pronounced difference in the final outcome, as a certain threshold distance between neighboring particles had been attained.

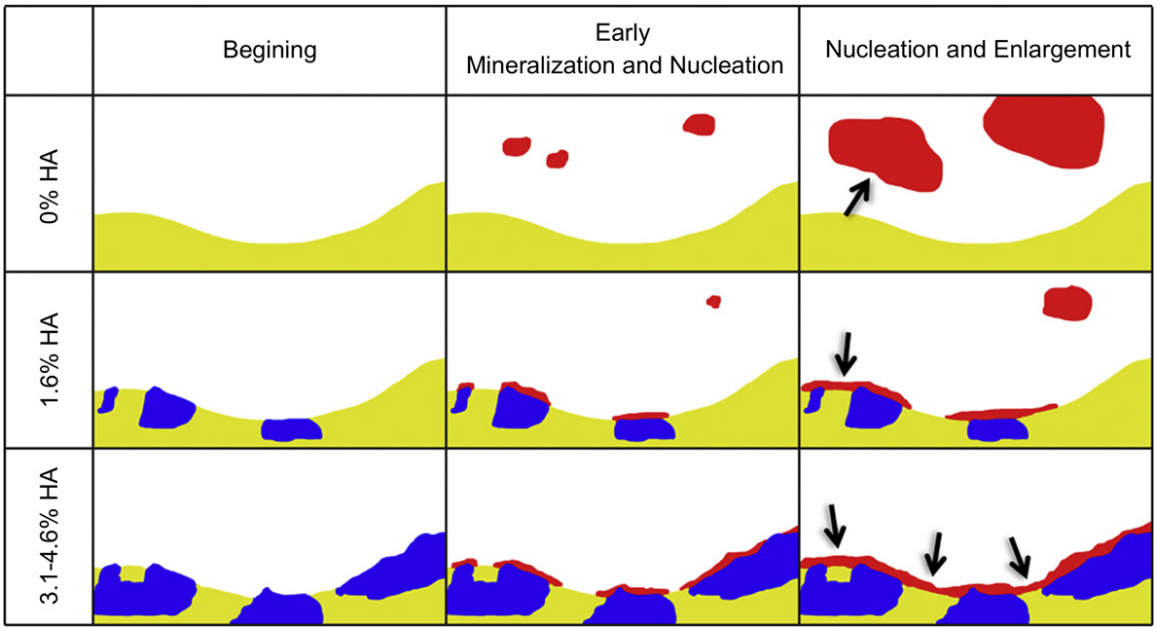

Figure V-7. Schematic of mineralization process. Yellow, blue and red regions represent silk, premineralized HA, and new mineral, respectively. Arrows indicate the connection of the new mineral structure. In 0% HA, newly produced mineral localized within the pore space and grew larger in size over time resulting in spherical-like mineral structure. In 1.6% HA, new mineral nucleated from premineralized HA as well as was deposited into the pore space. In 3.1e4.6% HA, the newly produced mineral nucleated from the premineralized HA. As the structure grew, structural connections occurred.

CONCLUSIONS

The effect of incorporating the HA mineral into porous silk scaffolds was investigated for tissue engineered bone formation with hMSCs. The HA mineral enhanced hMSCs osteogenic differentiation and provided a platform for bone-like structure formation when adequate HA content was incorporated. The HA mineral provided a platform for the formation of engineered bone by hMSCs, both through the osteoconductivity of the material and by providing nucleation sites for the newly produced mineral.

CHAPTER VI

Aim 1.2: Effect of silk sponge scaffold stiffness and surface roughness on mineral deposition and functional bone formation

INTRODUCTION

Large bony defects from either non-unions or trauma, can pose a significant problem for a patient and often require surgical intervention [217]. Current treatments rely on autografts or allografts, each of which has associated risks. Autografts require an additional surgical site, with a restricted amount of available donor tissue, and are often associated with donor site morbidity. In contrast, the issue of limited donor material is alleviated with the use of allografts, although there is a potential risk of disease transmission and possible long-term complications [186, 218]. In some cases, it has been shown that progenitor cells can be injected into the defect to aid in tissue repair. Although this approach has shown some promise, difficulty remains with immobilizing the cells at the site of bone regeneration. Therefore, tissue engineered constructs have been considered in order to sustain cells at the implant site and to act as conduits for growth factor, antibiotic, or therapeutic drug release [186].

There are several biological requirements that must be met for a successful tissue engineered graft device. Specifically for bone tissue, the device should be (i) biocompatible, (ii) osteoconductive, (iii) osteoinductive to attract progenitor cells in order to aid in regeneration, (iv) osteogenic to ensure osteoid deposition, and ultimately (v) osteointegrative. Additionally, material characteristics of scaffolding that msut be considered include surface roughness, mechanical integrity, and porosity [186]. Many polymeric materials, both natural and synthetic, have been studied for use as bone scaffolding substrates, including collagen, hyaluronic acid, chitosan, poly(L-lactide-co-glycolide) (PLGA), polymethylmethacrylate (PMMA), polycaprolactone (PCL), as well as several ceramic materials such as calcium phosphate, calcium

sulfate, and bioactive glass [219-222]. However, the search for a perfect bone scaffold that fulfills all biological criteria still continues. In addition to biological factors, an ideal bone tissue scaffold should also satisfy several physical requirements. For instance, a mismatch between the biomechanics of the orthopedic biomaterial and the native tissue can also be a source of failure [223]. Often in literature, the biomaterial scaffolding is too compliant to simulate native bone. For example, direct implementation of collagen for bone tissue engineering has been limited due to the relatively weak mechanical characteristics with respect to the native bone [224, 225]. Scaffolds made of collagen-based demineralized bone matrix (DBM) reportedly had a wet compressive modulus of 4.1 kPa [226]. This value increased to 31 kPa by cross-linking the DBM with heparin. Despite the significant improvement in rigidity, these values are still too low in comparison with native bone tissue [227].

To improve the mechanical properties and osteoinductive potential of bone scaffold materials, the use of composites has been explored. In many cases, a polymer matrix is augmented by the inclusion of a ceramic material such as hydroxyapatite (HAP), tricalcium phosphate, or bioactive glass [228-231]. For example, by synthesis of PLGA microspheres in the presence of amorphous calcium phosphate followed by sintering produces a porous scaffold with interconnected structures that contains mechanical properties within the range of the trabecular bone in the dry state [229]. However, the dependence of the mechanical properties of these materials in the hydrated state has not been reported. In another study, dispersing nano-hydroxyapatite (nHAP) throughout silicone rubber provided a more favorable matrix for cell attachment, viability, and proliferation of murine preosteoblasts as compared to the pure silicone rubber [231]. In these cases, a polymer matrix was mixed with a ceramic filler. This is in contrast to the present study where we reinforce a silk fibroin matrix with a silk fibroin microparticle filler to create a protein–protein composite. By controlling the interfacial bond between the two phases, we can improve the mechanical performance through interfacial stability.

Bombyx mori (silkworm) silk fibroin's desirable properties make it a potent alternative to many other biodegradable biopolymers for bone tissue engineering. Silk fibroin possesses a **β**-sheet (crystalline)-rich structure that provides superior physical characteristics, such as stiffness and toughness to most natural and synthetic polymers. For example, individual fibroin filaments have an ultimate tensile strength (UTS) between 610 and 690 MPa and a modulus between 15 and 17 GPa. In contrast, the UTS for rat tail type I collagen and polylactic acid (PLA) range between 0.9 and 7.4 MPa and 28 and 50 MPa, respectively. The moduli for these materials are 1.8-46 MPa, for collagen, and 1.2–3.0 GPa for PLA [232]. In addition to the mechanical properties, silk fibroin has favorable biological characteristics, such as excellent biocompatibility with low inflammatory and immunogenic response. As a consequence, silk has been used as a suture material for centuries and is an FDA approved biomaterial. Moreover, due to its amphiphilic nature, silk fibroin can easily be processed into fibers, hydrogels, thin films, sponges, and composite materials, with degradation rates that can be tuned from days to years. Additionally, silk can be produced in large quantities and at reasonable costs due to the commodity textile business. Due to the above properties and the ability to be processed into a range of material formats, silk is an excellent candidate material for bone tissue applications.

The goal of the present work was to investigate the effect of silk sponge stiffness and surface roughness on *in vitro* engineered bone development. Previously, no increase in either material strength or stiffness was observed after depositing hydroxyapatite (HAP) on the surface of preformed silk scaffolds, despite enhanced bone-specific development [216]. A recent study has shown that silk sponges can be reinforced by loading the matrix phase with different concentrations of silk microparticles in order to address these strength limitations [233]. Here, we intend to exploit the impressive mechanical properties of these silk–silk composite materials. By adding silk microparticles to the matrix of a silk sponge, both the surface roughness and mechanical properties can be enhanced. We systematically investigated the effect oftwo modifications of silk scaffolds on human stem cell differentiation and the development of

engineered bone. The modifications were as follows: (*i*) an increase in scaffold stiffness by alteration of total silk fibroin concentration (resulting in a smooth, single phase porous scaffold) and (*ii*) reinforcement by embedding silk microparticles (resulting in two-phase porous scaffolds with strong interfacial compatibility and surface roughness). Direct effect of scaffold surface roughness was investigated by adjusting the two silk modifications to exhibit similar stiffness.

Table VI: Composition and mechanical properties of the four types of scaffolds: material compositions and equilibrium compressive moduli. (^significant difference within SS and PS group; *significant difference from their respective SS groups)

Scaffolds	Concentration of silk fibroin (g/ml)	Concentration of silk micro particles (g/ml)	Equilibrium compressive modulus (kPa)
16-0 (SS)	0.16	0	61±37
32-0 (SS)	0.32	0	519±158^
16-16 (PS)	0.16	0.16	402±101*
32-16 (PS)	0.32	0.16	900±211^*

MATERIALS AND METHODS

Fabrication of porous silk scaffolds with embedded silk microparticles

Hexafluoro isopropanol (HFIP)-silk solution was fabricated from cocoons of *Bombyx mori* as previously described [234]. One ml of silk solution (16 or 32 w/v%) was added into the glass container containing 3.4 g granular NaCl (particle size; 500-600 μm) with or without silk particles (3.1 ± 1.84 μm, 16 w/v%), centrifuged, and dried at room temperature. After 2 days of MeOH treatment, the NaCl porogens were extracted to produce cylindrical microparticle-

embedded silk sponges (12 mm in diameter). Two types of silk sponges (SS group: 16-0 and 32-0) and two types of micro-particles-embedded silk sponges (PS group: 16-16 and 32-16) were fabricated (**Table VI**). Scaffolds were cut and cored into cylinders 4 mm diameter x 4 mm thick.

Scanning electron microscopy

SEM was performed to determine pore structure and surface topography on two scaffolds of 32-0 and 16-16 samples. In brief, scaffolds were washed in PBS and then fixed in 2% glutaraldehyde in PBS overnight. Constructs were washed in buffer and freeze-dried overnight in a lyophilizer. Before imaging, samples were coated with gold and palladium and used for SEM.

Compressive mechanical testing

The equilibrium compressive Young's modulus (n=4 per group) was determined at day 0, and at week 5 under unconfined compression in wet conditions using a modification of an established protocol [103]. An initial tare load of 0.2 N was applied and was followed by a stress-relaxation step where specimens were compressed at a ramp velocity of 1% per second up to 10% strain and maintained at the position for 1800 s. The Young's modulus was obtained from the equilibrium forces measured at 10% strain.

Human mesenchymal stem cell cultivation and seeding

Fresh bone marrow aspirates were obtained from Cambrex Life Sciences (East Rutherford, NJ), isolated and characterized as previously described [78]. Cells were expanded in high-glucose DMEM supplemented with 10% FBS, 1% pen-strep, and 0.1 ng/mL bFGF. The hMSCs were cultured up to the third passage and then used for seeding the scaffolds. The seeding process was previously described [87, 137]. In brief, scaffolds were seeded at the concentration of 30×10^6 cells per 1 ml of scaffold. A 40-μl aliquot of cell suspension was pipetted onto blot-dried scaffolds and allowed to percolate through. The scaffolds were flipped 180° every 20 minutes

and 10 μl of media was added to prevent the cells from drying out. Constructs were cultured with osteogenic medium (low-glucose DMEM supplemented with 10% FBS, 10 nM dexamethasone, 10 mM sodium-β-glycerophosphate, and 0.05 mM ascorbic acid-2-phosphate) for 3 days before insertion into the bioreactor.

Bioreactor cultivation

A perfusion bioreactor developed in our laboratory, as described and used previously [87, 204], was employed in this study. In brief, 6 scaffolds were placed in each bioreactor and medium flow rate was set to provide the superficial velocity of medium through the scaffolds at 400 μm/s. Half of the medium volume was replaced twice a week and scaffolds were harvested for analysis at week 5.

DNA quantitation

Constructs were cut in half in the longitudinal direction, washed in PBS and the wet weights were determined. For DNA analysis, the samples (n=8) were stored at -20°C in 1 ml of digestion buffer (10 mM Tris, 1mM EDTA and 0.1% Triton X-100) with 0.1 mg/ml of proteinase K in micro-centrifuge tubes. Samples were then thawed and maintained in this solution overnight at 56°C to extract the DNA. The DNA content was determined using a Picogreen assay (Molecular Probes, OR).

Histology and immunohistochemistry

Constructs were washed in PBS, fixed in 10% formalin, embedded in paraffin, sectioned into 4 μm slices and stained with haematoxylin and eosin (H&E), and Von Kossa. Immunohistochemistry staining for bone sialoprotein (BSP) was also conducted as previously described [87].

Statistical analysis

Multiway Analysis of Variance (ANOVA) to analyze groups at the same time point and within group at different time points was carried out followed by Tukey's *post hoc* analysis using STATISTICA software, with $p<0.05$ being considered as significant.

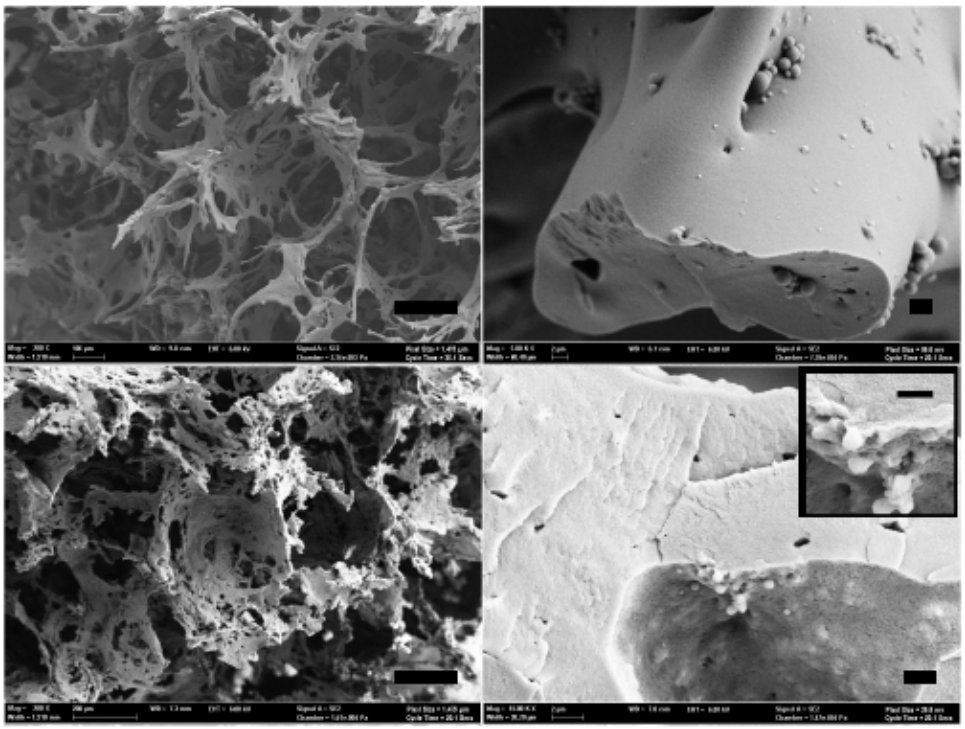

Figure VI-1: Scanning electron microscopy of the silk sponge (A and B) and microparticle-embeded silk sponge (C and D). Low magnification (A and C) shows the scaffold with similarly high porosity (Bar = 200 μm). High magnification (B and D) demonstrates the difference in the scaffold topography between the two groups (Bar =2 μm). The incorporation of silk microparticles (D and inset) increased surface roughness as compared to the silk sponge without microparticles (B).

RESULTS

Scanning electron microscopy

Low magnification SEM indicated similarity in scaffold porosity and pore structure between SS and PS groups (**Fig.VI-1 A and C**). Greater detail of scaffold surface property was detected at

high magnification. The scaffold surface of SS was smooth while the surface of PS was much rougher (**Fig.VI-1 B and D**). SEM also showed incorporation of microparticles in silk scaffold (**Fig.VI-1 D inlet**)

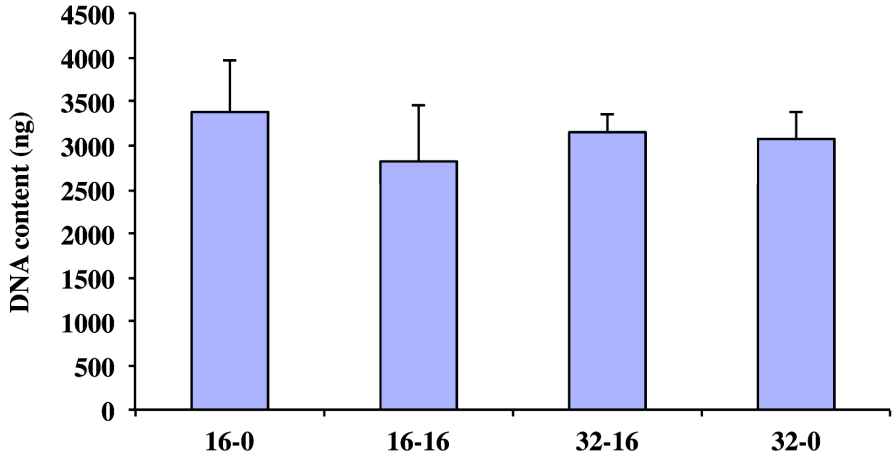

Figure VI-2: DNA contents after 5 weeks of cultivation for 16-0, 16-16, 32-16, and 32-0. Groups were not significantly different (3392±581, 2819±634, 3139±216, and 3072±309 ng per scaffold, respectively).

Scaffold mechanical property

Increasing silk fibroin concentration from 16 to 32 w/v % significantly increased the equilibrium compressive modulus (16-0 vs. 32-0 and 16-16 vs. 32-16, **Table VI-1**). Embedding silk microparticles into silk sponges also resulted in a significantly higher equilibrium compressive modulus compared to their respective SS group (16-0 vs. 16-16 and 32-0 vs. 32-16, **Table 1**).

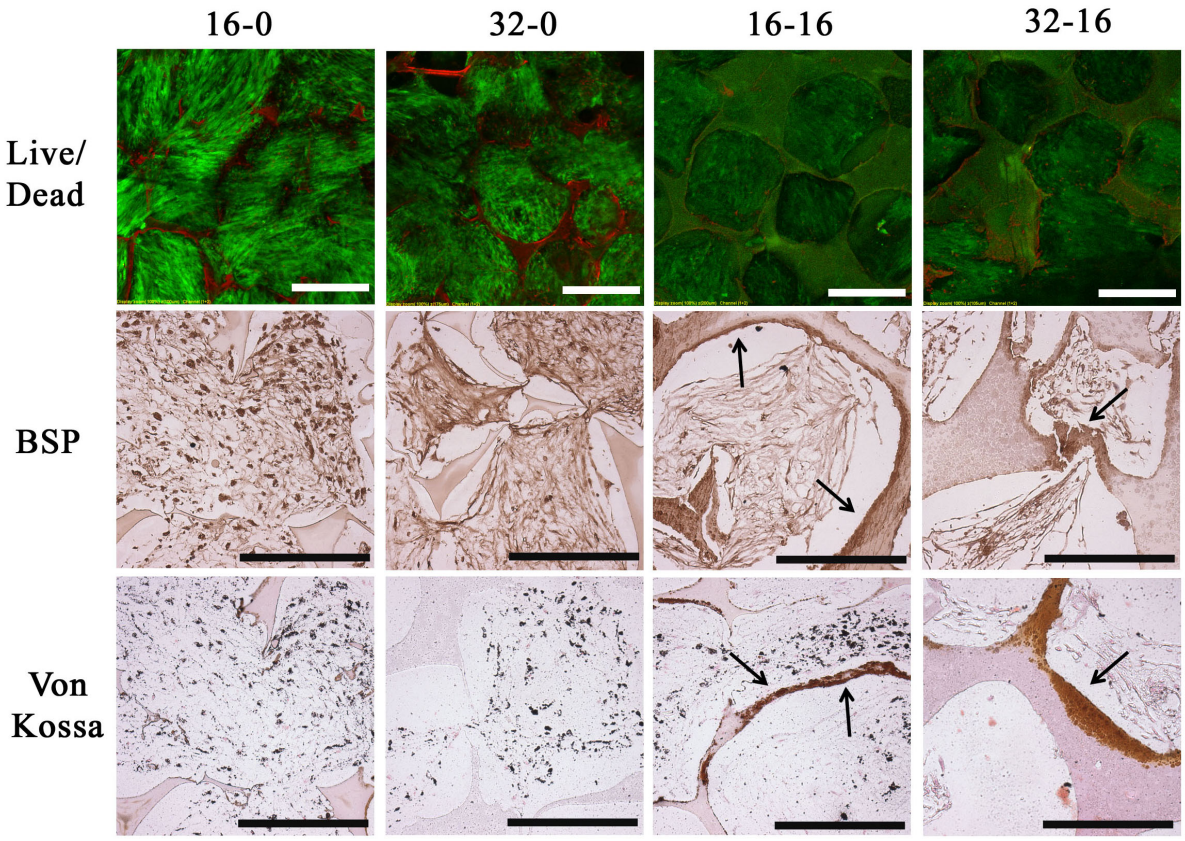

Figure VI-3: Histomorphology of engineered human bone. Live/Dead confocal microscopy (top row), BSP (middle row), and Von Kossa staining (bottom row) of the four types of silk scaffolds after 5 weeks of cultivation. Arrow indicates matrix deposition at the internal scaffold surfaces. Scale bar: 400 μm.

Tissue engineered bone construct

After 5 weeks of culture, the DNA contents were similar in all study groups (**Fig.VI-2**). Live/dead assay displayed good cell viability in all four groups of scaffolds (**Fig.VI-3**). Histological analysis revealed that there were more cells at the periphery than in the central regions of the scaffolds. BSP (**Fig.VI-3**) were expressed in all four groups. In addition, calcium deposition detected by Von Kossa staining was observed for all groups (**Fig.VI-3**). Under high magnification, PS groups showed mineralization (Von Kossa) and matrix deposition (BSP) along the scaffold surface while no such evidence occurred in SS groups (**Fig.VI-3, arrow**). The increases in equilibrium Young's modulus in the two PS groups were significantly higher than

their respective SS groups (**Fig.VI-4**). By comparing the effect of initial scaffold stiffness (16-0 vs. 32-0 and 16-16 vs. 32-16), the Young's modulus increased significantly (**Fig.VI-4 blue box**). In addition, when comparing on the effect of surface roughness (32-0 vs 16-16 groups), the Young's modulus of the 16-16 group increased significantly more than the 32-0 group (**Fig.VI-4 yellow box**)

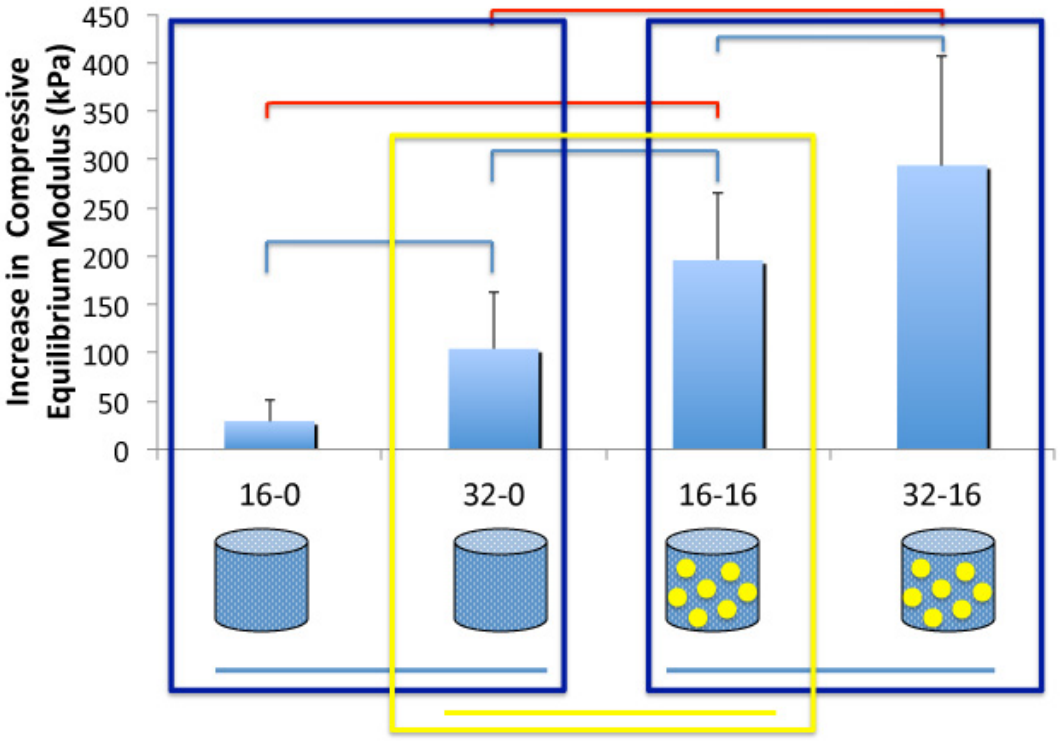

Figure VI-4: Increase in compressive equilibrium modulus after 5 weeks of cultivation. Blue and yellow box illustrates comparison on the effect of stiffness and roughness, respectively. Red and blue line indicates significant differences ($p<0.05$ and $p<0.1$, respectively).

DISCUSSION

In the present study, silk microparticles were incorporated into the silk matrix during processing to create a protein–protein composite. The ability to optimize the interfacial contact between the matrix and filler phases is critical to maximize the mechanical properties of a composite. For

example, if the reinforcing agent has superior mechanical properties but the interface between the filler and the matrix is weak, the composite will fail along the interface. Therefore, strong interfacial binding is essential to facilitate transfer of the mechanical load from the matrix to the reinforcing agent and vice versa [235].

In the present study, silk microparticles were incorporated into the silk matrix during solution processing. The inclusion of particles into silk solution with low silk concentration (16-0) and high silk concentration (32-0) increases equilibrium compressive modulus by approximately 6.6 and 1.7 folds, respectively, (**Table VI-1**). The inclusion of particles allowed the constructs to approach the native trabecular bone (~10 MPa) [234] while maintaining scaffold structure and porosity (**Fig.VI-1**). These results suggest that an effective load transfer was achieved between the silk fibroin sponge matrix and the silk fibroin microparticle reinforcement, presumably due to the strong interfacial contact produced through solution processing.

The study was designed to independently investigate the effects of *scaffold stiffness* (by comparison within the SS groups or within PS groups), and *scaffold roughness* (by comparison between the corresponding PS and SS groups). The changes in scaffold stiffness and surface roughness did not alter proliferative capabilities of the hMSCs (**Fig.VI-2**). Over 5 weeks of culture, hMSCs remained viable inside the scaffolds and differentiated into bone forming cells (**Fig.VI-3**). According to the histology and immunohistochemical staining, no significant differences were detected due to the initial stiffness on hMSC proliferation and differentiation amongst the different scaffolds (**Fig.VI-3**). However, live/dead analysis (**Fig.VI-3**) showed more cells were present on the scaffold surface of PS groups. The difference in concentration indicates better cell attachment and proliferation due to the surface roughness. The cell differentiation led to the deposition of BSP and mineral on the surface of the microparticle-embeded scaffolds (**Fig.VI-3**). On the other hand, BSP and mineral deposition on silk scaffolds without microparticles occurred only within the pore space. This trends was consistent with that suggested by many other studies [136, 137, 216]. With the localization of BSP and mineral

deposition, the mechanical property of the tissue-engineered constructs was enhanced. The compressive mechanical properties of the PS scaffolds significantly increased after culture when compared to their respective SS group (**Fig.VI-4 red line**). Furthermore, the mechanical property increased due to both the effect of initial stiffness and surface roughness (**Fig.VI-4 blue and yellow box**).

It is not surprising that increasing the rigidity of the scaffold enhanced the differentiation of hMSCs into osteoblasts as defined by mineral deposition. Mechanical forces are known to be vital for wound healing and tissue homeostasis in adult organisms [236]. Matrix stiffening may increase cellular contractibility and matrix deposition. In addition, the role of matrix stiffness in cell motility and behavior has also been explored [237] and shown to influence differentiation. Particularly, hMSCs differentiate into an osteogenic lineage on stiffer substrates, whereas the cells appear more neurogenic on more compliant matrices [238]. While vast evidence has demonstrated the positive effect of substrate stiffness toward osteogenic differentiation and bone formation of hMSCs, the true effect of surface roughness is unknown. A previous study has suggested that surface roughness may play a role in stimulating hMSC osteogenic differentiation; however, the study was not able to decouple surface roughness from other effects such as chemical composition or scaffold stiffness [193]. This study successfully investigated the true effect of surface roughness in a silk sponge scaffold system. Results of the study show that surface roughness enhanced bone matrix deposition onto the scaffold surface, which resulted in enhancement of tissue engineered bone function.

CHAPTER VII

Aim 1.3: Effect of Bone Sialoprotein on Cell-Mediated Collagen Mineralization

INTRODUCTION

Until recently, the process in which mineral crystals nucleation on non-collagenous proteins (NCP) bind to the collagen fibrils was believed to be the dominating mechanism for bone mineralization. New discoveries have proposed a detailed mechanism of mineralization of collagen fibrils [167, 168]. The studies showed that calcium-based biominerals could be formed via stable pre-nucleation clusters [239] with aggregation into an amorphous calcium phosphate (ACP) and subsequently, transformation of this phase into a crystal [240]. These findings suggested that collagen is an active scaffold for the formation of oriented hydroxyapatite platelets, with domains of charged amino acids in both the gap zone and the overlap zone acting as nucleation sites for crystalline hydroxyapatite. Interestingly, the mineralization of collagen fibrils in these studies contains no NCPs to initiate mineral formation. Instead, hydroxyapatite crystallization inhibitors, polyaspartic acid or fetuin, were employed to mimic the polyanionic character of the NCPs [165, 166].

Bone sialoprotein (BSP) is one of the most important NCPs involved in bone mineralization. BSP is expressed nearly exclusively in mineralizing tissue [148]. The findings suggested that the BSP-mineral complex acts as a carrier for mineralizing collagen fibril. It can specifically bind to collagen via a 20 AA long domain. Furthermore, BSP can bind hydroxyapatite through two glutamic acid-rich regions, which are both required for its functional activity as a nucleator of hydroxyapatite [149]. In addition, it has been demonstrated that after treatment with organophosphate for 4-8 h, BSP localizes to the ECM in osteoblastic cultures, well before the first appearance of apatite crystals [51,58]. This suggests that inorganic phosphate triggers BSP

secretion into the ECM, where it can subsequently nucleate calcium phosphate in metastable solutions. In contrast, opposing findings suggested that bone sialoprotein is associated with a population of vesicle-like structures, defined as crystal ghosts, which are 500 – 800 nm in size prior to infiltration into collagen fibrils [145]. It is unknown as which of these mechanisms is dominant under cell-mediated collagen mineralization.

Collagen mineralization by cells is a complex process. Cells must (i) produce collagen matrix, the platform for mineralized tissue, (ii) introduce metastable conditions of calcium and phosphate ions by releasing calcium and alkaline phosphatase to cleave organic phosphate molecules, and (iii) express and release NCPs such as BSP which play important roles in initiating mineral nucleation. However, the specific role of BSP in cell-mediated collagen mineralization is unclear. This study employed tissue-engineering techniques to study the effects of initial BSP in its native state on collagen mineralization by osteogenic progeny of human mesenchymal stem cells (hMSC).

If the mechanism in which BSP binds to collagen fibrils prior to mineral nucleation is dominant, the pre-existing BSP in collagen matrix will enhance collagen mineralization by nucleating more minerals. However, if BSP binds to calcium phosphate ions prior to collagen infiltration, the pre-existing BSP may not have any effect on collagen mineralization or could even inhibit the process by reducing the binding affinity of infiltrating BSP-mineral complex. We hypothesized that the presence of native BSP in bone collagen matrix would not enhance collagen mineralization, but rather inhibit MSC-mediated mineralization. The study employed the processing of bone matrix to preserve or remove BSP from native bone collagen matrix.

Demineralized bone matrix (DBM) is a common clinically used bone graft due to its superior osteoinductivity and osteoconductivity. The process of bone demineralization removes cellular materials and mineral but preserves collagens and some NCP of the native bone structure, including BSP. Bone processing techniques to isolate BSP have been previously developed.

Cellular and other protein components not bound to the mineral phase can be extracted using 4M guanidine hydrochloride (GuHCl), prior to demineralization with 0.5 M EDTA [241, 242]. This process was applied on a variety of mineralized vertebrate tissues to isolate a number of other mineral-related phosphorylated NCPs [241, 243, 244]. A second dissociative extraction, after demineralization, was added to the protocol to remove tightly bound mineral-protected BSP molecules from the structural collagen matrix [242]. As a result, the native bone collagen matrix without BSP and other NCPs can be generated for the study.

METHODS

Scaffold preparation

The process for scaffold preparation is illustrated previously (**Ill.VII-1**). Briefly, trabecular bone plugs (4 mm in diameter) were cored from the subchondral region of calf carpometacarpal joints. All solutions contained proteinase inhibitors consisting of 100 mM 6-amino-n-hexanoic acid, 5 mM benzanidine hydrochloride, 5 mM N-ethylmaleimide, and 1 mM phenylmethane sulphonyl fluoride, in order to preserve protein function. Plugs were washed in water to remove marrow and rinsed in PBS with 0.1% ethylenediaminotetraacetic acid (EDTA) for 1 h at room temperature. This was followed by sequential washes in hypotonic buffer (10 mM Tris, 0.1% EDTA, pH 8.0), decellularizing solution (10 mM Tris, 0.1% EDTA, 0.5% Triton-X-100, 200 rpm for 3 days). Decellularized bone plugs were rinsed in PBS, freeze-dried, and ground to yield cylinders of 4 mm in diameter and 2 mm thickness. Scaffolds of density between 0.29 to 0.42 mg/μl were selected for the study. The scaffolds were washed in 2:1 chloroform:methanol (100 mg scaffolds per ml solution) for 1 hr to remove additional fat and allowed to air dry overnight. All subsequent washes were conducted at 4°C. The scaffolds were washed in 4 M guanidine hydrochloride (GuHCl), and 50 mM Tris-HCl (20 mg scaffolds per ml solution) for 24 hours with one solution change. The scaffolds were washed twice in PBS, prior to demineralization in 0.5 M EDTA in 50mM Tris-HCL (20 mg scaffolds per ml solution) for 36 hours with one

solution change at 24 hours. Following demineralization, the scaffolds were washed in PBS twice and split into two groups: (i) BSP+ and (ii) BSP-. For BSP+ scaffolds, PBS was used to sequentially wash the scaffolds. BSP- scaffolds were sequentially washed with strong detergent (4 M GuHCl, 50 mM Tris-HCl, 20 mg scaffolds per ml) to also remove BSP from the matrix, and washed with PBS twice. The scaffolds were sterilized in 70% ethanol for 2 days prior to cell seeding.

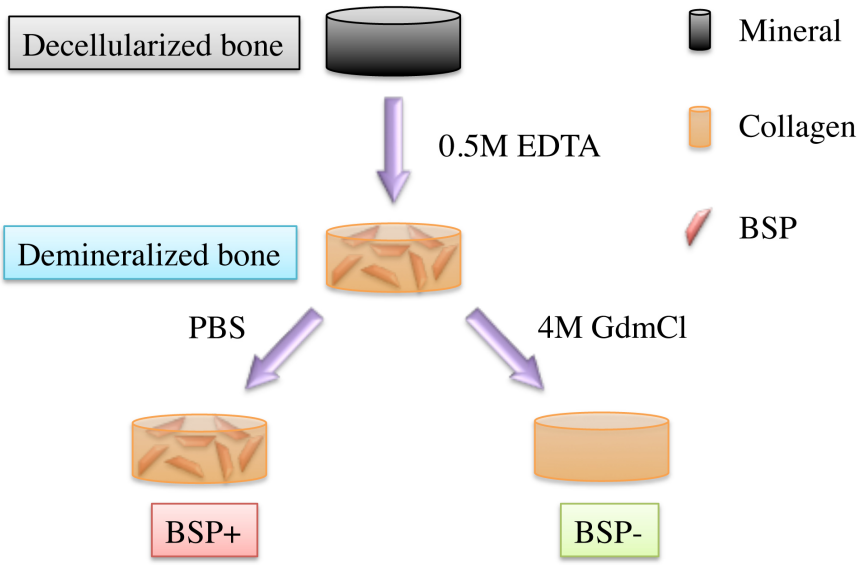

Figure VII-1 Scaffolds fabrication process.

Human mesenchymal stem cell culture and seeding

Fresh bone marrow aspirates were obtained from Cambrex Life Sciences (East Rutherford, NJ). The cells were isolated and characterized as previously described [78]. Cells were expanded in high glucose DMEM supplemented with 10% FBS, 1% penicillin-streptomycin, and 0.1 ng/mL bFGF. Scaffolds were seeded with 7.5×10^5 passage 4 hMSC each (30×10^6 cells per ml tissue volume). Briefly, a 20 µl volume of cell suspension was added onto dry scaffolds and allowed to percolate through. The scaffolds were flipped every 20 minutes, and 5 µl of media was added each time to prevent the cells from drying. The seeded constructs were cultured in osteogenic media (low glucose DMEM supplemented with 10% FBS, 10 nM dexamethasone, 10 mM

sodium-β-glycerophosphate, 0.05 mM ascorbic acid-2-phosphate) for up to 5 weeks. Scaffolds (*n*=15) from each group were harvested at day 1 (D1), week 1 (W1), 3 (W3), and 5 (W5).

Mechanical testing

The equilibrium compressive Young's modulus (n=4 per group) was measured under unconfined compression using a modification of an established protocol [103]. An initial tare load of 5 g was applied, followed by a stress-relaxation step in which specimens were compressed at a ramp velocity of 1% per second up to 10% strain and then maintained for 1800 s. The Young's modulus was obtained from the equilibrium force measured at 10% strain. Mechanical properties of decellularized trabecular bovine bones were also measured with the same method.

Biochemical assays

Calcium quantitation was conducted on samples after mechanical testing (*n*=4), which were rapidly frozen in liquid nitrogen and stored at -20°C. Calcium was extracted in 500 µl of 5% TCA solution using a bead beater and analyzed with the Calcium (CPC) Liquicolor® kit (Stanbio Laboratory, USA). For DNA and alkaline phosphatase (ALP) quantitations (*n*=4), constructs were cut in half longitudinally, washed in PBS, and the wet weights were determined. For DNA analysis, the samples were stored at -20°C in 1 ml of digestion buffer (10 mM Tris, 1mM EDTA, 0.1% Triton X-100) with 0.1 mg/ml proteinase K in microcentrifuge tubes. Samples were then thawed and maintained in this solution overnight at 56°C to extract the DNA. The DNA content was determined using the PicoGreen assay (Molecular Probes, OR). For ALP content analysis (*n*=4 halves), constructs were rapidly frozen in liquid nitrogen and stored at -20°C. The ALP quantitation was conducted using the Sensolyte® pNPP Alkaline Phosphatase Assay Kit (Anaspec, CA).

Gene Expression

Samples from each group at each time point (n=4) were analyzed for Runx2, Col1a, BSP, OPN, and ON gene expression with quantitative PCR. Each gene was normalized by a housekeeping gene, GAPDH, and then normalized relative to BSP+ day 1 samples.

Histology and Immunohistochemistry

Constructs were washed in PBS and fixed in 10% formalin, then embedded in paraffin and sectioned into 8 μm slices, before staining with Alizarin Red S and Von Kossa to detect mineralized matrix.

Statistical Analysis

Multiway Analysis of Variance (ANOVA) was used to analyze groups at the same time point and within groups at different time points, followed by Tukey's *post-hoc* analysis using STATISTICA software, with α=0.05.

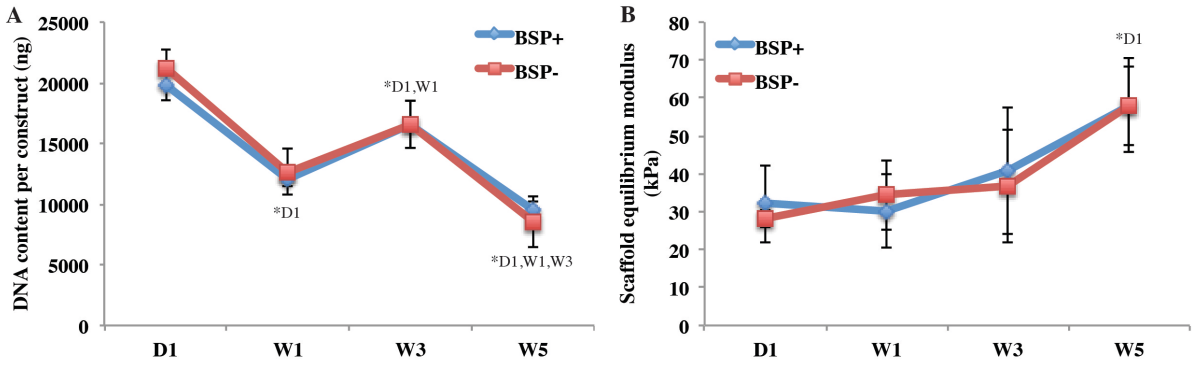

Figure VII-2: (A) DNA content per construct and (B) Scaffold equilibrium modulus for BSP+ and BSP- after cultivation for 1 day (D1), 1 week (W1), 3 weeks (W3), and 5 weeks (W5). *significantly different from the indicated time point ($p<0.05$)

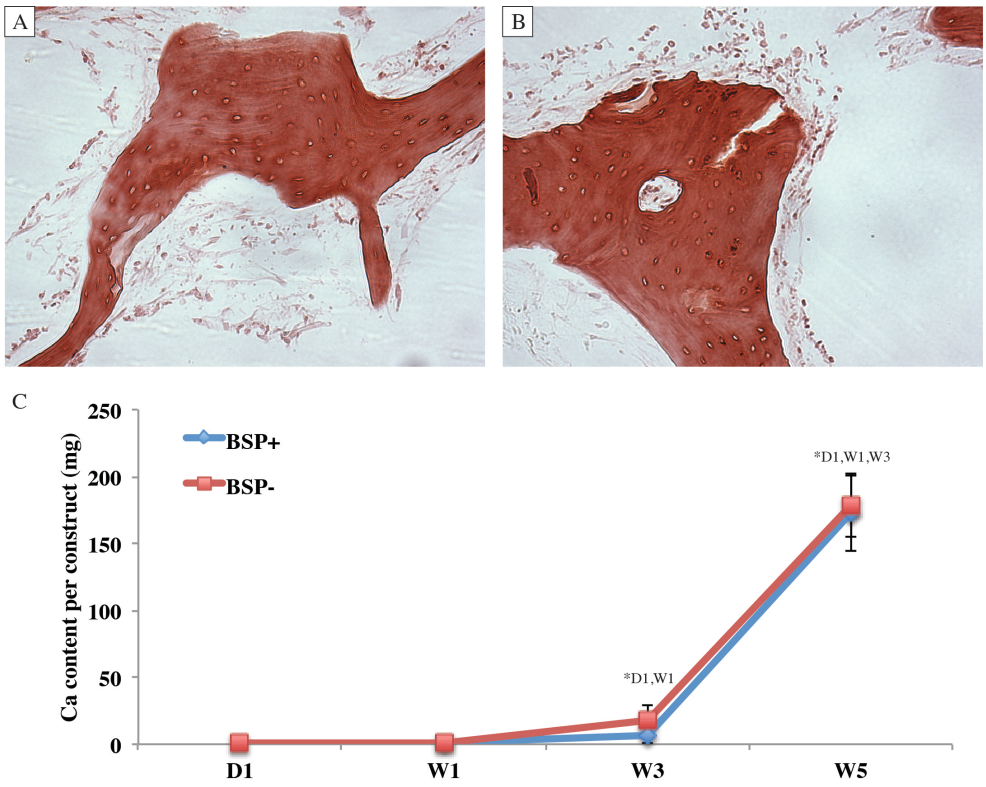

Figure VII-3: Alizarin Red staining of calcium deposition on (A) BSP+ and (B) BSP- at 5 weeks of cultivation. (C) Calcium quantitation which corresponding to the Alizarin Red stain. There are no statistically significant differences between BSP+ and BSP- at all time point. *significantly different from the indicated time point ($p<0.05$).

RESULTS

Scaffold fabrication and tissue engineered bone property

Demineralization removed mineral leaving behind protein approximately 30% of the decellularized bone dried weight. The demineralization process with EDTA maintained the original trabecular bone architecture. In addition, sequential washes with PBS or GuHCl did not alter the scaffold seeding efficiency [**Fig.VII-2A]** or mechanical properties [**Fig.VII-2B**]. The cell seeding efficiencies on BSP+ and BSP- matrix were not significantly different at 61.9±4.7% and 66.0±3.3%, respectively. hMSC-seeded BSP+ and BSP- scaffolds were cultured statically in osteogenic media for up to 5 weeks. Both DNA quantification and Young's moduli measurement

showed no significant differences in DNA content between the groups at all time points (data not shown).

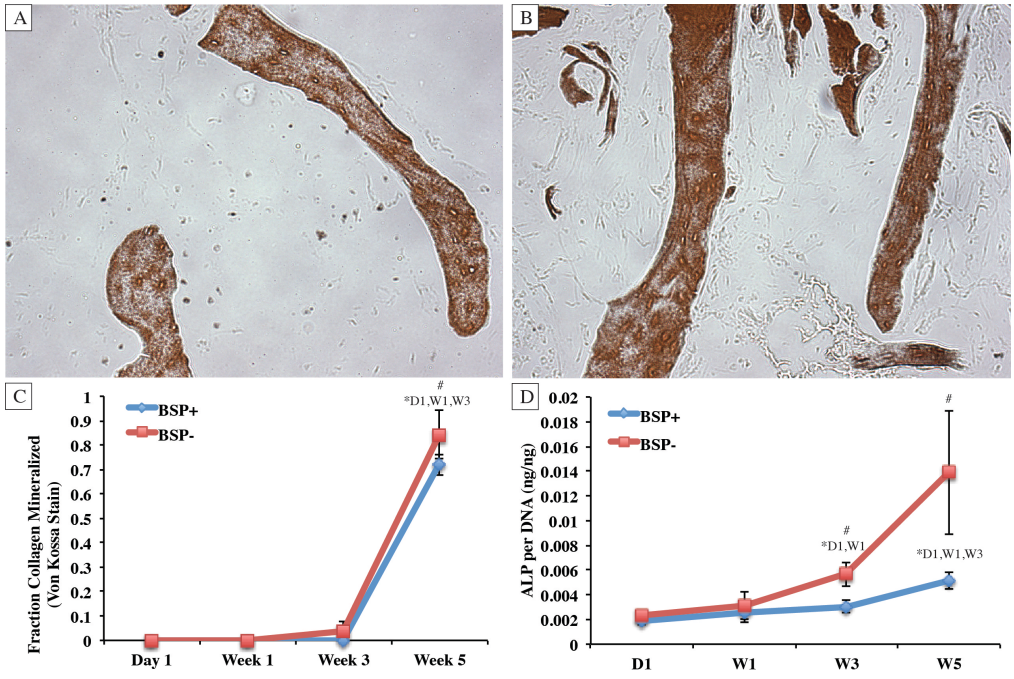

Figure VII-4: Von Kossa staining of phosphate deposition on (A) BSP+ and (B) BSP-. The images selected were the most representative of the average fraction of mineralized collagen within the group (72.1% and 85.7% for BSP+ and BSP-, respectively). (C) Fraction of mineralized collagen obtained from image analysis of Von Kossa staining. (D) ALP per DNA for BSP+ and BSP- at different time points. #significantly different between BSP+ and BSP- (p<0.05). *significantly different from the indicated time point (p<0.05).

Mineralization of collagen matrix

Alizarin Red showed no calcium deposition at day 1 and week 1 and minimal calcium deposition inside collagen fibrils at 3 weeks of culture. Calcium fully occupied collagen fibrils at 5 weeks for both BSP+ and BSP- scaffolds [**Fig.VII-3A,B**]. Calcium quantitation [**Fig.VII-3E**] corresponded with the Alizarin Red stain. Calcium content at Day 1, Weeks 1, 3 and 5 were 1.1±1.2, 1.2±0.6, 7.1±6.2, and 172.0±28.1 μg, respectively, for BSP+ and 0.4±0.3, 1.0±0.5, 18.0±11.4, and 178.6±23.7, respectively, for BSP-. The calcium content was not significantly

different between groups at each time point. Von Kossa, which stains for phosphate, another component of bone mineral, revealed particulate staining inside collagen fibrils at 3 weeks, and positive staining occupying most of the collagen fibrils at 5 weeks of culture for both groups (**Fig.VII-4A,B**). Based on both the Alizarin Red and Von Kossa stains, the proportion of mineralized collagen consisting of both calcium and phosphate was determined using image analysis. There was no mineralized collagen present after 1 day and 1 week of culture. The fraction of mineralized collagen area for BSP+ and BSP- was not significantly different (0.004±0.008% and 3.5±4.0%, respectively) at week 3, but was significantly different (71.8±4.1% and 84.3±9.8%, respectively) at week 5 (**FigVII-4C**). ALP content at week 3 and 5 was significantly higher in the BSP- group relative to the BSP+ (**Fig.VII-4D**).

Osteogenic gene expression

hMSCs differentiate into osteogenic lineage over 5 weeks of culture. Runx2 gene expression was similar between the two groups, such that expression was highest at day 1, lowest at week 1, and then gradually increased over the rest of the culture period (**Fig.VII-5A)**. Col1A1 (**Fig.VII-5B**) and SPARC (**Fig.VII-5C**) gene expression were stable throughout the culture period. Increases in SPP1 gene expression in BSP+ relative to BSP- were detected at all time points, with a significant increase in expression for BSP+ at week 1 (**Fig.VII-5D**). Interestingly, BSP gene expression (**Fig.VII-5E**) significantly increased over time for both study groups after 3 weeks of culture; further, this increase was significantly higher in BSP+ compared to BSP- (fold increase of 89±6 vs. 30±6 at week 3, 591±87 vs. 309±146 at week 5 for BSP+ vs. BSP-).

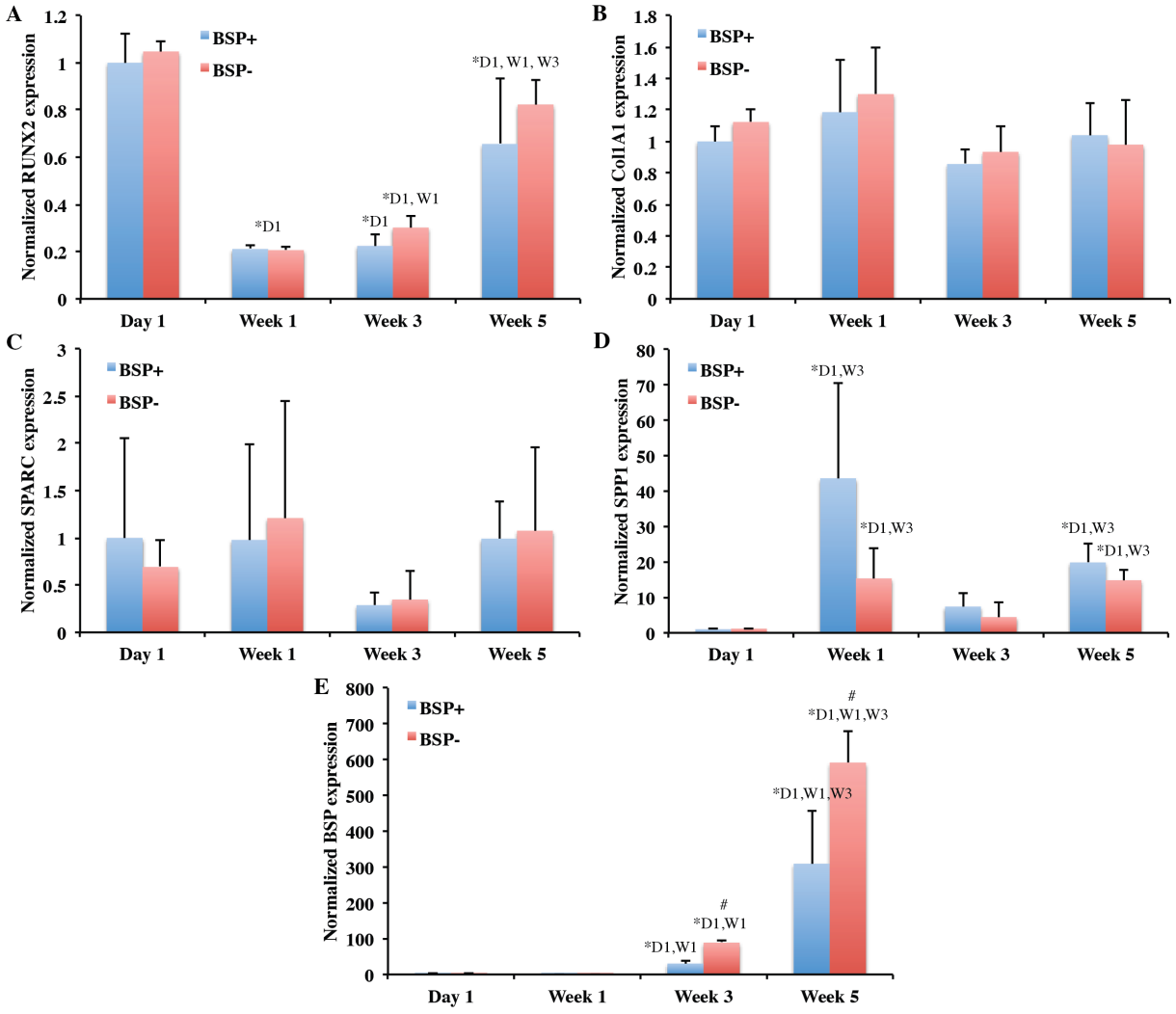

Figure VII-5: Normalized (A) Runx2, (B) Col1A1, (C) SPARC, (D) SPP1, and (E) BSP osteogenic gene expression for BSP+ and BSP- at all time points. #significantly different between BSP+ and BSP- ($p<0.05$). *significantly different from the indicated time point ($p<0.05$).

DISCUSSION

Previous theories and findings illustrated that mineralization of bone occurred by either (i) precipitation of mineral or (ii) formation of ACP infiltrating collagen fibrils. The mechanisms of the two methods were distinctively different. The precipitation of mineral crystals was suggested to be induced by NCP, which act as an origin of nucleation. NCPs adhere to collagen fibrils, followed by mineral nucleating from the collagen-bound NCPs. In contrast, ACP consisting of

NCP and calcium phosphate minerals are created prior to infiltration into collagen fibrils. Although, BSP has been shown to undergo both mechanisms, the function of BSP in mineralized bone tissues is not clear. This study employed a tissue engineering approach to study the mechanism of cell-mediated collagen mineralization in native bone protein matrix in the presence of native BSP.

Bone collagen matrix with (BSP+) and without (BSP-) native BSP was successfully produced while maintaining the original demineralized bone matrix architecture. Removing BSP from native bone protein matrix allowed the investigation of the effects of BSP and the mechanism of cell-mediated collagen mineralization in osteogenically-induced cells. Although BSP contains a classical integrin-binding motif (RGD) near the C-terminal, BSP+ did not play a significant role in hMSC attachment, as seeding efficiency was similar between BSP+ and BSP-. In addition, the presence of native BSP did not affect cell proliferation (**Fig.VII-2**).

Over 5 weeks of cultivation, hMSCs differentiated into osteogenic lineage, as indicated by RUNX2 gene expression (**Fig.VII-5A**), which exhibited an increase after 1 week of culture. The high expression at day 1 was likely due to the rapid change caused by osteogenic media induction, which stimulated the hMSCs to initiate osteogenic differentiation. The hMSCs began producing bone matrix at 3 weeks, regardless of the presence of pre-existing BSP. Calcium and phosphate deposition were detected in bone collagen matrix after 3 weeks of culture. Alizarin Red, which stains for calcium deposition, was an indication of osteoid formation, or developing bone (**Fig.VII-3**). In contrast, Von Kossa, which stains for calcified bone but not osteoid, was an indication of mature, mineralized collagenous tissue (**Fig.VII-4 A&B**). Image analysis of Von Kossa staining suggested that more mineral crystallization occurred when BSP was not initially present in the scaffold, which was counterintuitive since BSP was previously suggested to initiate mineral formation (**Fig.VII-4C**). The fraction of mineralized collagen matrix was proportional to the increase in ALP production (**Fig.VII-4D**) and BSP expression (**Fig.VII-5E**). The results suggested that osteogenically differentiated hMSCs recognized the presence of BSP

in the collagen matrix. In the absence of native BSP in the collagen matrix, hMSCs expressed more BSP and produced more ALP in order to mineralize collagen fibrils. In contrast, when BSP was initially present, the hMSCs did not initiate the process to nucleate and mineralize these pre-existing BSP. Furthermore, BSP expression and ALP production were reduced, indicating an inhibitory mechanism. Interestingly, osteopontin (SPP1) expression was increased in BSP+ at week 1 (**Fig.VII-5D**). Osteopontin has been implicated as an important factor in bone remodeling [245], and may play a role in anchoring osteoclasts to the mineral matrix of bone [246]. The results of this study suggested that the presence of BSP signal hMSCs to undergo matrix remodeling, rather than initiate mineralization. Collagen type I and SPARC expressions remained constant over the culture period (**Fig.VII-5 B&C**). The environment, with a large quantity of unmineralized collagen type I, did not require further collagen production. SPARC, an acidic cysteine-rich glycoprotein that plays a vital role in bone mineralization, cell-matrix interactions, and collagen binding, did not seem to be required in this cell-mediated collagen mineralization.

The study suggested that collagen matrix devoid of BSP was a more favorable environment for cell-mediated collagen mineralization. The presence of BSP-bound collagen matrix neither initiated nor enhanced calcium phosphate deposition, but rather inhibited the mineralization process of osteogenically differentiated hMSCs. In addition, the enhancement of collagen mineralization in collagen matrix without BSP, as well as the inability for pre-existing BSP in collagen matrix to stimulate mineral formation, suggested that the infiltration of BSP-mineral complexes was the more likely mechanism, advocating cell-mediated collagen mineralization.

CHAPTER VIII

Aim 2 Experimentation: Engineering articular cartilage using novel cell pellet compression technique

INTRODUCTION

Osteochondral tissue engineering has the potential to provide biological grafts for the repair of poorly healing or degenerated articular cartilage. Previous attempts to fabricate osteochondral grafts, consisting of articular cartilage interfaced with bone, employed clinically unfavorable primary chondrocytes [184, 185], while grafts fabricated from bone marrow stem cells lacked physiological mechanical properties [136, 137]. Though scaffold-free grafts have previously exhibited dense matrix structure, controlling graft size and shape has proven to be challenging [134, 184, 185]. Our study employed a novel technique to engineer osteochondral grafts with a scaffold-free cartilage layer, using human bone marrow-derived mesenchymal stem cells (hMSC) and decellularized bone scaffolds. With this approach, the hMSCs developed into physiologic-like articular cartilage tissue with excellent integration to subchondral bone.

METHODS

hMSC cultivation

Fresh bone marrow aspirates were obtained from Cambrex Life Sciences (East Rutherford, NJ). The hMSC were isolated and characterized, as previously described [78]. Cells were expanded in high glucose DMEM supplemented with 10% FBS, 1% penicillin-streptomycin, and 0.1 ng/mL bFGF, up to passage 4.

Decellularized bone scaffolds

Decellularized bone was obtained, as previously described [87]. Briefly, trabecular bone plugs (4 mm in diameter) were cored from the subchondral region of carpometacarpal joints of 2-4 month-old cows. The plugs were washed to remove marrow and rinsed in PBS with 0.1% ethylenediaminotetraacetic acid (EDTA) for 1 h at room temperature, followed by sequential washes in hypotonic buffer, detergent and enzymatic solution. Decellularized bone plugs were rinsed in PBS, freeze-dried, and cut to 5 mm in length, yielding cylinders of 4 mm in diameter × 5 mm in height. The weights and dimensions of each plug were measured in order to calculate scaffold density, and scaffolds within the range of 0.30-0.40 mg/cm^3 were used. Scaffolds were sterilized in 70% ethanol, washed in PBS, and incubated in expansion medium, prior to seeding cells. The distribution of bone scaffolds of different densities was randomized.

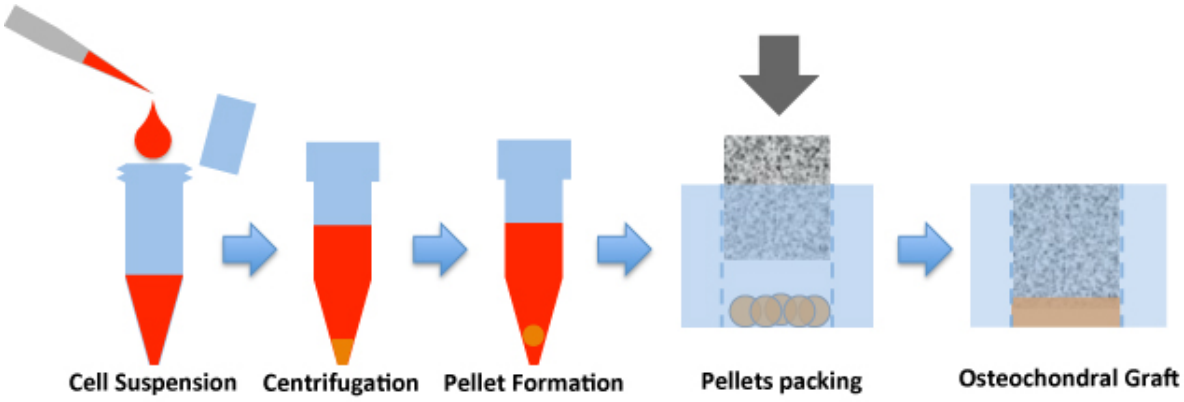

Figure VIII-1. Osteochondral construct fabrication process.

Osteochondral graft fabrication

Fig.VIII-1 illustrated the novel pellet compression technique for producing osteochondral grafts. hMSCs were centrifuged to form pellets of 5×10^5 cells and cultured in chondrogenic media (high glucose DMEM supplemented with 10 ng/ml TGF-β3, 100 nM dexamethasone, 50 mg/ml

ascorbic acid-2-phosphate, 100 mg/ml sodium pyruvate, 40 mg/ml proline, 1% insulin, transferrin, and selenous acid (ITS)+ mix and 1% pencillin-streptomycin). Osteochondral constructs were fabricated using cell pellets pre-cultured for 3, 5, and 7 days. Decellularized trabecular bone cores (4 mm in diameter × 4 mm thickness), processed as previously described [134], were inserted into sterile PDMS rings (4 mm diameter × 4.5 mm thickness) containing 8 cell pellets, such that the edge of the bone core was level with the PDMS ring, to produce a cartilage region of 500 μm thickness. The constructs were inverted to expose the cartilage region and cultured in chondrogenic medium with two medium changes weekly for 5 weeks.

Biochemical assays

Constructs (*n*=4) were washed in PBS. Three layers were separated from each construct: the cartilage layer above the edge of the bone scaffold; the 1 mm interface layer of the scaffold directly under the cartilage layer; and the subchondral bone layer consisting of the remainder of the scaffold. Samples were placed in digestion buffer (50 mM Tris-HCl, 1 mM EDTA, 50 mM iodoacetaminde, 10 μg/ml pepstatin, 0.5 mg/ml proteinase K), incubated at 60°C overnight, and centrifuged at 300×g for 5 min. The supernatants were used to measure DNA and GAG content using a PicoGreen assay and a 1,9-dimethylmethylene blue dye with chondroitin-6-sulfate as a standard, respectively.

Mechanical testing

The Young's modulus (*n*=4) of cartilage was determined using unconfined compression. Scaffolds were placed in a chamber containing PBS and compressed at a low speed of 500 nm/s (~0.1%/s strain rate) to allow equilibration during ramping. The force was recorded, and the Young's modulus was determined from the initial slope of the stress-strain curve. Friction tests (*n*=4) were conducted to determine the lubricating properties of the articular cartilage surface using a previously described testing apparatus [247], and the protocol consisted of measuring the

time-dependent friction coefficient of the cartilage surface against smooth glass in PBS. A constant 50 g load was applied with a sliding velocity of 1 mm/s, for a total translation of 10 mm for 1800 seconds. The time-dependent friction coefficient was calculated from the ratio of the friction force to the normal force. The minimum and maximum friction coefficient, denoted as μ_{min} and μ_{max}, respectively, were reported.

Histology and immunohistochemistry

Samples were fixed in 4% formaldehyde, decalcified, dehydrated, embedded in paraffin, and sectioned to 8 μm. Cartilage formation was verified by overall histomorphology (H&E), and the presence of total collagen (Masson's trichrome), GAG (Alcian blue), and Collagen Types I, II, and X (immunohistochemistry).

RESULTS

Pellet maturity

Cells in chondrogenic media condensed into spherical pellets overnight after centrifugation. The cell pellets became smaller and denser within 5 days, as seen by H&E staining (**Fig.VIII-2 A-C**). Total hydroxyproline content and hydroxyproline per DNA, representing the amount of collagenous matrix, were significantly higher in day 7 pellets (**Fig.VIII-2D&E**). After compressing the pellets under decellularized bone scaffolds, the osteochondral constructs were successfully fabricated to obtain a cartilage layer of approximately 500 μm thickness, interfaced with decellularized bone cores (**Fig.VIII-2F**).

Engineered articular cartilage

After 5 weeks of culture, the constructs developed into articular cartilage-like tissue. All constructs contained cartilage regions above the edge of the subchondral bone with strong cartilage-bone interfaces. Interestingly, the mechanical properties of the cartilage approached

physiological values (**Table VIII**). The Young's moduli of constructs fabricated from day 3 and 5 pellets were significantly higher than those constructed from day 7 pellets. The friction coefficients of the engineered cartilage surface were on the same order of magnitude as physiological values. Similar to the Young's modulus results, both μ_{min} and μ_{max} were significantly lower in constructs formed using day 7 pellets. Biochemical assays showed that DNA content in the cartilage layer was similar in all groups and was significantly higher than in the interface and subchondral bone regions (**Fig.VIII-3A**). The DNA content in the interface and subchondral bone regions of constructs from day 3 and 5 pellets were significantly higher than that of constructs from day 7 pellets. GAG content per construct wet weight also exhibited similar trends as shown in DNA content (**Fig.VIII-3B**).

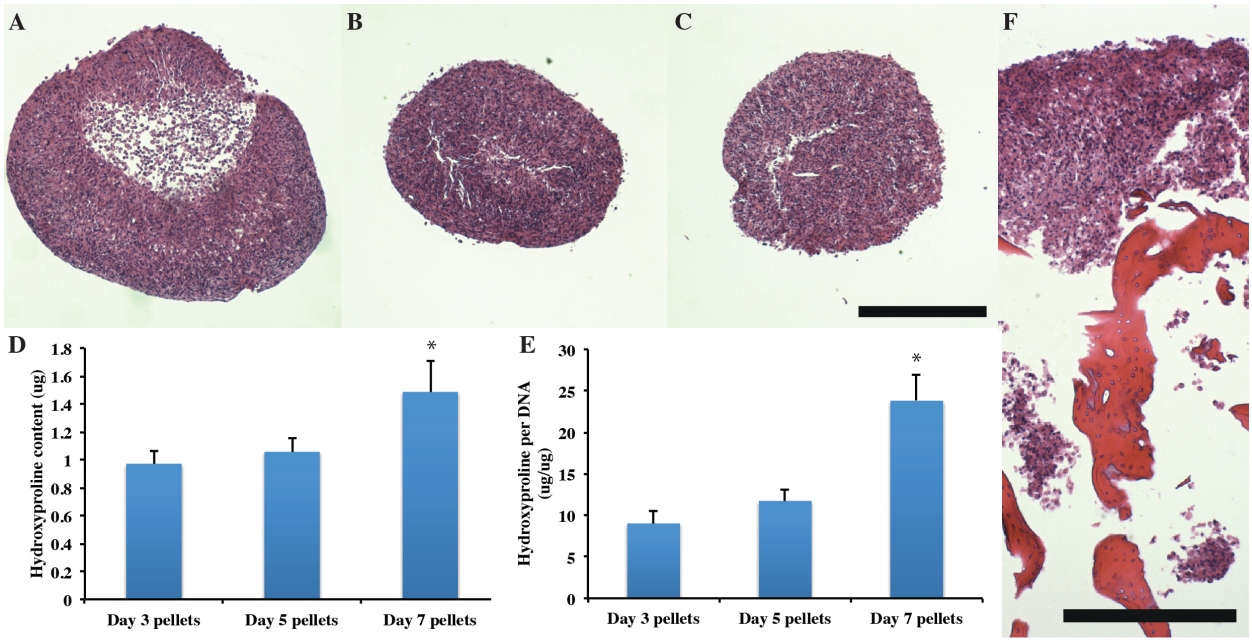

Figure VIII-2: H&E of (A) Day 3, (B) Day 5, and (C) Day 7 pellets (scale bar = 500 μm). Biochemical assays for (D) total hydroxyproline content and (E) hydroxyproline per DNA of pellets at different time points. (* significantly different from the other groups). (F) H&E of an osteochondral construct fabricated from Day 3 pellets after 1 day of culture (scale bar = 500 μm). The thick, extremely dense cell cartilage layer and the penetration of cells into the subchondral bone was produced

Table VIII: Mechanical properties of engineered articular cartilage

Group	Young's modulus (kPa)	μ_{min}	μ_{max}
Day 3 pellets	771±241	0.049±0.015	0.281±0.032
Day 5 pellets	837±239	0.046±0.010	0.298±0.023
Day 7 pellets	454±56*	0.066±0.015*	0.343±0.049*

Histology and immunohistochemistry revealed the structure resembling articular cartilage (**Fig.VIII-4**). H&E and trichrome staining demonstrated a thick articular cartilage layer with a cellularized interface integrating with the subchondral bone. Cell lacunae in the cartilage layer were surrounded by matrix rich in GAG. The interface region contained markedly less GAG than the bulk of the cartilage tissue (**Fig.VIII-3**). Immunohistochemistry showed light staining of collagen type I, whereas collagen type II exhibited intensely positive staining at the surface, in the deep cartilage region and the interface region. Moderate collagen type X stain was also detected in the interface region and on differentiated hMSCs.

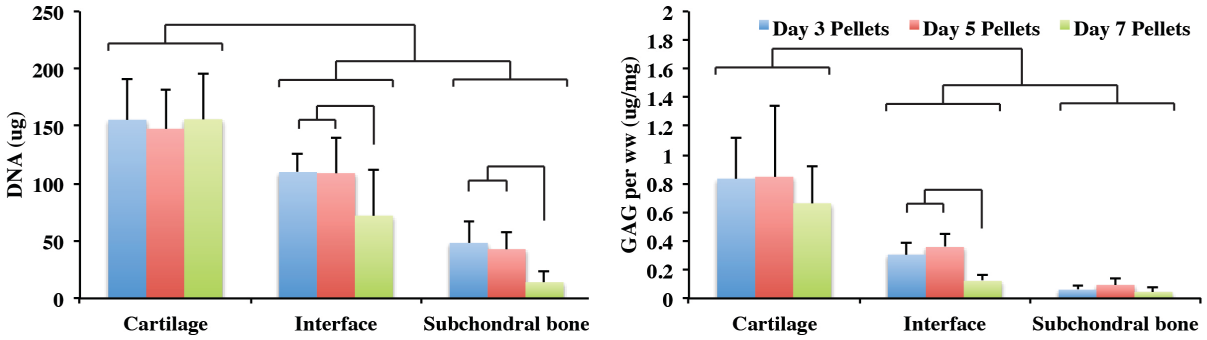

Figure VIII-3: (A) DNA content and (B) GAG per wet weight of cartilage, interface, and subchondral layers after 5 weeks of cultivation. (lines indicated significant differences; $p<0.05$).

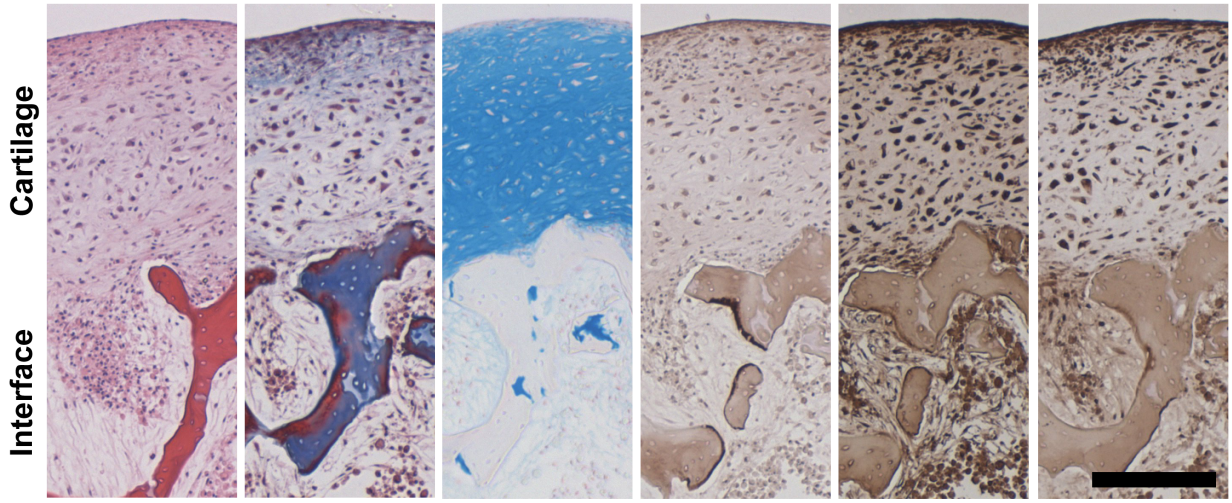

Figure VIII-4: Histology and immunohistochemistry of osteochondral constructs (of day 3 pellets). Left to right: H&E, Masson's trichrome, Alcian blue, Collagen Type I, Collagen Type II, and Collagen Type X. (Scale bar = 250 μm)

DISCUSSION

The compression of bone cores onto pellets in a confined space forced the pellets to fuse and penetrate into the subchondral bone. Over the course of *in vitro* culture, a dense cartilage layer and a well-developed cartilage-bone interface region formed. The hMSCs differentiated along the chondrogenic lineage and produced chondrogenic extracellular matrix, forming a cartilage layer integrated with subchondral bone. The constructs formed from day 7 pellets exhibited inferior properties compared to constructs from day 3 and day 5 pellets for all analyses. Histology and biochemical assays dictated that day 7 pellets were more mature and denser than pellets from day 3 and day 5. As such, day 7 pellets may not fuse or penetrate into subchondral bone well, resulting in a less continuous structure than constructs fabricated with less mature pellets from day 3 and 5.

Quantitation of DNA content and GAG per wet weight after culture confirmed the results. The interface and subchondral bone regions of constructs from day 3 and 5 pellets contain significantly greater cellularity that constructs from day 7 pellets, suggesting that less mature

pellets penetrate into subchondral bone more than the mature pellets. More GAG production also occurred at the interface, as a result of the differences in cellularity. The inferior ability of mature pellets to fuse together and integrate into subchondral bone resulted in constructs with poorer functional properties.

Articular cartilage engineered using the pellet compression technique exhibits similar structure to native tissue, with cells in deep zone cartilage demonstrating lacunae-like morphology and cells at the superficial zone appearing flat and aligned. The two extracellular matrix proteins, collagen and GAG, which play great roles in cartilage function, were deposited in the desired regions, i.e., collagen was predominantly present in the superficial zone whereas dense GAG matrix was present in the deep zone. High production of collagen type II in the cartilage layer indicates successful hyaline cartilage development. The interface region contained extracellular matrix providing strong anchorage to the subchondral bone. Collagen type X, a hypertrophic cartilage marker, has been reported in chondrogenic MSC cultures [248]. Interestingly, the expression of collagen type X in the interface region further indicates strong integration between cartilage and subchondral bone.

By using the pellet compression technique, we were able to produce osteochondral constructs with cartilage layers that are thicker than any previous scaffold-free fabrication technique reported thus far [185]. Most strikingly, this technique produced osteochondral constructs with physiologic mechanical properties. The mechanical Young's moduli of the constructs approached 1 MPa, a value measured for young bovine articular cartilage. Notably, such a high compressive stiffness has not been previously accomplished by any method of cartilage tissue engineering using adult human mesenchymal stem cells. In addition, the surface lubrication properties of the engineered constructs were also similar to the values previously reported for native cartilage. [247, 249]

In conclusion, the pellet compression technique using immature hMSC pellets with decellularized bone scaffolds provides a platform for the development of native-like engineered cartilage within osteochondral grafts. The method successfully fabricated osteochondral grafts from human mesenchymal stem cells with excellent integration, physiologic structure, and native function.

CHAPTER IX

Aim 3 Experimentation: Spatial regulation of human mesenchymal stem cell differentiation in engineered osteochondral constructs: effects of pre-differentiation, soluble factors and medium perfusion

INTRODUCTION

One method of the treatment of cartilage injuries is to replace the full-thickness defects with osteochondral plugs, where the bony region anchors the graft and facilitates the integration of the cartilage graft with the host tissue [250]. This approach is limited by insufficient availability of autograft material, donor site morbidity and the risks of disease-transmission associated with the allografts. To alleviate these limitations, it is possible to engineer biological replacements of cartilage and bone tissues using multi-potent human mesenchymal stem cells (hMSCs). There are, however, some inherent technical and scientific challenges to growing osteochondral constructs from hMSCs where bone and cartilage should ideally develop in tandem to facilitate functional integration of the two tissues. Most importantly, spatial regulation of hMSC differentiation is necessary to guide hMSCs down the chondrogenic or osteoblastic lineages in vitro and generate discrete cartilaginous and osseous regions within a single construct.

Previously, hMSCs were separately differentiated into bone and cartilage constructs before physically opposing and suturing these constructs into biphasic units [136]. This approach required considerable manipulation of cultured tissues under sterile conditions and resulted in poor integration between the two tissue constructs. An alternative approach exposed the mouse MSCs to chondrogenic or osteogenic supplements during their monolayer expansion, and sequentially encapsulated the cells in gel substrates to create two distinct but contiguous constructs [135, 251, 252]. After 12 weeks in the dorsum of nude mice, the bone and cartilage remained grossly distinct with apparent regions of integration at the interface. While these results

are clearly promising, the use of in vivo mouse cultivation limits the clinical utility of these constructs. A distinct 'pre-induction' method has also been reported for hMSCs [134]. The resulting composites were cultured in a medium containing a cocktail of osteogenic and chondrogenic supplements for another 5 weeks. Encouraging results for bone-cartilage integration were achieved in this study with the main drawback being the long (10 weeks) cultivation times.

Bioreactors can be utilized to provide biophysical stimulation and improved nutrient transfer to the cells on scaffolds, and enhance their functional assembly into tissues. Several bioreactor designs have been used for engineering bone [90, 137, 253] and cartilage [183, 254] from hMSCs. Most recently, we utilized a perfusion bioreactor for the cultivation of bone constructs [87]. The interstitial flow facilitated cell growth and differentiation, leading to the deposition of mineral and extracellular matrix (ECM) proteins throughout the bone region. We adapted this perfusion bioreactor for use in the present study.

For scaffold materials, we selected those shown to be optimal in previous studies of cartilage and bone tissue engineering. Agarose gel was used for the cartilage phase, as it has been demonstrated that it yields the best mechanical properties of engineered cartilage among all materials studied with immature chondrocytes [103]. Likewise, decellularized bone was selected as a scaffold for the bone region, as it provides osteo-inductive architecture, mechanical properties and biochemical composition [201, 255]. Additionally, in our numerous previous studies, agarose and decellularized bone were used independently and in combination as scaffolds for cartilage, bone and osteochondral constructs [256, 257]. Therefore, we hypothesized that the agarose-bone scaffolds, alone or in combination with molecular and cellular parameters and biophysical stimuli, could provide hMSCs with differential cues necessary to induce spatially confined chondrogenesis (in agarose) and osteogenesis (in bone) while facilitating interfacial communication between the two developing tissues. To test this hypothesis, we explored the effects of three sets of experimental variables on hMSC

differentiation in biphasic constructs: (1) supplementation of chondrogenic factors vs a cocktail of chondrogenic and osteogenic factors, (2) pre-differentiation of hMSCs, (3) medium perfusion (interstitial flow).

MATERIALS AND METHODS

hMSCs cultivation and pre-differentiation

Cryopreserved passage 2 bone-marrow derived hMSCs were kindly provided by Dr Caplan, after isolation using previously described protocols [258]. Cells were expanded for one passage (P3) in control medium (low glucose Dulbecco's Modified Eagle Medium (DMEM) supplemented with 10% Fetal Bovine Serum (FBS), 1 ng/ml Fibroblast Growth Factor (FGF) and 1% antibiotics). Passage 4 cells were split into three groups, and cultured for one more passage (8±1 days) in (1) control medium (undifferentiated hMSCs), osteogenic medium (osteo-induced hMSCs), and chondrogenic medium (chondro-induced hMSCs). Undifferentiated and osteo-induced hMSCs were plated at a density of 5000 cells/cm^2 while the chondro-induced hMSCs were plated at 60,000 cells/cm^2 [259, 260]. Osteogenic medium was low glucose DMEM supplemented with 10% FBS, 1% antibiotics, 10 mM sodium-β-glycerophosphate, 100 nM dexamethasone, and 50 mg/ml ascorbic acid-2-phosphate. Chondrogenic medium was high glucose DMEM supplemented with 10 ng/ml Transforming Growth Factor-beta 3, 100 nM dexamethasone, 50 mg/ml ascorbic acid-2-phosphate, 100 mg/ml sodium pyruvate, 40 mg/ml proline, 1% Insulin, transferrin, sodium selenite (ITS)+ mix and 1% antibiotics. Passage 4 cells were then used for experiments.

Pellet culture

Cells cultured under the various conditions were resuspended in a specific medium (undifferentiated, osteo-induced and chondro-induced), counted, and 2.5×10^5 cells per aliquot were centrifuged to form pellets. Pellets from each group were then cultured in control,

osteogenic, and chondrogenic medium, resulting in 9 different conditions. Three pellets for each condition were cultured for 4 weeks in 1 ml of culture medium, with medium change three times per week.

Decellularized bone scaffolds

Decellularized bone was obtained as previously described [87]. In brief, trabecular bone plugs (4 mm in diameter) were cored from the subchondral region of carpometacarpal joints of 2-4-month- old cows. They were washed to remove marrow and rinsed in PBS with 0.1% ethylenediaminotetraacetic acid (EDTA) for 1 h at room temperature. This was followed by sequential washes in hypotonic buffer, detergent and enzymatic solution. Decellularized bone plugs were rinsed in PBS, freeze-dried, and cut to 5 mm lengths to yield cylinders 4 mm diameter × 5 mm high. The weights and dimensions of each plug were measured and used to calculate scaffold density. Scaffolds within the range of 0.30-0.40 mg/cm^3 were used. Scaffolds were sterilized in 70% ethanol, washed in PBS and incubated in culture medium prior to seeding cells. The distribution of bone scaffolds with different densities was randomized.

Biphasic scaffolds

Bone scaffolds were seeded as previously described [87]. In brief, scaffolds were blot-dried and seeded with 1.8×10^6 cells suspended in 40 ml of media (45×10^6 cells/ml). The scaffolds were flipped every half hour and 10 ml media were added. After 2 h, 5 ml of media were added and scaffolds were incubated overnight. Agarose gels were made the following day by mixing equal volumes of 4% agarose solution and cell suspension to yield 25×10^6 cells/ml in 2% agarose. This was pipetted into cylindrical wells (4 mm ⊘ × 2.5 mm height) in PDMS molds. Bone scaffolds seeded on the previous day were overlaid allowing a penetration depth of 500 mm of gel into the bone scaffold. The agarose was then allowed to solidify at room temperature to complete the

formation of biphasic constructs. The seeded scaffolds were cultured for 4 days under static conditions to allow cell attachment, prior to applying medium perfusion.

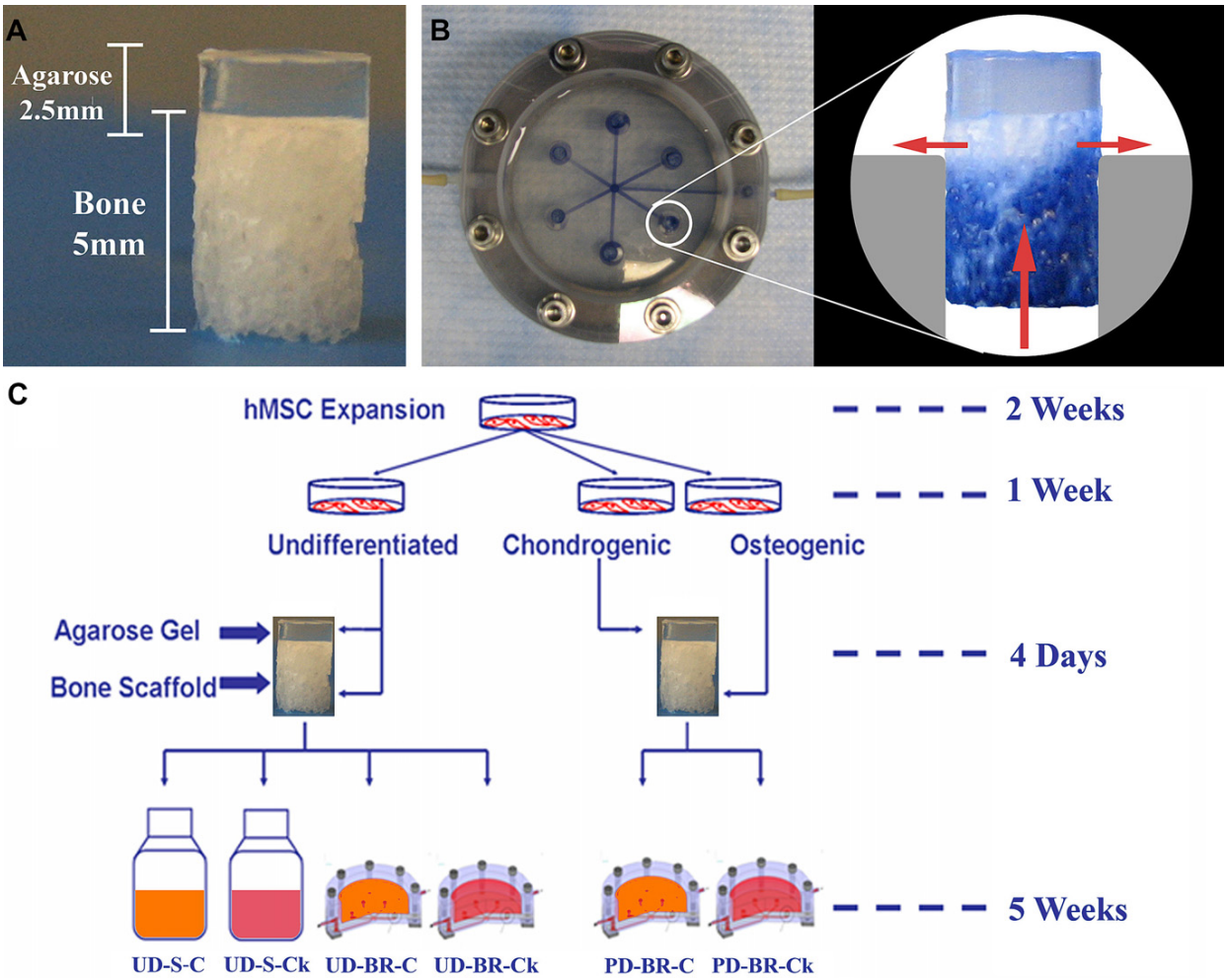

Figure IX-1. Experimental design. (A) Biphasic scaffold made by interfacing agarose and trabecular bone scaffolds. (B) Perfusion bioreactor for cultivation of biphasic scaffolds. Enlarged view shows predicted path of medium flow through the scaffolds and through the sides into the reservoir. (C) Schematic of experimental design.

Perfusion bioreactor

A perfusion bioreactor developed in our laboratory and described previously [87] was used for cultivating biphasic tissue constructs. The constructs were positioned with the bone region secured in wells and agarose region in the reservoir. The bone region protruded 1 mm from the well. Culture medium was pumped axially upwards through the interstices of the bone region,

and out into the medium reservoir. The agarose region was completely submerged in culture medium in the reservoir, and was not perfused (**Fig.IX-1B**). The medium flowed through the bone scaffolds at a superficial velocity of 400 μm/s [87].

Experimental design

The experiment was set-up to test the effects of three distinct variables: cell pre-differentiation, medium perfusion and medium supplements (**Fig.IX-1C**). To evaluate the influence of cell pre-differentiation, constructs were made from undifferentiated hMSCs (UD) or hMSCs pre-differentiated to chondrocytes and osteoblasts (PD). To evaluate the effects of perfusion, each of the cell groups was cultured either in perfused bioreactor (BR) or statically (S). To evaluate the effects of medium supplements, each of the cell-bioreactor groups was cultured in either chondrogenic (C) or cocktail (Ck) medium (high glucose DMEM containing both chondrogenic and osteogenic supplements: 10% FBS, 10mM sodium-b-glycerophosphate, 100 nM dexamethasone, 50 mg/ml ascorbic acid-2-phosphate, 10 ng/ml TGF-β3, 100 mg/ml sodium pyruvate, 40 mg/ml proline, 1% ITS+ mix and 1% antibiotics). As a result, we obtained six experimental groups as shown in (**Fig.IX-1C**). This way, the effects of cell pre-differentiation were compared for two culture conditions and two sets of medium supplements (UD-BR-C/Ck vs PD-BR-C/Ck). Likewise, the effects of biophysical stimulation via medium perfusion were determined for both differentiated and undifferentiated cells, and both media compositions (UD-S-C/Ck vs UD-BR-C/Ck). Finally, chondrogenic medium (which already contained dexamethasone and ascorbic acid) and the cocktail medium (containing additional osteogenic supplements) were compared for both cell groups and both sets of culture conditions (UD/PD-BR-C vs UD/PD-BR-Ck). Data were obtained in two independent series of experiments.

Micro computerized tomography (μ-CT)

μ-CT imaging was performed using a modified protocol from Liu et al. [208]. Constructs were aligned along their axial direction in a 15 ml centrifuge tube and stabilized with wet gauze. The tube was clamped in the specimen holder of a vivaCT 40 system (SCANCO Medical AG, Basserdorf, Switzerland). Constructs were scanned at 21 mm isotropic resolution, and the bone volume (BV) was obtained by global thresholding technique that detected only the mineralized tissue.

Mechanical testing

The equilibrium Young's modulus of the cartilage region was measured in unconfined compression using a modification of an established protocol [103]. An initial tare load of 0.02 N was applied. This was followed by a stress-relaxation step where the specimens were compressed to 10% strain of the cartilage region at a ramp velocity of 0.05%/s and maintained at that position for 1800 s. The Young's modulus was calculated from the equilibrium forces measured at 10% strain.

Biochemical assays

The gel and bone regions of three constructs per group were separated along the flat surface of the bone scaffold and the wet weight of the gel and bone regions determined. The samples were stored at 20°C. until assay. For analysis, the gel regions were digested in 1 ml proteinase K solution at 50°C. The bone regions were placed in 100 ml of proteinase K digestion buffer at 50°C. DNA content was determined using the Picogreen assay (Molecular Probes, OR). The sulfated GAG (s-GAG) content of the extracts was determined using the 1,9-dimethylmethylene blue (DMMB) dye colorimetric assay with chondroitin-6-sulfate as a standard.

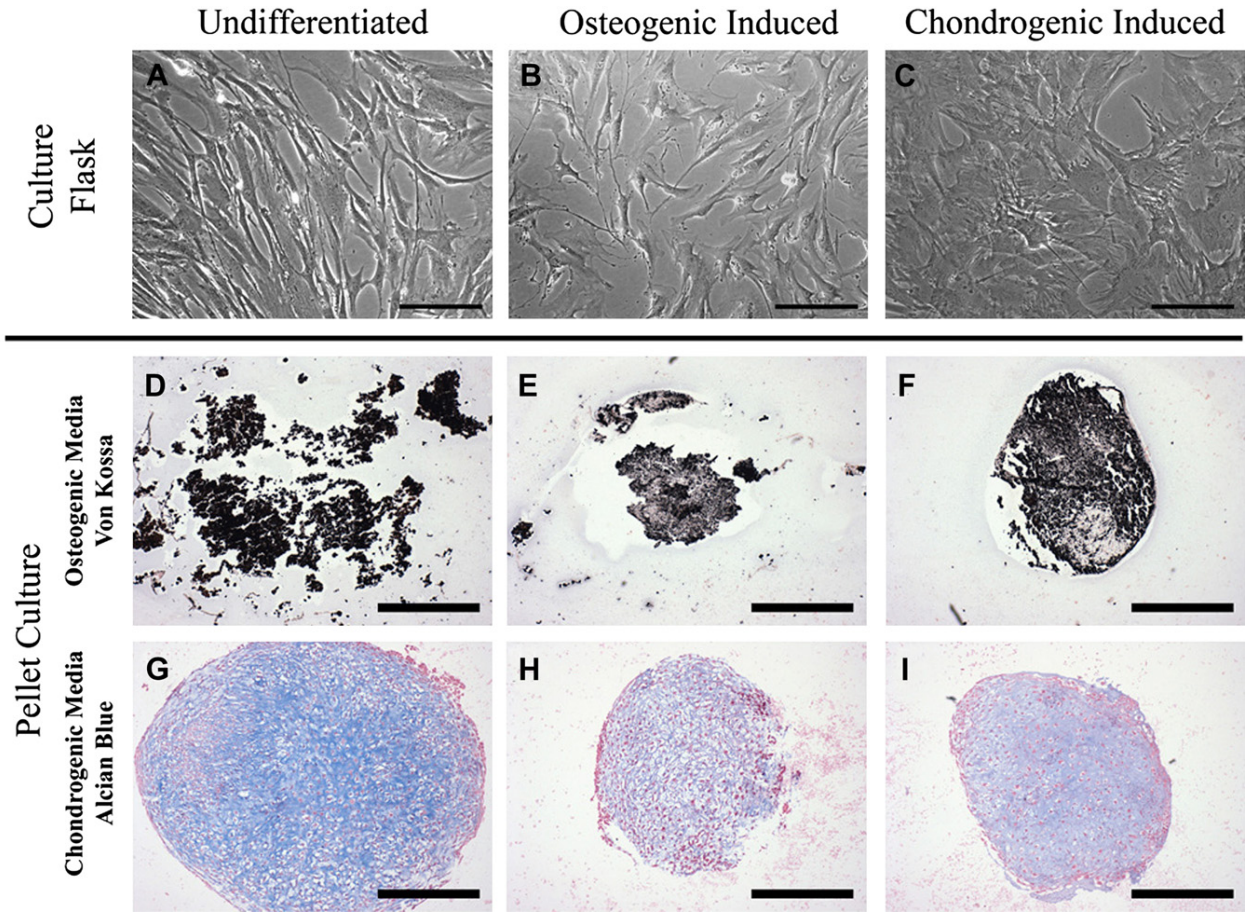

Figure IX-2. Cell differentiation studies. (A-C) Morphology of hMSCs cultured using (A) expansion medium, (B) osteogenic supplements and (C) chondrogenic supplements. (D-F) Von Kossa staining of pellets cultured under osteogenic conditions for 4 weeks. (G-I) Alcian Blue staining of pellets cultured under chondrogenic conditions for 4 weeks.

Histology and immunohistochemistry

Constructs were washed in PBS and fixed in 10% formalin, decalcified with Immunocal solution, embedded in paraffin, sectioned into 5 mm slices and stained with haematoxylin and eosin (H&E) and Alcian Blue (GAG). Samples were also immunohistochemically stained for collagens I and II and bone sialoprotein (BSP) as previously described[87].

Statistical analysis

Pair-wise comparisons of results were carried out using multi- way Analysis of Variance (ANOVA) followed by Tukey's post hoc analysis using STATISTICA software. P<0.05 was considered as significant.

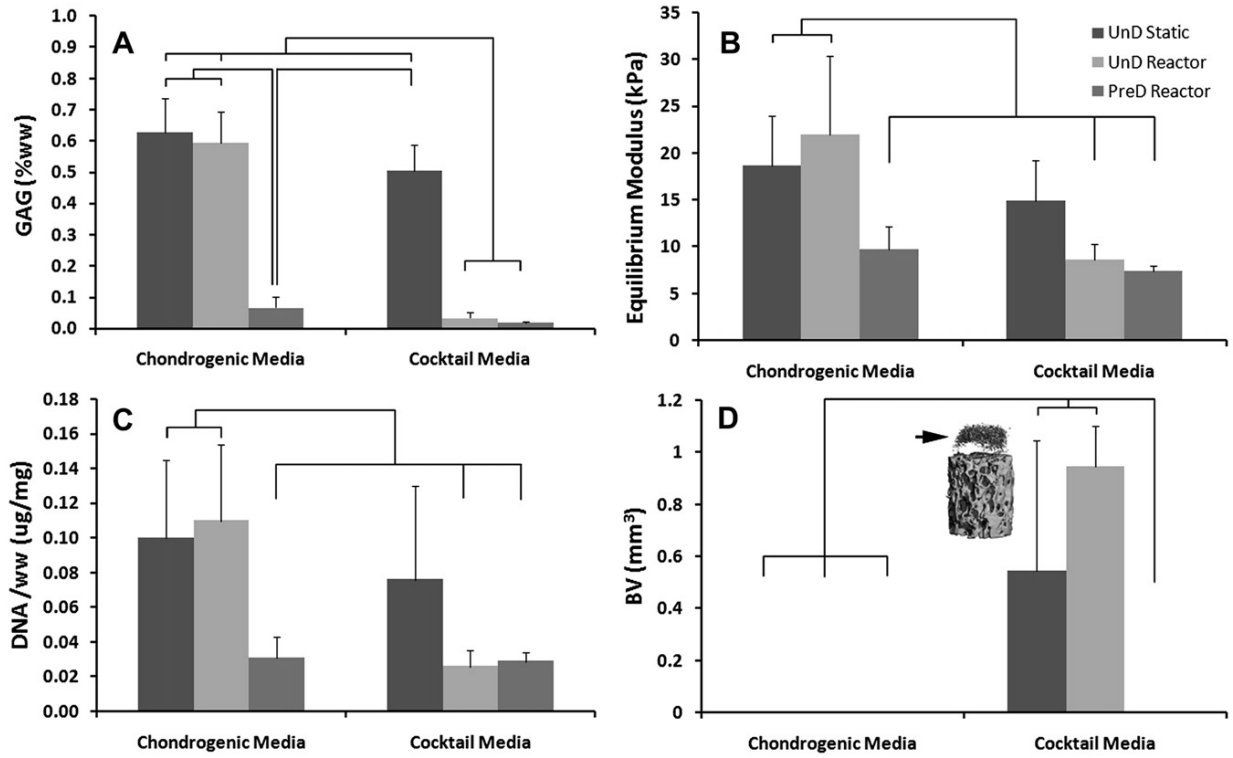

	GAG/DNA (µg/µg)		Equilibrium Modulus/DNA (kPa/ug)	
	Chondrogenic	Cocktail	Chondrogenic	Cocktail
UD-St	75.2±42.7	93.2±59.2*	7.55±5.71	7.54±4.37
UD-BR	65.1±43.6	14.2±7.3	7.22±5.18	11.40±6.86
PD-BR	21.9±6.6	6.6±2.0	8.37±3.30	7.34±1.48

Figure IX-3. Quantitative properties of cartilage region. (A) GAG content of gels normalized by wet weight. (B) Equilibrium modulus. (C) DNA content normalized by wet weight. (D) BV of gels measured by µCT. (n 1⁄4 3; *P < 0.05; **P < 0.001) (E) Table of GAG expression and equilibrium modulus values normalized to DNA (n 1⁄4 3; *P < 0.05 as compared to the experimental groups using the same culture medium).

RESULTS

Characterization of undifferentiated and pre-differentiated hMSCs

Undifferentiated hMSCs maintained their fibroblast-like morphologies throughout the two-dimensional (2D) cultivation period while osteo-induced hMSCs grew faster and appeared thinner but less elongated and less aligned to each other. Despite the high seeding densities and chondro-inductive medium, hMSCs were unable to adopt a spherical morphology, instead becoming broad and flat (**Fig.IX-2 A-C**). Pre-differentiation of hMSCs by 1-week monolayer cultivation in chondrogenic or osteogenic medium did not improve their subsequent three-dimensional (3D) differentiation along the same lineage (osteo/osteo or chondro/chondro) during pellet culture (**Fig.IX-2 D-I**). Under osteogenic conditions, pellets from all three groups stained positively for mineral deposition (**Fig.IX-2D,F**) and expressed BSP (not shown). Under chondrogenic conditions, pellets from all three groups expressed GAG and formed lacunar structures. Both osteogenic and chondrogenic pre-differentiation appeared to decrease their subsequent chondrogenic potential in pellet culture relative to undifferentiated hMSCs. Pellets formed by undifferentiated hMSCs were approximately twice the size of those in other groups, and stained more intensely for GAG (**Fig.IX-2G-I**) and collagen type II (not shown).

Cartilage region in biphasic constructs

The highest GAG contents (expressed as a fraction of wet weight) were achieved for UD-S-C constructs (**Fig.IX-3A**). Biochemical and mechanical properties of engineered cartilage were significantly affected by the combination of cocktail medium and perfusion, but not by either stimulus alone. For example, GAG content was statis- tically similar when comparing UD-S-C (P 1⁄4 0.61%), UD-BR-C (P 1⁄4 0.59%) and UD-S-Ck (P 1⁄4 0.53%) constructs but there was a decrease in GAG contents for UD-BR-Ck group (P 1⁄4 0.02%) where both bioreactor cultivation and cocktail medium were used. Pre-differentiated hMSCs did not express significant quantities

of GAG (<0.1%). The equilibrium Young's modulus values reflected the trend of the GAG content [Fig. 3(B)]. Similar values were obtained for UD- S-C (18 kPa), UD-BR-C (22 kPa) and UD-S-Ck (15 kPa) while the modulus of UD-BR-Ck, PD-BR-C and PD-BR-Ck were all less than 10 kPa. The normalized DNA values were consistent with these findings as the DNA contents of UD-S-C, UD-BR-C and UD-S-Ck were approximately three times higher than the other three groups (**Fig.IX-3C**). It should be pointed out that the trend for GAG content remained the same when normalized to DNA content, but the differences observed between groups for equilibrium modulus disappears. μ-CT data indicated mineral deposition in the gel regions of UD-S-Ck and UD-BR-Ck groups only [**Fig. 3D (inset)**].

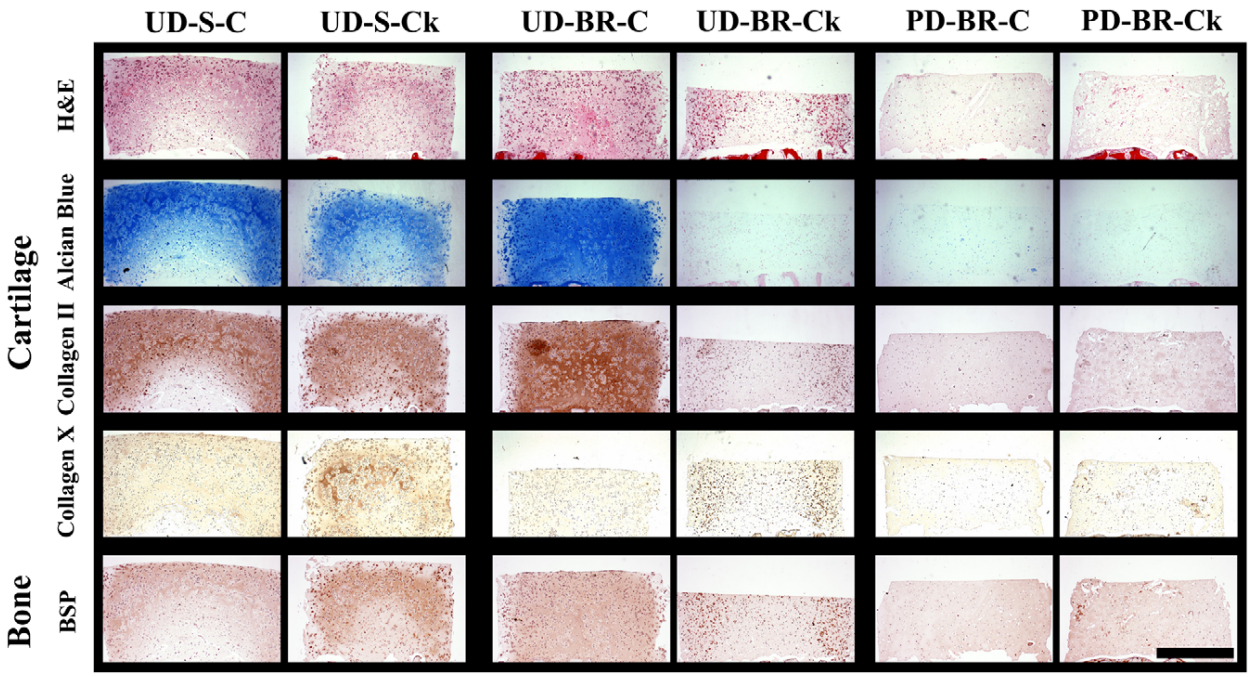

Figure IX-4. Representative images of immunohistochemical properties of cartilage region. First row: H&E staining. Second row: Alcian Blue staining for GAG content. Third row: collagen II expression. Fourth row: collagen expression. Fifth row: BSP expression.

H&E staining indicated differences in cell distributions throughout the gel regions between the experimental groups. Under static conditions (UD-S-C and UD-S-Ck), the central regions closer

to the bony substrates were less densely populated than the edges, an effect that can be attributed to the diffusional limitations of nutrient transport (**Fig.IX-4**, first row). This pattern was less pronounced for the UD-BR groups (UD-BRC and UD-BRCk) where medium was perfused directly into the lower face of the gel construct. Decreased matrix deposition was again evident in PD-BR constructs (PD-BR-C and PD-BR-Ck).

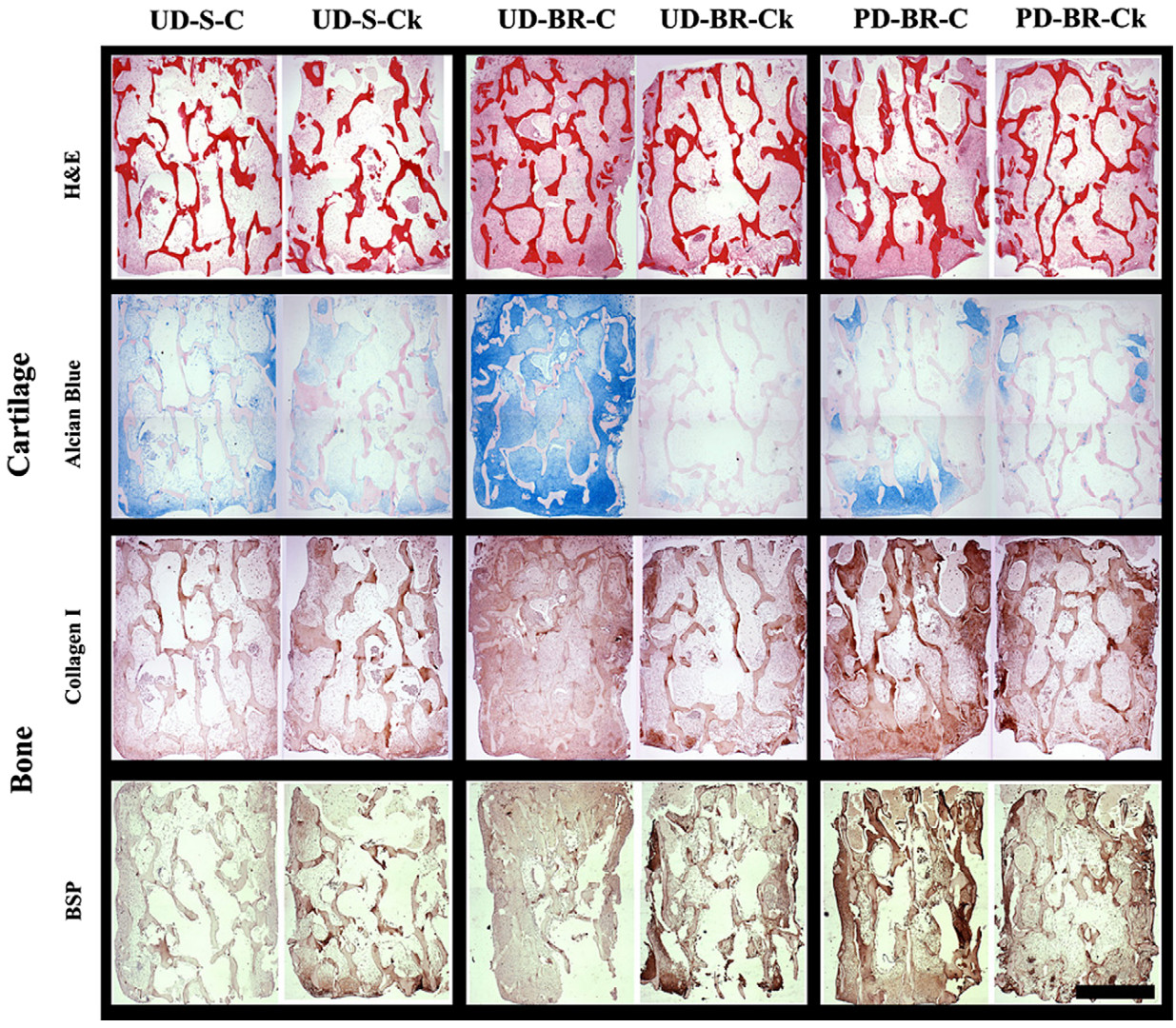

Figure IX-5. Representative images of immunohistochemical properties of bone region. First row: H&E staining. Second row: Alcian Blue staining for GAG content. Third row: collagen I expression in gels. Fourth row: BSP expression.

Bone region in biphasic constructs

Quantitative evaluation of DNA content within the bone region of the constructs demonstrated little variation between the experimental groups (data not shown). The large variability in initial mineral content (obtained from m-CT) made it difficult to rigorously evaluate relative changes in mineralization based on cultivation conditions. However, histological analysis showed interesting effects of cultivation conditions on the properties of bone regions. H&E staining demonstrated that constructs cultured under static conditions resulted in cell growth and matrix deposition up to approximately 1 mm from the periphery of the bone scaffolds leaving the central regions largely unpopulated. In contrast, medium perfusion resulted in more uniform cell distribution and matrix accumulation throughout the pore spaces of the bone scaffolds (**Fig.IX-5**, first row). GAG deposition was evident for undifferentiated cells cultivated in chondrogenic medium (Un-S-C and Un-BR-C), and rather low in the groups cultivated in cocktail medium. Again, the combined effects of perfusion and cocktail medium were evident: Un-S-Ck groups also showed patches of light GAG staining while the Un-BR-Ck groups showed no GAG staining (**Fig.IX-5**, second row).

Osteogenic pre-differentiation alone was not sufficient to eliminate chondrogenic differentiation in the bone region: PD-BR-C showed light GAG staining, but this was eliminated in the presence of osteogenic supplements (PD-BR-Ck group). Undifferentiated groups cultured in chondrogenic medium (Un-S-C and Un-BR-C) did not exhibit collagen I or BSP staining. Interestingly, the pre-induced osteoblasts cultured in chondrogenic medium (PD-BR-C) expressed BSP and collagen I throughout the scaffold. Cocktail supplements without flow were sufficient to elicit minimal BSP expression (Un-S-Ck), but the expression of BSP and collagen I increased with perfusion (Un-BR-Ck and PD-BR-Ck) (**Fig.IX-5**, third and fourth rows).

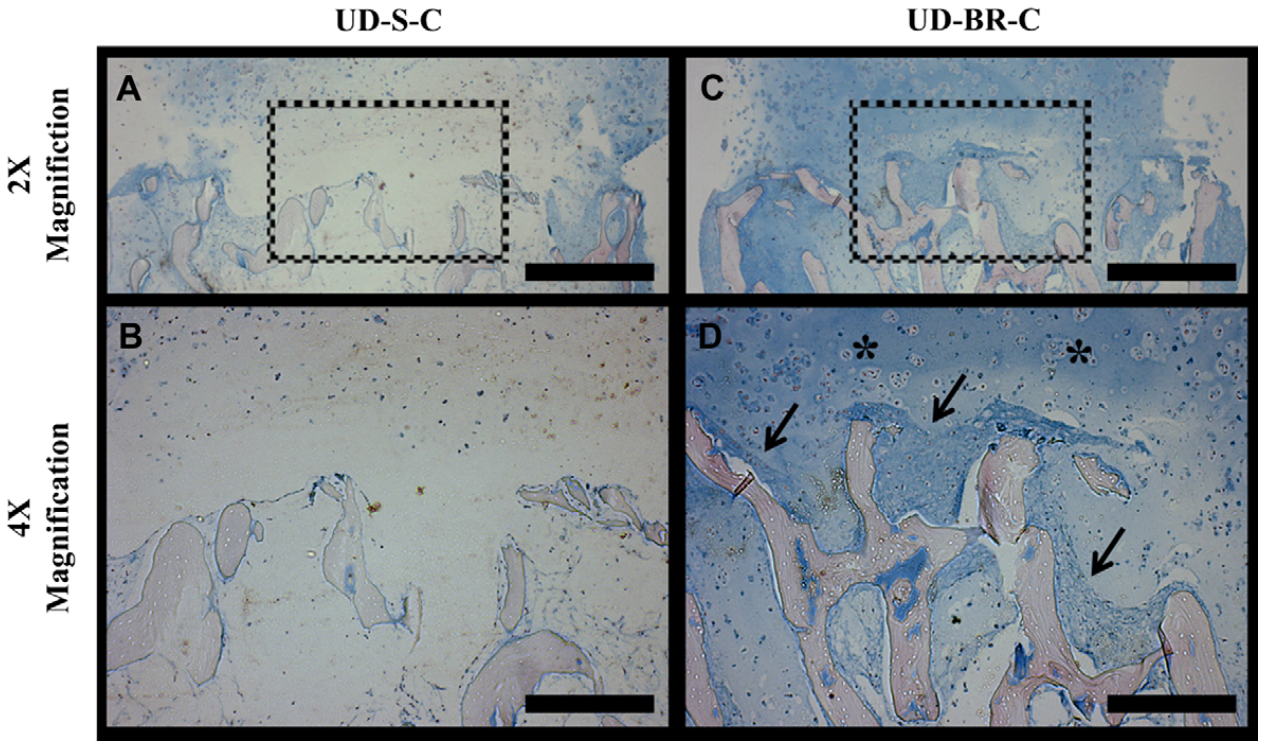

Figure IX-6. Integration of bone and cartilage regions. (A) Integration region of static constructs (UD-S-C) is mostly acellular. (B) High magnification image of region indicated by box in (A) showing different morphologies in gel and scaffold regions and minimal GAG expression. (C) Integration between cartilage and bone is enhanced under bioreactor conditions. (D) High magnification image of region indicated by box in (C) shows high matrix production in central regions of integration zone. Distinct spherical morphology in gel is indicated by * whereas the elongated, fibrous morphology is evident in regions close to bone by arrows ([).

Integration of cartilage and bone regions

The integration in the region where agarose gel penetrated into the porous bone scaffold was assessed by examining the properties of cell and tissue matrix. Constructs cultured under static condi- tions demonstrated the presence of cells only at the outer edges of the integration zone (**Fig.IX-6A**) but no cells were observed in the inner regions (**Fig.IX-6 A,B**). To evaluate the effect of perfusion on integration, the integration zone for the Alcian Blue-stained Un-BR-C construct is shown in **Fig.IX-6C**. Cells were present throughout the integration zone in these constructs. Interestingly, while cells throughout the entire region are expressing GAG, indicative of chondrogenic differentiation, there is evidence of morphological differences. Cells embedded

completely within the agarose gel are spherical and reside within lacunae, while cells within close proximity to the bone scaffold exhibit more fibrous morphologies (**Fig.IX-6D**). It was noted that the fibrous regions did not form as a uniformly horizontal layer throughout the integration zone hence there was no evidence of a discrete layer separating bone from cartilage.

DISCUSSION

Early tissue engineering studies investigated the feasibility of forming osteochondral constructs from two separate regions containing differentiated chondrocytes and osteoblasts, and using the resulting composites for the repair of focal defects [261, 262]. However, differentiated cells do not provide a practical clinical option as they are limited in supply, their harvest is associated with morbidity and the danger of secondary joint disease, and it is difficult to procure healthy cells for therapeutic use. One attractive cell source for cartilage and bone tissue engineering is hMSCs because of their innate capability to make osteochondral tissues. Numerous reports have demonstrated the feasibility of growing either bone-like or cartilage-like tissues from hMSCs, although the functional outcomes for cartilage have never been comparable to those ach- ieved using immature chondrocytes. Still, growing 'complex' tissues is dependent upon the ability to provide the hMSCs with the appropriate chondrogenic or osteogenic cues in a site-specific manner. Therefore, the primary objective of our study was to evaluate various experimental conditions which could enable the simultaneous development of integrated, yet distinct, bone and cartilage tissues from a homogenous hMSC population.

hMSC pre-differentiation reduces subsequent chondrogenesis

We tested the hypothesis that pre-differentiating the cells would turn on lineage-specific genes, expedite the formation of cartilage and bone regions within the osteochondral plugs and predispose cells to respond to either osteogenic or chondrogenic stimuli in cocktail medium, but not both. The results of pellet culture experiments, which were used to determine the phenotypic

stability of cells after differentiation, demonstrated that pre-differentiated hMSCs could still respond to opposing stimuli even though the effect was attenuated relative to undifferentiated hMSCs (**Fig.IX-2**). It was also found somewhat counter- intuitively that the chondrogenic pre-differentiation reduced the hMSCs' potential to form cartilage matrix in 3D culture. A similar approach was taken and shown to be successful using rat MSCs. This difference may reflect an inherent distinction in the capacity of rat vs human cells under similar cultivation conditions. In retrospect, this is not surprising, because the chondrogenic potential of hMSCs is heavily dependent upon their ability to maintain a spherical morphology [200]. By providing chondrogenic stimuli during monolayer culture, the cells were essentially presented with conflicting stimuli, which negatively affected subsequent development.

Chondrogenesis is reduced by the combination of flow and cocktail medium

Undifferentiated hMSCs cultured statically in agarose gels (UD-S-C) produced 0.6% GAG and had Young's moduli of approximately 20 kPa. These values are considerably lower than those observed for constructs grown with immature bovine chondrocytes [106], but are in the range of values reported for bovine MSCs [183]. These results underscore the inherent difficulty in elucidating and providing the appropriate cues for directing stem cells into mature chondrocytes in vitro. Yet, the scaffold-bioreactor system provided critical insights into the ability of hMSCs to integrate multiple stimuli in cell-fate decisions. Notably, relative to the UD-S-C group, changing to perfusion only (Un-BR-C) or cocktail medium only (UD-S-Ck) had no significant effect on tissue composition content and mechanical stiffness, while both param- eters were negatively affected by the combination of cocktail medium and perfusion (UD-BR-Ck) (**Fig.IX-3**). Collagen X stains (**Fig.IX-4**) suggested hypertrophy of hMSC-derived chondrocytes in all groups where undifferentiated hMSCs were used to form the cartilage layer, with the strongest expression in the cultures where cocktail medium was used. This is consistent with the notion that hypertrophy is generally associated with MSC chondrogenesis.

Pre-differentiation, flow and cocktail medium provide the best osteogenic conditions

Our study tested whether the biochemical environment of trabecular bone matrix combined with flow-induced shear stress through the constructs may have been sufficiently osteo-inductive for new bone formation. It was evident that the soluble factors in the medium had the most potent effects on cell differentiation: extensive GAG and collagen II staining were evident throughout the bone regions of UD-S-C and UD-BR-C groups (**Fig.IX-5**) indicating that the combination of flow and the trabecular bone biochemistry was insufficient for osteogenesis. Cells in the scaffold did, however, appear to be predisposed to an osteogenic phenotype since cultivation in cocktail medium (UD-S-Ck and UD-BR-Ck) virtually eliminated GAG and collagen II staining while upregulating BSP expression. Perfusion considerably improved cell distribution throughout the bone regions of the constructs (**Fig.IX-5**). There was also decreased collagen II and increased BSP expression in the UD-BR-Ck relative to UD-S-Ck groups indicating flow might play a role in further stimulating osteogenesis of hMSCs at the expense of chondrogenesis. However, further investigations are required to elucidate whether it is due to biophysical stimulation or improved cell-cell communication associated with high cell densities.

Spatial regulation of hMSC differentiation and bone-cartilage integration

In this study we have explored the combination of *in vitro* culture conditions that give rise to suitable chondrogenic or osteogenic differentiation of hMSCs in pre-determined regions of osteochondral constructs. Static culture of undifferentiated hMSCs in chondrogenic medium elicited the best cartilage properties while perfusion culture of pre-differentiated osteoblasts or undifferentiated hMSCs with cocktail medium provided the best osteogenic response.

The collected data support the notion that an osteochondral bioreactor should contain two discrete compartments [263, 264], which would enable cells in either region to be exposed to optimal stimuli, including different medium compositions. In comparison to the previous *in vitro*

studies [134, 136], we used an experimental design that allowed the cartilage and bone phases to develop in tandem. The interface formed in biphasic constructs remains different from that in a native issue where the bone cartilage cross-talk occurs at a clearly demarcated zone of mineralized cartilage. Future studies may focus on clarifying the conditions required to recapitulate the native interface and investigating the heterogenous cell-cell communication in this region. It is also interesting to note that the gel region of this group (UD-BR-Ck) constructs strongly expressed GAG (**Fig.IX-3A**) while simultaneously depositing considerable amounts of mineral (**Fig.IX-3D**). Future studies may determine whether hMSCs are capable of expressing the osteogenic and chondrogenic phenotypes simultaneously similar to the immature cell phenotype which exists during intramembranous ossification [4] or whether these are two distinct populations which co-exist in the gel regions. Such studies may provide insight into mechanisms of stem cell differentiation and cellular interactions at the osteochondral interface.

In conclusion, the study demonstrated the feasibility of engineering biphasic tissue constructs using biphasic scaffolds and perfusion bioreactors enabling spatial regulation of hMSC differentiation. Pre-differentiation of hMSCs in monolayer culture was beneficial for bone tissue development but not cartilage. It was shown that undifferentiated hMSCs are capable of integrating signals from biological factors and perfusion stimuli into decisions to differentiate into chondrocytes or osteoblasts, and perfusion culture considerably enhanced tissue development and improved integration of bone and cartilage tissues. Future studies will focus on the development of an osteochondral bioreactor, and the facilitation of the biological communication necessary to foster functional bone-cartilage interface.

CHAPTER X

Personalized Osteochondral Bioreactor for Engineering TMJ Condyle

Regeneration of the normal shape, architecture, and function of tissues following congenital abnormality, trauma, or surgical treatment presents special problems to tissue engineering. Because of the great variation in properties of these tissues, currently available treatment options fall short of adequate care. The engineering of personalized grafts customized to the patient would revolutionize craniofacial defect treatments. This dissertation demonstrated the ability to engineer bone, cartilage, and osteochondral tissue with native structure and physiologic function from a clinically favorable cell source, hMSC. The following study utilized a personalized bioreactor for the engineering of anatomically shaped oesteochondral grafts. The design of this bioreactor is suitable for clinical translation. The TMJ condyle-specific bioreactor was created as the first in a family of systems. The TMJ was chosen as the target graft of this study because of its complex shape, moderate size, mechanical loading properties, and the great need for this graft in craniofacial reconstructions. Although the bioreactor was specifically designed for the TMJ condyle, the flexibility of its design allows for extensions to numerous other grafts.

RECONSTRUCTION OF THE HEAD AND FACE: RECENT ADVANCES AND CURRENT NEEDS

Defects in the head and face regions due to trauma, tumor removal, or congenital abnormalities not only leave patients with reduced tissue structure and function, but also render them psychologically scarred. The burden of craniofacial injuries extends far beyond medical expenses, as these injuries often impair the patient's social integration. Due to the complexity of craniofacial reconstructions [265][266], the currently available treatment options fall short of adequate care [267][268]. There is a pressing need for functional and esthetic restoration of a multitude of bones including TMJ, zygomatic arch, cranial, nose, temple, mandible, and orbital bone. The current market for craniofacial bone is estimated at $390 million for trauma alone, a

figure based on the overall trauma market of $3 billion in 2010, with facial trauma representing 13% of all traumatic bone injuries [269].

Numerous bone-grafting options exist for head and face reconstruction, depending on the specifics of the defect and the patient's clinical condition. Autologous bone implantation is widely adopted because of the superior osteogenic, osteoinductive, and osteoconductive properties of native bone [270]. Sources of autologous grafts determine their quality and functionality in the craniofacial complex. The membranous bone grafts, such as those harvested from cranium [271], are superior to endochondral bone grafts in terms of volume maintenance [272]. Highly vascularized grafts, such as vascularized bone flap from fibula or iliac bone [51], have the advantage of rapid incorporation into the host bone and vascular flow [270]. Finally, costcochondral grafts can repair composite defects of bone and fibrocartilage [50, 51]. Autologous grafts are considered a gold standard for head and face reconstruction due to their bioactivity, mechanical competence, and immediate cellular function. However, the restricted availability of harvestable bone, donor site morbidity, the lack of precision in carving delicate shapes of craniofacial bones, and differences in the structure and biomechanics of bones from different parts of the body call for alternative methods.

Allografts and alloplastic substitutes provide an unlimited off-the-shelf supply of implants in a range of sizes and shapes. Bone allografts are osteoconductive and may also contain osteoinductive capability [273, 274]. For comparison, a demineralized bone matrix (DBM) exhibits significant osteoinductive behavior and imparts osteoconductivity to the collagen matrix [275]. However, the use of allografts is often associated with infection, disease transmission, and immunological rejection. Processing bone allografts into a demineralized bone matrix can significantly reduce these complications [274].

In contrast, alloplastic grafts are fabricated from synthetic materials, such as hydroxyapatite, calcium phosphates, polymers, plastics, and metals, and carry less burden of infection or immune rejection. Nonbiological grafts can also be designed to provide desired mechanical strength, size, and shape to meet specific implantation requirements. However, the osteoinductivity and osteoconductivity of alloplastic grafts are generally inferior to those exhibited by autologous or allogeneic bone grafts [270]. Also, the nonbiological nature of alloplastic grafts does not provide metabolic function, adaptation, and remodeling of bone (e.g., in response to mechanical loading and aging), all of which are critical for long-term function of implanted grafts.

Existing grafting techniques offer a variety of tools to reconstruct head and face defects, with tolerable success. Nevertheless, disadvantages and complications of existing bone grafts inspire clinicians, scientists, and engineers to develop more effective bone treatment modalities. A major trend in this direction is the development of personalized bone grafts that are autologous in nature and have properties tailored to the patient and the specific clinical situation.

The important criteria for developing functional grafts for head and face reconstruction include (i) superior bioactivity for successful graft incorporation, (ii) native-like graft shape and architecture for aesthetic purposes, and (iii) maintenance of tissue volume during and beyond the bone remodeling period. Patient-specific bone grafts can be designed to synergize the advantages of autologous and alloplastic grafts. A personalized graft (with respect to its shape, architecture, and immune compatibility) is readily accepted by the patient's immune system and designed to match, with great precision, the structural and biomechanical features of the donor site to ensure full reconstruction of both esthetics and function. The availability of personalized human bone graft customized to the patient and the specific clinical condition would revolutionize the way we currently treat craniofacial defects.

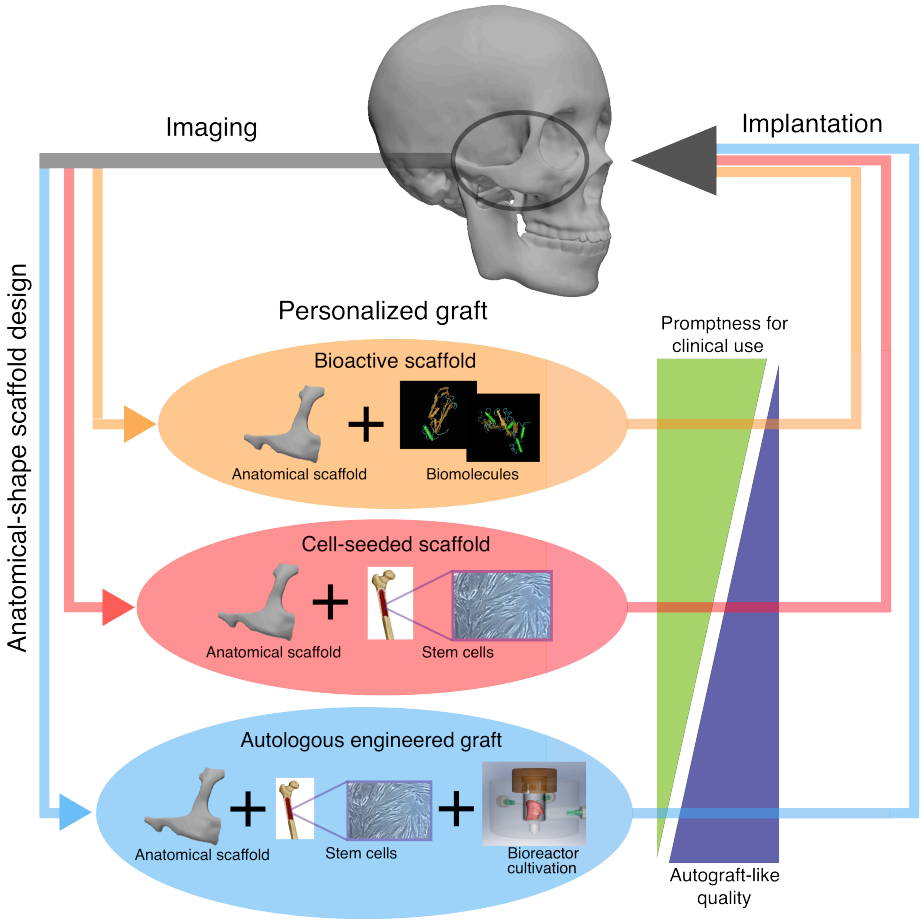

Figure X-1: Key strategies for engineering personalized grafts. (i) Bioactive scaffolds with incorporation of bioactive molecules, designed to recruit the host cells, (ii) cell-seeded scaffolds, with or without additional bioactive factors, designed to foster rapid bone growth inside a scaffold providing structural and mechanical competence, and (iii) autologous bone grafts grown in vitro to various levels of maturity, designed to provide immediate function along with the capacity for integration with the adjacent tissues and blood supply. The similarity to native bone tissue increases from bioactive scaffolds to cell-seeded scaffolds and to preformed bone, whereas the readiness for clinical application decreases in this same order.

ENGINEERING PERSONALIZED HUMAN GRAFTS

A fundamental requirement for personalized craniofacial reconstruction is to fulfill the functional and aesthetic properties of native bone. This is achieved through fabrication of an anatomically shaped, functionally resilient graft that is able to integrate with the host bone, adjacent soft

tissues, and vascular supply. Due to the complex shapes and dynamic properties of the facial skeleton, in addition to patient defect variability, imaging-guided tissue engineering technologies are of great interest. Computer-assisted imaging and preoperative planning are increasingly used to predetermine the surgical location and to facilitate manufacturing of patient-specific implants. Rudman et al. summarized the innovations in computer- assisted reconstructive surgery, including anatomic considerations, implant materials available, technologies for preoperative planning, and the process of obtaining a patient-specific graft [276]. Clinical experience demonstrates that virtual planning, rapid prototype modeling, and stereotactic navigation for complex craniofacial defects can provide the reconstructive surgeon with innovative options for treating challenging and patient- specific reconstructions [277]. The use of computer-assisted imaging allows an exact fabrication of a personalized graft matching the aesthetic requirements of head and facial reconstructions.

Three strategies of great interest for engineering personalized bone grafts rely on the use of (i) bioactive scaffolds, (ii) cell-seeded scaffolds, and (iii) autologous bone grafts grown in vitro (**Fig.X-1**). These three strategies result in different maturities of the implanted tissue (from scaffold alone, over immature cellular graft, to preformed bone) and the promptness for translation (with cell-free scaffolds being closer to clinical application than cellular or bone grafts).

Option 1: Bioactive acellular scaffolds

The first option for personalized bone reconstruction is biodegradable synthetic scaffolds with incorporated osteoinductive factors that can recruit the host cells and guide bone ingrowth. Ideally, bone healing responses to implantation of these scaffolds involve host inflammatory reaction, cell proliferation, migration, differentiation, revascularization, and new bone formation [270]. The biodegradation can progress through hydrolysis or osteoclastic resorption at rates allowing isomorphic replacement of scaffold material with new bone tissue. The bioactive

function should support all processes involved in bone tissue formation—vascularization, osteogenic differentiation, and prevention of scar formation. In addition, mechanical properties of the scaffold are important, especially for load bearing sites. Two techniques are being actively pursued for the design of bioactive scaffolds: (i) fabrication of hierarchical structures resembling those of the native tissue to provide mechanical support and direct cell migration and differentiation and (ii) incorporation of biomolecules to recruit cells and guide bone formation.

Considerations for scaffold architecture include porous channels for cell migration, surface features for cell attachment, and mass-transport conduits for cell nutrient delivery. Due to the complexity of facial bones, an "ideal" scaffold would have a hierarchical porous structure to attain desired mechanical function and mass transport and would allow manufacturing of complex three-dimensional anatomical shapes [278]. Common methods for fabrication of anatomically shaped scaffolds include molding and machining [279, 280]. An example of highly anisotropic structure is the TMJ that contains vertical lamina of cancellous bone, with the matrix density decreasing from superior to inferior across the condyle [281, 282]. Another example is the zygomatic arch (cheek bone) that has a porous central region and a compact rim, with trabeculae arranged vertically and anteroposteriorly [283-286].

Recently, manufacturing techniques known as solid free-form fabrication (SFF) and rapid prototyping have been successfully used to fabricate complex scaffolds. SFF builds parts by selectively adding materials, layer-by-layer, as specified by a computer program [287]. Using this technique, scaffolds were fabricated to match the anisotropic structure of human mandibular condyle from polycaprolactone [278]. Optimizing architecture and scaffolding material for biocompatibility and osteoconductive properties would greatly improve the quality of tissue engineered human bone graft.

Incorporation of biomolecules into alloplastic scaffolds could be utilized to recruit specific cell types to promote bone regeneration. With advances in scaffold fabrication and controlled release

of bioactive factors [288, 289], "smart" scaffolds are becoming available to provide both a structural template and the temporal control of osteoinductive factors. The utilization of growth factors, including transforming growth factor beta, bone morphogenetic proteins (BMP), fibroblast growth factors, insulin-like growth factors, and platelet-derived growth factor in the repair of bone have previously been reviewed [290]. Scaffolds releasing multiple factors in a timely fashion— for example, initial release of cytokines to recruit cell migration followed by the release of vasculogenic and osteogenic factors to direct bone formation—would be most effective for guiding bone regeneration. Cytokines, such as BMP-2, are currently being used commercially, whereas the more complex systems, such as multiple cytokines incorporation, are only being investigated in vitro.

Option 2: Cell-seeded scaffolds

Cellularized grafts, in general, provide better remodeling and integration with the host tissue than acellular scaffolds. Cell-seeded scaffolds combine the benefits of exogenous cells with the incorporation of bioactive molecules and the use of customized scaffolds. In order to prevent immunological response, the graft can be made using autologous materials. Harvesting osteoblasts from native tissue would cause donor site morbidity and is, therefore, not a method of choice. Instead, less invasive harvesting methods are preferred to obtain autologous cells from whole bone marrow (BM), adipose tissue or the platelet-rich plasma (PRP). Bone marrow is rich in biomolecules and cells responsible for normal maintenance of bone, including three types of stem cells: hematopoietic, mesenchymal, and vascular precursor cells. Autologous PRP is commonly used in clinical settings to treat injury and defects. PRP consists of concentrated platelets in a small volume of plasma extracted from whole blood. It comprises seven fundamental protein growth factors proven to be actively secreted by platelets to initiate wound healing and three blood proteins known to act as cell adhesion molecules for osteoconduction and synthesis of connective tissues and epithelial migration [291]. Both the bone marrow and

PRP can be harvested and seeded into anatomical shape scaffolds in a point-of-care setting immediately prior to implantation. Adult stem cells, particularly MSC, have also demonstrated high clinical potential in the application of personalized grafts for head and facial reconstructing. MSCs are the most extensively investigated and utilized therapeutic cells for bone regeneration. These cells have been successfully used in orthopedic cell-based reconstructive therapies [292]. However, the utilization of any type of adult stem cells in cellularized bone grafts requires isolation, purification, and in vitro expansion in order to obtain an adequate number of high-quality stem cells.

Immature cellularized grafts, obtained by seeding of scaffolds immediately prior to implantation, enhance osteogenesis in the site of bone defects through the signaling of biological factors and constituent cell populations. The enhancement in craniofacial reconstruction was investigated using various combinations of cellular and scaffolding materials in several autologous implantation models: BM in a scaffold [293], PRP in a scaffold [291], BMSC in a scaffold [294], and BMSC with PRP [295]. In general, grafts containing cells were superior to their respective no-cell controls, conclusively suggesting that implanted autologous cells contribute to the reconstruction process. Challenges for fabricating personalized immature cellular graft include obtaining sufficient amounts of cellular material, providing spatially uniform and rapid seeding of large anatomically shaped scaffolds, maintaining graft survival postimplantation, and controlling cells to undergo tissue-specific formation *in vivo*.

Option 3: Customized autologous bone grafts

Stem cell biology has advanced to the point that allows biologists and bioengineers to manipulate cells into specific tissue types and form *in vitro* skeletal tissues. Engineering clinically sized autologous bone grafts requires a large number of cells and advanced cultivation systems to provide adequate cell seeding of anatomically shaped scaffolds, sufficient nutrition to the cells within scaffolds, and regulatory signals for cell differentiation and functional assembly [77].

Various technologies have been developed for engineering human bone grafts by utilizing scaffolds and bioreactors [77, 84, 85]. In a suitable environment and with adequate stimulation, stem cells differentiated into osteogenic cells, producing bone proteins and minerals [296, 297]. Notably, tissue engineered bone grafts were superior to scaffold alone and cell-seeded scaffold in terms of graft incorporation into the critical size mouse calvarial bone defects [225].

Maintaining cellularity in large, anatomically shaped bone grafts *in vitro* can be a challenging task. Recently, Grayson et al. [78] reported that clinically sized, anatomically shaped, viable human bone grafts can be engineered in vitro using human mesenchymal stem cells and a "biomimetic" scaffold-bioreactor system. Human TMJ was selected as a model because of the tremendous clinical importance of TMJ and the challenges associated with reconstructing its complex shape and load-bearing function. Anatomically shaped scaffolds were generated from fully decellularized trabecular bone using digitized clinical images and seeded hMSCs. A novel bioreactor with a chamber in the exact shape of a human TMJ was designed for controllable perfusion throughout the engineered construct. By employing computer software to analyze fluid flow patterns, the medium perfusion was optimized to ensure nutrient transport within the forming tissue.

After five weeks of cultivation, tissue growth was evidenced by the formation of confluent layers of lamellar bone (by scanning electron microscopy), markedly increased volume of mineralized matrix (by quantitative microcomputer tomography), and the formation of osteoids (histologically). For the first time in bone grafts of this size and complexity, cells were fully viable at a physiologic density, likely an important factor in graft function. The density and architecture of the bone matrix correlated with the intensity and pattern of the interstitial flow, as determined in experimental and modeling studies. This approach has the potential to overcome a critical hurdle—*in vitro* cultivation of viable bone grafts of complex geometries—and to provide patient-specific bone grafts for craniofacial and orthopedic reconstructions.

The potential of engineering autologous craniofacial grafts with precise anatomical shapes, internal architectures, and biomechanical properties matching the properties of native tissues is tremendous and requires further investigation on bench-top and in large animal studies. The technology could impact research in developmental biology (where high-fidelity tissue models can be used to study bone formation), as much as clinical translation (by providing large and viable anatomically shaped bone grafts for treating craniofacial or orthopedic defects). Current developments are nearing a point where such an approach could become clinically feasible for reconstruction of small- to moderate-sized bone defects.

CLINICAL TRANSLATION OF ENGINEERED CRANIOFACIAL AUTOLOGOUS GRAFTS

The availability of customized, living, engineered tissues would significantly enhance graft function, reduce surgical time, and eliminate issues with donor site morbidity by substituting the use of harvested autografts with engineered autologous grafts. Engineered autologous grafts (option 3), though less prompt in terms of clinical translation than bioactive scaffolds (option 1) and cellularized grafts (option 2), exhibit superior bioactivity for successful graft incorporation, the most important criteria for medical reconstruction. Recent years have brought significant advances in the synergistic utilization of stem cells and bioengineering for craniofacial reconstruction, and identified some of the remaining challenges in clinical translation.

The ultimate goal of tissue engineering is to create native-like tissue grafts *in vitro* for therapeutic purposes. TMJ condyle is one of the most complex bones in the craniofacial skeleton in term of its load-bearing and osteochondral properties. **Table X-1** summarizes the requirements and key findings obtained from the studies in this dissertation. The ideal grafts must be readily accepted by the body and exhibit native tissue function. Clinical knowledge has proven that the use of autologous tissue or cell sources would eliminate the medical complications caused by graft rejection; thus, autologous MSC are the most therapeutic-ready cell source. In addition to autologous property, essential aspects in the context of osteochondral tissue engineering are the

ability to form bone and cartilage tissue, and the ability to provide strong tissue interface. Mimicking physiologic structure, biological expression, and mechanical function would allow for graft incorporation and survival post implantation.

Table X-1 Engineered osteochondral graft requirements and solutions

Requirements	Solutions
Graft immunogenic suppression	Autologous MSC isolated from bone marrow or fat
Bone formation	Regulating bone mineral and protein matrix deposition (Aim 1)
Cartilage formation	Directing articular cartilage formation with cell pellet compression technique (Aim 2)
Bone-cartilage integration	Supplying nutrient and factor through perfusion bioreactor (Aim 3)

This dissertation has shown success in controlling tissue matrix assembly to form bone and articular cartilage structures from hMSC and in providing an adequate system to enhance bone-cartilage integration. In Aim 1, bone architecture was engineered under the regulation of mineral and bone protein deposition. Further, articular cartilage was engineered by directing hMSC differentiation through mesenchymal condensation under the novel cell pellet compression technique (Aim 2). Finally, integration between bone and cartilage was enhanced with sufficient supply of culture media and biological factors with perfusion through bone region (Aim 3).

PERSONALIZED OSTEOCHONDRAL BIOREACTOR DESIGN CONSTRAINTS

The accomplishments and key findings obtained in this dissertation provided understanding on the important features required for successful personalized osteochondral bioreactor design. Ideally, a complete bioreactor system should be capable of (i) supporting cell proliferation and differentiation throughout the complex-shaped multi-phase constructs, (ii) coordinating biological, physiological and mechanical stimuli, (iii) applying stimuli in a spatially and temporally controlled manner to provide lineage-specific stimulation within the cartilage and bone regions, and (iv) providing sufficient nutrient supply to all compartments of the graft.

The design constraints for successful engineering of personalized osteochondral grafts are to allow for (i) manufacturing of anatomical grafts, (ii) cellular support, (ii) stimulation of bone development, (iv) regulation of articular cartilage formation, and (v) spatial control of tissue formation. Based on key findings in the recent studies, the tissue engineering techniques were developed to address these requirements (**Table X-1**). Anatomically-shaped scaffolds can be fabricated using SFF or 3D milling from computerized 3D program. Medium perfusion provides sufficient supply of nutrient to support cellularity in large constructs. To engineer osteochondral constructs from hMSC, undifferentiated cells must be seeded into the bi-phasic construct and spatially supplied with osteogenic and chondrogenic media in bone and cartilage region respectively.

DESIGN OF PERSONALIZED OSTEOCHONDRAL BIOREACTOR

A personalized osteochondral bioreactor was developed, which fulfills the previously mentioned designe constraints. **Fig.X-2** shows the schematic of the system. The system consists of one culture chamber where the cellularized construct is located, and two reservoirs containing osteogenic and chondrogenic media. The two media are perfused into the chamber to provide nutrients and stimulating factors to the different region of the bi-phasic osteochondral construct.

The culture chamber consisted of five main components (**Fig.X-3A**): (i) scaffold, (ii) PDMS block, (iii,iv) two manifolds, and (v) case. To assemble the bioreactor, the scaffold is inserted into the PDMS block, which is specifically fabricated to match the construct anatomical shape. The PDMS block is then sandwiched between two polycarbonate fluid-routing manifolds, while a tubular enclosure slides over the assembly, providing a compressive force to tightly seal the components together (**Fig.X-3B**). The polycarbonate manifolds are designed with four ports for medium perfusion: two inlets and two outlets each for chondrogenic and osteogenic media (**Ill.X-2**). Chondrogenic media enters the chamber at the articular side of the manifolds and is perfused into the PDMS block on top of the articular surface of the condyle. Osteogenic media enters the chamber at the subchondral side and is perfused into the PDMS and through the bone scaffolds.

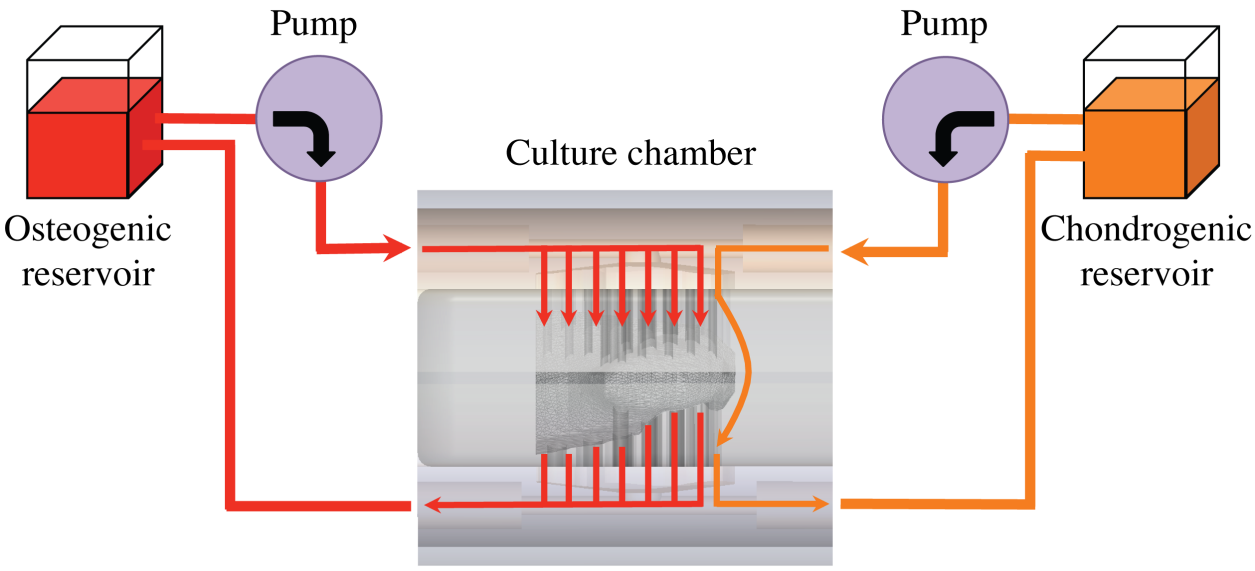

Figure X-2: Schematic of a complete personalized osteochondral bioreactor

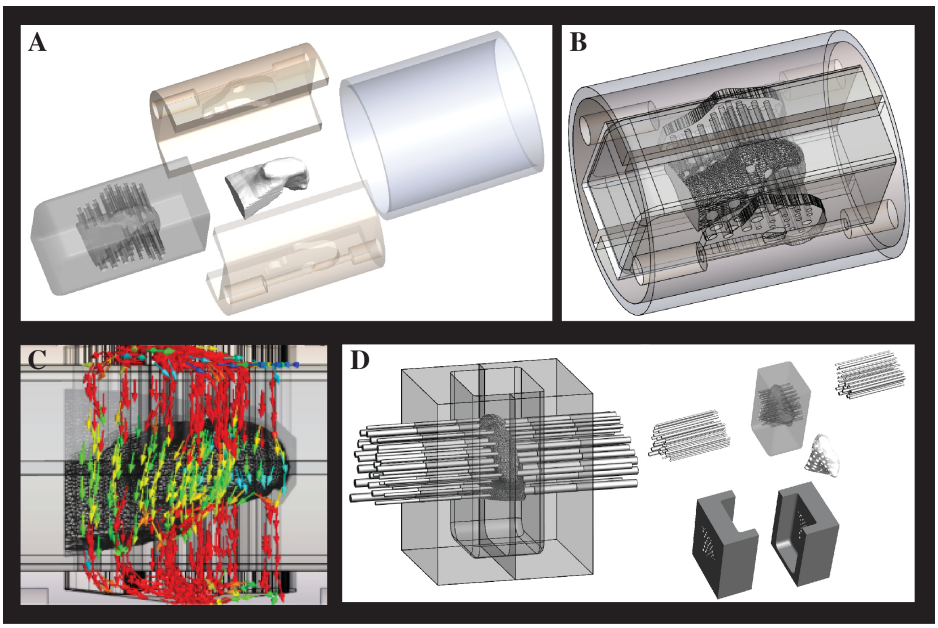

Figure X-3 Culture chamber consists of (A) five main components assemble together (B). (C) Modeling of flow dynamics to determine channels size and location that provide homogenous flow. (D) Components to create PDMS block with pre-determined channels.

Large anatomically shaped constructs require a well-controlled nutrient supply to support cell viability and stimulate tissue formation. For homogenous medium perfusion, channels within the PDMS block are sized according to the local scaffold thickness and are positioned to provide a near-uniform flow velocity throughout the scaffold of the bone region (**Fig.X-3C**). The sizes and placement of perfusion channels were determined by computational flow dynamics modeling to ensure the homogenous distribution of medium flow. Once the location and the size of channels to provide homogenous flow was determined, the mold to create PDMS block was created (**Fig.X-3D**). The positive TMJ shape mold and the outside casing containing the pre-determined holes for channels were 3D print. Multiple channels were inserted through the pre-determined holes of the outside casing into the TMJ shape mold. PDMS was poured into the empty space between the two casing and let cured to create negative PDMS block with pre-determined channels.

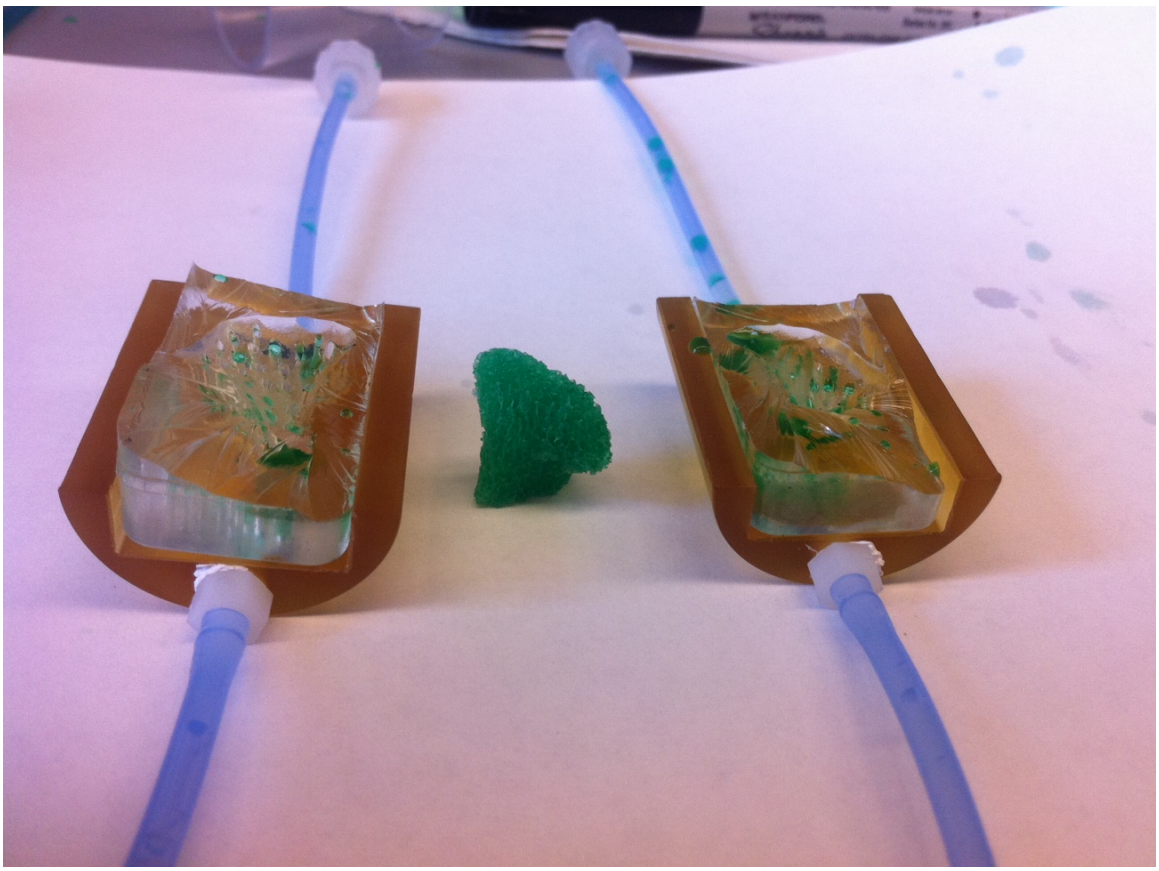

Figure X-4: Flow testing. The whole scaffolds turned green after 30 seconds of perfusing green dye solution confirming the homogeneity of media flow through the scaffolds.

In comparison to a previously developed perfusion bioreactor for engineering anatomical bone graft which was successful in delivering sufficient factors through out complex cellularized bone constructs of small and moderate size [78], the new system offers several additional advantages. This new system allows for multi-phase tissue formation with spatially-controlled nutrient supplies, the most important requirement in engineering osteochondral and other complex constructs. A major drawback of the previously developed perfusion bioreactor was the inability to control the homogenous medium flow scheme, which resulted in a different cellular response and morphology across the volume of the constructs. The design was simplified by reducing the number of inlet/outlet ports while providing a more homogenous perfusion scheme through the porous scaffolds. The improvement in design allows for cultivation of constructs with any size and shape while sufficiently providing nutrient supply to the whole construct. The prototype of

the bioreactor was fabricated and tested (**Fig.X-4**). Within less than 30 seconds of introducing green dye solution, the anatomically shaped TMJ scaffold fully dyed indicating the effectiveness of the new perfusion bioreactor in supplying nutrients. In conclusions, this design addressed all the design constraints of a successful system for engineering personalized osteochondral grafts which are summarized in **Table X-2**.

Table X-2 Personalized osteochondral bioreactor design constraints and solutions

Design constraints	Solutions
Manufacture cellularized anatomical graft	Fabricate and culture cell-seeded anatomically-shaped scaffold
Support cellularity	Provide homogenous media perfusion throughout the anatomically-shaped scaffolds
Stimulate bone development	Induce undifferentiated hMSC-seeded constructs with osteogenic media
Regulate cartilage formation	Induce undifferentiated hMSC layer with chondrogenic medium
Spatially stimulate tissue formation	Completely separate osteogenic and chondrogenic media

CHAPTER XI

Feasibility, Efficacy, and Future Challenges of Engineered Autologous Grafts

Tissue engineering offers promising alternative treatment modalities for regenerative medicine. The ability to create autograft-like constructs will have tremendous benefit clinically, socially, and economically. Thus far, the sophisticated process in generating engineered autologous grafts from stem cells limits the progress to laboratory bench and small animals. With advancement in stem cells biology and bioreactor systems, the ability to engineer autologous grafts with clinically relevant size has become possible. This chapter presents the feasibility in generating engineered autologous bone grafts in a pre-clinical set up and demonstrates the efficacy in implementing the engineered autologous grafts for treating craniofacial defect.

CRANIOFACIAL RECONSTRUCTION WITH ENGINEERED AUTOLOGOUS GRAFTS

Maxillofacial surgeons are faced with the challenge of reconstructing complex deformities that require functional and cosmetic aesthetic precision. Clinically-used grafts must be predictable, and shoud exactly matching the 3D form unique to every patient defect. The current standard of practice depends on lengthy procedures, secondary surgical sites, and immense resources, but, in many instances, still yields non-ideal results. With advancements in tissue engineering, we are increasingly able to produce autogenous bone grafts engineered *in vitro* through regulation of osteogenic differentiation and functional assembly of stem cells. Here we report our experience with custom-made bone grafts of the TMJ condyle and ramus with the use of autogenous adipose stem cells (ASCs) in a large-animal study (Yucatan minipig). The planned duration of the study is 6 months. Here, the mid-point analysis was reported in which 2 pigs from each implantation group were sacrificed at 3 months post-implantation.

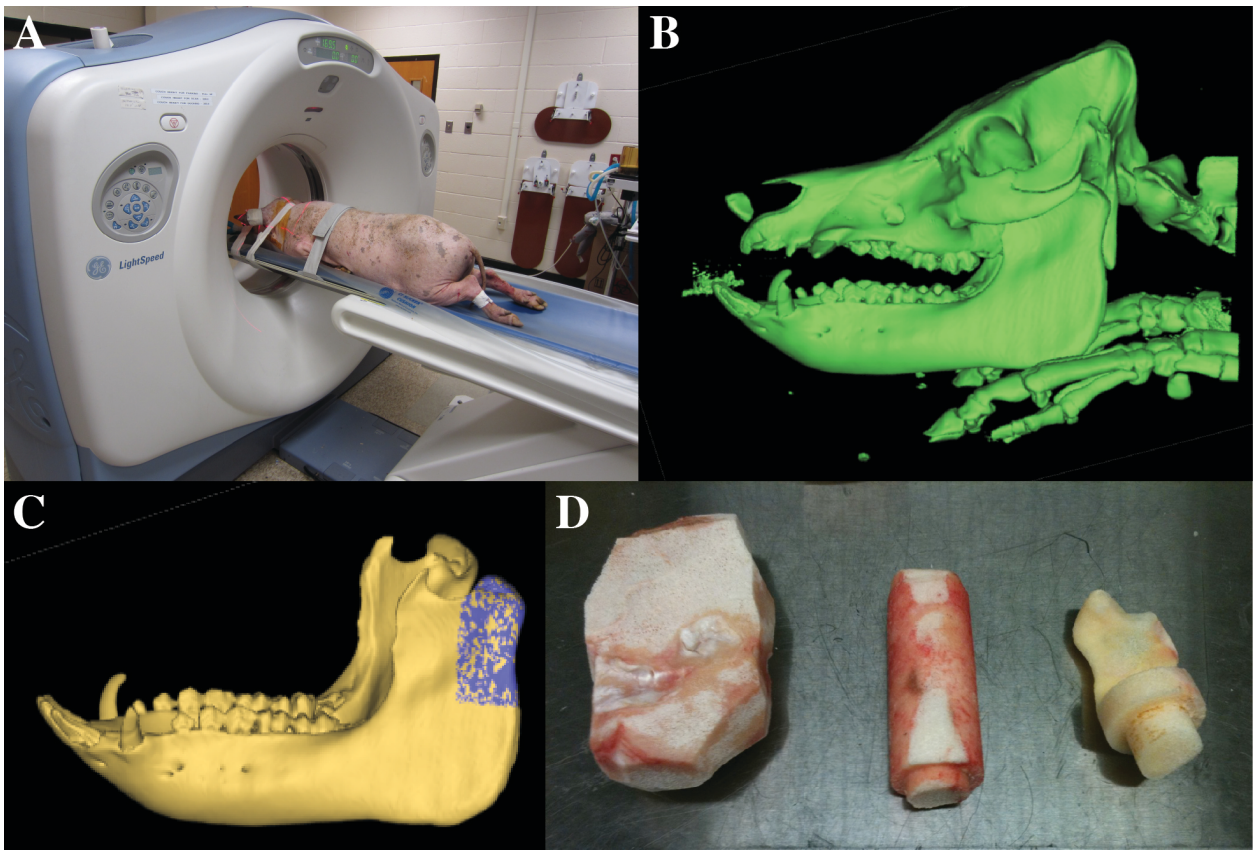

Figure XI-1: Surgical planning and RCU scaffold fabrication were conducted for each pig. Each pig was CT scanned (A) and the facial skeleton was 3D reconstructed (B). Left RCU was selected for reconstruction (C) and used as a template for scaffold fabrication from adult bovine trabecular knee bone block (D).

Preparation of personalized TMJ scaffolds

Yucatan minipigs were randomly divided into 3 groups: (i) condylectomy (n=2) as negative control (to verify that there is no spontaneous regrowth), (ii) scaffold implantation (n=6) as a cell control (to determine the relative contributions of the cells in performed bone), and (iii) engineered autogenous bone graft implantation (n=6). The process for fabricating anatomically-shaped TMJ condyles for implantation was adapted from our previous work [78]. In brief, facial skeletons of each pig were CT-scanned and reconstructed in the form of 3D digital files (**Fig.XI-1A&B**). Left ramus-condyle units (RCU) of 4 cm in width and 6 cm long were chosen for reconstruction (**Fig.XI-1C**). Anatomically-shaped scaffolds for each pig were fabricated from

trabecular bone of adult bovine knees based on previously reported methods [78] (**Fig.XI-1D**). In brief, adult bovine knees were cut to remove cartilage and cortical bone to obtain large inner trabecular bone blocks. The blocks were lathed to obtain long cylinder of at least 5 cm in diameter and 8 cm long. The blocks were placed onto a 4-axis 3D milling machine and, based on the selected 3D construct RCU, the blocks were milled into the exact shape and size for each pig. The anatomical RCU grafts were washed and decellularized using the method previously described in Chapter VII. The scaffolds were autoclaved to obtain sterility for implantation. At this point, the sterile anatomical RCU grafts were ready for pig scaffold implantation.

Engineered personalized autologous TMJ condyle grafts

To engineer the autologous bone graft, the scaffolds were seeded with autologous ASCs isolated from subcutaneous fat of each pig, as previously described [298]. The cells were expanded in culture and 80 million cells were seeded into each pig-specific TMJ condyle scaffold. The newly designed personalized bioreactor, described in Chapter X, was modified in this experiment to investigate feasibility and efficacy of engineered autologous bone grafts for craniofacial bone reconstruction. The size of the bioreactor design was increased to allow for cultivation of the much larger pig TMJ and the design was modified to only support the cultivation of the bone region (**Fig.XI-2A**). Personalized PDMS blocks were fabricated using the method described in the previous chapter (**Fig.XI-2B**). Pig-specific scaffolds were seeded with autologous ASC within the personalized perfusion bioreactor setup. In brief, anatomical-shaped decellularized bone scaffolds were placed in personalized perfusion bioreactor. The cells were suspended in 40 ml osteogenic media and injected into the bioreactor chamber until the suspension fully penetrated into the porous scaffolds (**Fig.XI-2C**). The bioreactors were placed in an incubator for 2 hours prior to initiation of media perfusion to allow cell attachment. This technique resulted in ~50% seeding efficiency. The grafts were cultured in osteogenic medium in specially designed perfusion bioreactors at 37°C for 3 weeks prior to implantation to allow for stem cell growth,

osteogenic differentiation, and bone matrix deposition (**Fig.XI-2D**). The perfusion velocity used was 40 μm/s for the first 3 days and increased to 400 μm/s for the rest of the cultivation period as this has shown to be the optimized velocity for culturing tissue engineered bone constructs [297].

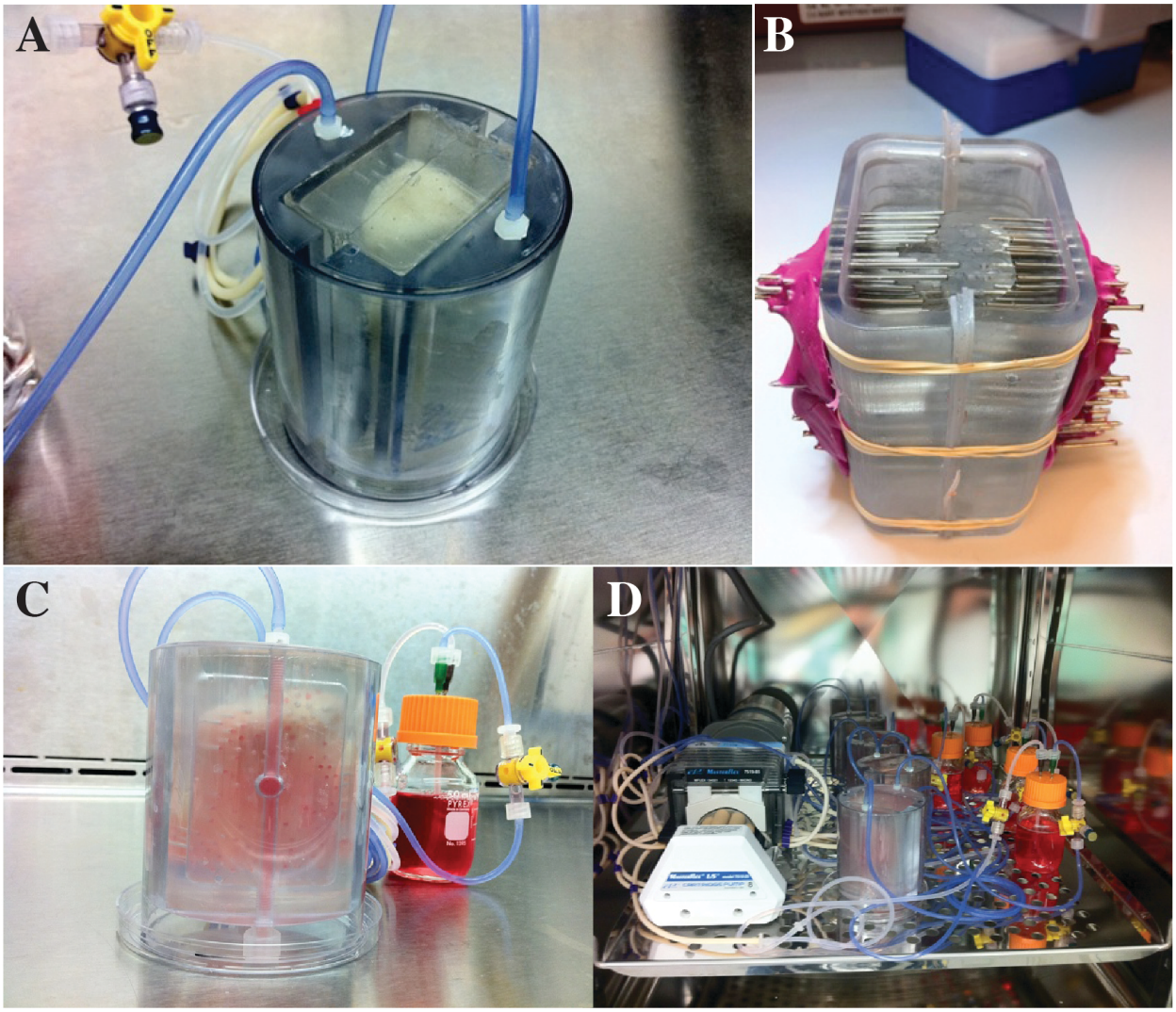

Figure XI-2: (A) Personalized perfusion bioreactor for engineering pig TMJ condyle graft. (B) Mold to create PDMS block with pre-determined channels, the main component to regulate homogenous perfusion. (C) Scaffold was filled with cell suspension after injection. (D) Bioreactors were connected to a pump and placed in 37°C humidified incubator for cultivation.

Graft implantation

Grafts were transported from New York, NY to Baton Rouge, LA for implantation. During the transportation, the personalized perfusion bioreactor containing engineered autologous grafts were disconnected from the pump and placed in an insulated container with cold packs to reduce cell metabolism rate. The total disconnection time was approximately 12 hours. The bioreactor was reconnected to the pump upon arrival at the final destination and placed in an incubator at least overnight prior to implantation. Though we detected some evidence of cell detachment due to transportation, the implanted scaffolds contained of approximately 2.9 times more cells than the scaffolds immediately after seeding.

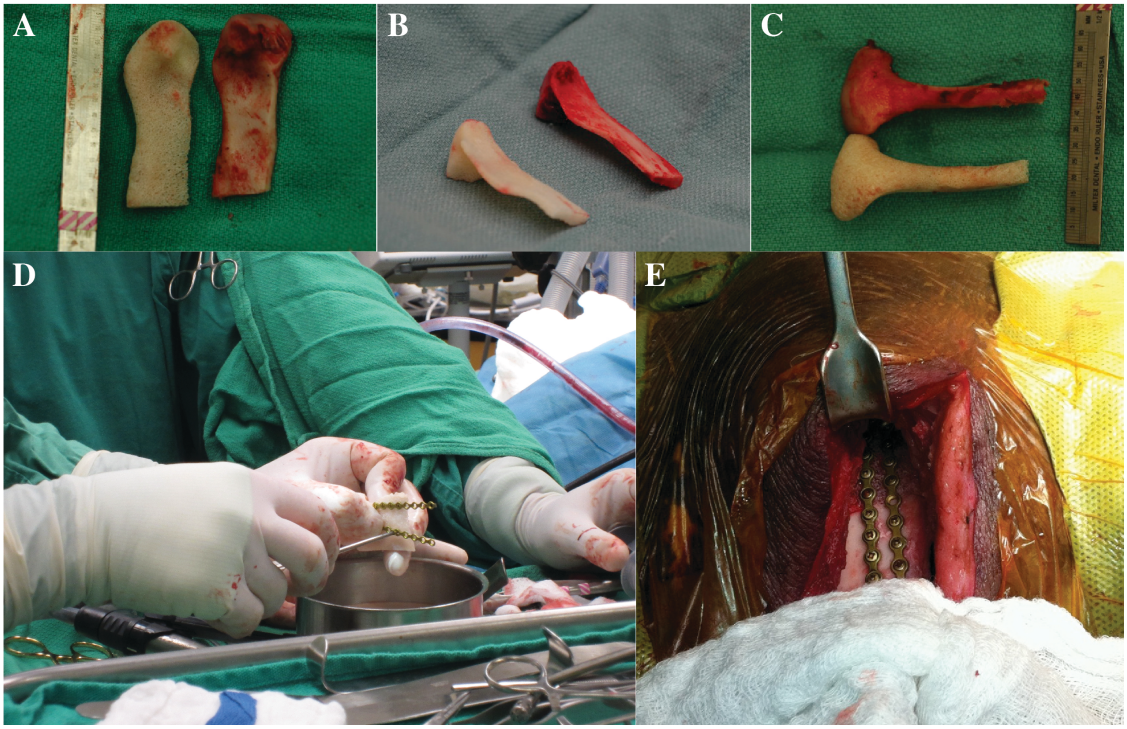

Figure XI-3: Anatomical TMJ graft implantation. The anatomical grafts generated had the exact shape and size as the extracted RCU. (D) The graft was fixated with two titanium plates and (E) inserted and fixated onto the defect.

Condylectomies to include a portion of the ramus were planned virtually and carried out under general anesthesia. The pigs selected for implantation were reconstructed using either scaffold

alone or engineered autologous bone graft. Bone grafts were successfully fabricated to contain the exact shape and size unique to each condyle (**Fig.XI-3A-C**). All grafts were rigidly fixated using 2.0 mm titanium miniplates (**Fig.XI-3D&E**).

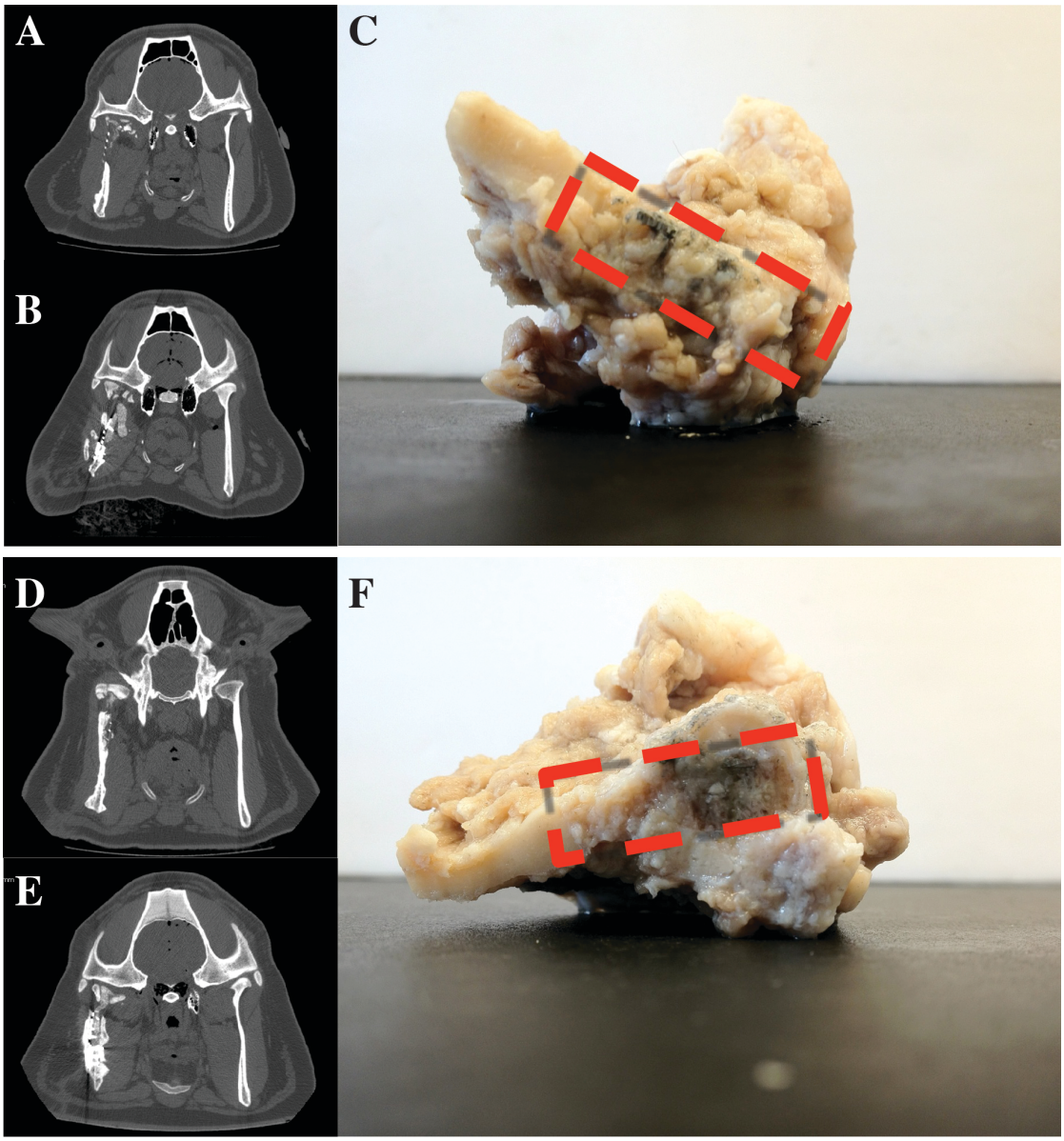

Figure XI-4: Regeneration of RCU in scaffold implantation (A-C) and engineered autologous graft implantation (D-F). CT images at 3 months showed graft resorption in scaffold implantation (A&B) while the engineered autologous graft implantation showed regeneration of RCU (D&E). Gross section of ramus showed fibrous ingrowth in scaffold implantation (C) at the implanted area (box) as opposed to bone regeneration in engineered autologous graft implantation.

Regeneration of ramus-condyle unit

CT scans were conducted after surgery (day 0), at 6 weeks, 3 months, and 6 months (in progress). TMJ condyles were harvested after sacrifice and assessed for graft remodeling in terms of compactness, integration, and resorption. All pigs survived the surgery without complications. At 3 months, pigs with untreated condylectomies regenerated incomplete ramus-condyle units (RCU). Pigs with scaffold implantation showed incomplete regeneration with significant scaffold resorption (**Fig.XI-4 A-C**). In contrast, pigs with autologous tissue engineered bone displayed regeneration as well as integration of the RCU (**Fig.XI-4 D-F**). The harvested condyles at 3 months demonstrated clear differences between the groups, with regeneration of a rigid and functional mandible in the engineered autologous bone graft group. The scaffold-only group failed to obtain comparable results, and healed with graft resorption and fibrous ingrowth. Based on the results of large animal model thus far, autologous tissue engineered bone is a promising treatment for facial bone reconstruction due to its ability to maintain tissue volume and enhance regeneration.

WHAT HAS BEEN DONE AND WHAT NEEDS TO BE DONE

The large animal study validated the feasibility in implementing the engineered autologous graft technology. The overall process represented the procedure that would be applied clinically. Anatomical scaffolds were fabricated to exactly match the defect to facilitate implantation and reconstruction. Autologous adult porcine stem cells were isolated and employed in order to prevent immune rejection. The cells were transported from medical facility to the laboratory and expanded, and the engineered autologous grafts were created within 5 weeks from the day of stem cells isolation. Furthermore, the grafts were successfully transported back to the medical facility for implantation with good cellularity, the key component responsible for engineered tissue function. As a result, the engineered autologous graft exhibited great efficacy in reconstructing craniofacial bone defect.

Optimizing and innovating systems to transport engineered grafts will likely increase cellular maintenance thus improving graft quality. Furthermore, understanding the essential biological signals and mechanisms for tissue regeneration would provide a thorough knowledge toward controlling stem cell differentiation. The techniques and systems established in this dissertation theoretically would allow for successful engineering and initial validation of osteochondral grafts. A more detailed validation in an animal study with larger group sizes is an obvious need.

CONCLUSIONS

The ability to generate native-like autologous grafts relies on the ability to regulate stem cells to produce native tissue matrix architecture by providing a suitable environment (physically, chemically, and biologically) and the right tools (bioreactor system). This dissertation successfully demonstrated the ability to control tissue matrix assembly by hMSCs cultured in scaffolds using advanced bioreactor systems towards the engineering of native-like bone, cartilage, and osteochondral grafts. By combining concepts and approaches of developmental biology and tissue engineering, bone, cartilage, and osteochondral constructs with physiological structures and functions were engineered *in vitro*. The feasibility and efficacy of implementing engineered autologous grafts progressed the technology closer toward clinical reality.

References

1. Hench, L. and J. Wilson, *Introduction to Bioceramics*1993, Singapore: World Scientific.

2. Baron, R., *Diseases of Bone and Mineral Metabolism*, ed. A. Arnold2008, Darmouth, MA.

3. Scott, C.K. and J.A. Hightower, *The matrix of endochondral bone differs from the matrix of intramembranous bone*. Calcif Tissue Int, 1991. **49**(5): p. 349-54.

4. Abzhanov, A., et al., *Regulation of skeletogenic differentiation in cranial dermal bone*. Development, 2007. **134**(17): p. 3133-44.

5. Solheim, E., *Growth factors in bone*. Int Orthop, 1998. **22**(6): p. 410-6.

6. Gerber, H.P., et al., *VEGF couples hypertrophic cartilage remodeling, ossification and angiogenesis during endochondral bone formation*. Nat Med, 1999. **5**(6): p. 623-8.

7. Trippel, S.B., *Biologic regulation of bone growth, in Bone Formation and Repair*, ed. C.T. Brighton, G.E. Friedlander, and J.M. Lane1994, Rosemont, IL: American Academy of Orthopedic Surgeons.

8. Rosenfeld, R.G., A.L. Rosenbloom, and J. Guevara-Aguirre, *Growth hormone (GH) insensitivity due to primary GH receptor deficiency*. Endocr Rev, 1994. **15**(3): p. 369-90.

9. Gonzalez, A.M., et al., *Distribution of basic fibroblast growth factor in the 18-day rat fetus: localization in the basement membranes of diverse tissues*. J Cell Biol, 1990. **110**(3): p. 753-65.

10. Hebert, J.M., et al., *Isolation of cDNAs encoding four mouse FGF family members and characterization of their expression patterns during embryogenesis*. Dev Biol, 1990. **138**(2): p. 454-63.

11. Bostrom, M.P. and P. Asnis, *Transforming growth factor beta in fracture repair*. Clin Orthop Relat Res, 1998(355 Suppl): p. S124-31.

12. Rosier, R.N., R.J. O'Keefe, and D.G. Hicks, *The potential role of transforming growth factor beta in fracture healing*. Clin Orthop Relat Res, 1998(355 Suppl): p. S294-300.

13. Joyce, M.E., et al., *Role of growth factors in fracture healing*. Prog Clin Biol Res, 1991. **365**: p. 391-416.

14. Urist, M.R., *Bone: formation by autoinduction*. Science, 1965. **150**(698): p. 893-9.

15. Wozney, J.M. and V. Rosen, *Bone morphogenetic protein and bone morphogenetic protein gene family in bone formation and repair*. Clin Orthop Relat Res, 1998(346): p. 26-37.

16. Frost, H.M., *Intermediary Organization of the Skeleton, vol II*. 1-331 ed1986, Boca Raton, FL: CRC Press.

17. Raisz, L.G., *Physiology and pathophysiology of bone remodeling*. Clin Chem, 1999. **45**(8 Pt 2): p. 1353-8.

18. Bilezikian, J.P., L.G. Raisz, and G.A. Rodan, *Principles of Bone Biology*. Vol. one. 1996, New York: Academic Press.

19. Cruess, R.L. and J. Dumont, *Fracture healing*. Can J Surg, 1975. **18**(5): p. 403-13.

20. Bolander, M.E., *Regulation of fracture repair by growth factors*. Proc Soc Exp Biol Med, 1992. **200**(2): p. 165-70.

21. Sfeir, C., et al., *Fracture Repair*. Bone Regeneration and Repair, ed. J.R. Lieberman and G.E. Friedlaender2005, Totowa, NJ: Humana Press.

22. Finkemeier, C.G., *Bone-grafting and bone-graft substitutes*. J Bone Joint Surg Am, 2002. **84-A**(3): p. 454-64.

23. Gazdag, A.R., et al., *Alternatives to Autogenous Bone Graft: Efficacy and Indications*. J Am Acad Orthop Surg, 1995. **3**(1): p. 1-8.

24. Mow, V.C. and M. Lai, *Biorheology of swelling tissue*. Biorheology, 1990. **27**(1): p. 110-9.

25. Eyre, D.R., *Collagen: molecular diversity in the body's protein scaffold*. Science, 1980. **207**(4437): p. 1315-22.

26. Clarke, I.C., *Articular cartilage: a review and scanning electron microscope study. 1. The interterritorial fibrillar architecture*. J Bone Joint Surg Br, 1971. **53**(4): p. 732-50.

27. Muir, H., P. Bullough, and A. Maroudas, *The distribution of collagen in human articular cartilage with some of its physiological implications*. J Bone Joint Surg Br, 1970. **52**(3): p. 554-63.

28. Lipshitz, H., R. Etheredge, 3rd, and M.J. Glimcher, *Changes in the hexosamine content and swelling ratio of articular cartilage as functions of depth from the surface*. J Bone Joint Surg Am, 1976. **58**(8): p. 1149-53.

29. Maroudas, A., *Physicochemical properties of articular cartilage*, in *Adult Articular Cartilage*, M.A.R. Freeman, Editor 1979, Pitman Medical: Kent. p. 215-90.

30. Stockwell, R.A., *Biology of cartilage cells*. Biological structure and function, 71979, Cambridge ; New York: Cambridge University Press. viii, 329.

31. Guilak, F., A. Ratcliffe, and V.C. Mow, *Chondrocyte deformation and local tissue strain in articular cartilage: a confocal microscopy study*. J Orthop Res, 1995. **13**(3): p. 410-21.

32. Buckwalter, J.A. and H.J. Mankin, *Articular cartilage: tissue design and chondrocyte-matrix interactions*. Instr Course Lect, 1998. **47**: p. 477-86.

33. Donzelli, P.S., et al., *Contact analysis of biphasic transversely isotropic cartilage layers and correlations with tissue failure*. J Biomech, 1999. **32**(10): p. 1037-47.

34. Mankin, H.J., *Alterations in the structure, chemistry, and metabolism of the articular cartilage in osteoarthritis of the human hip*. Hip, 1982: p. 126-45.

35. Felson, D.T., et al., *Osteoarthritis: new insights. Part 1: the disease and its risk factors*. Ann Intern Med, 2000. **133**(8): p. 635-46.

36. Tew, S.R., et al., *The reactions of articular cartilage to experimental wounding: role of apoptosis*. Arthritis Rheum, 2000. **43**(1): p. 215-25.

37. Quinn, T.M., et al., *Matrix and cell injury due to sub-impact loading of adult bovine articular cartilage explants: effects of strain rate and peak stress*. J Orthop Res, 2001. **19**(2): p. 242-9.

38. Chen, C.T., et al., *Compositional and metabolic changes in damaged cartilage are peak-stress, stress-rate, and loading-duration dependent*. J Orthop Res, 1999. **17**(6): p. 870-9.

39. Chen, C.T., et al., *Chondrocyte necrosis and apoptosis in impact damaged articular cartilage*. J Orthop Res, 2001. **19**(4): p. 703-11.

40. Mowery, C., M. Botte, and G. Bradley, *Fracture of polyethylene tibial component in a total knee replacement. A case report*. Orthopedics, 1987. **10**(2): p. 309-13.

41. Bradley, G.W., et al., *Evaluation of wear in an all-polymer total knee replacement. Part 2: clinical evaluation of wear in a polyethylene on polyacetal total knee*. Clin Mater, 1993. **14**(2): p. 127-32.

42. Whiteside, L.A., *Clinical results of Whiteside Ortholoc total knee replacement*. Orthop Clin North Am, 1989. **20**(1): p. 113-24.

43. Ayers, D.C., *Polyethylene wear and osteolysis following total knee replacement*. Instr Course Lect, 1997. **46**: p. 205-13.

44. Ahsan, T., et al., *Integrative cartilage repair: inhibition by beta-aminopropionitrile*. J Orthop Res, 1999. **17**(6): p. 850-7.

45. Harper, M.C., *Viscous isoamyl 2-cyanoacrylate as an osseous adhesive in the repair of osteochondral osteotomies in rabbits*. J Orthop Res, 1988. **6**(2): p. 287-92.

46. Caplan, A.I., et al., *Principles of cartilage repair and regeneration*. Clin Orthop, 1997(342): p. 254-69.

47. Zuger, B.J., et al., *Laser solder welding of articular cartilage: tensile strength and chondrocyte viability*. Lasers Surg Med, 2001. **28**(5): p. 427-34.

48. O'Driscoll, S.W., F.W. Keeley, and R.B. Salter, *The chondrogenic potential of free autogenous periosteal grafts for biological resurfacing of major full-thickness defects in joint surfaces under the influence of continuous passive motion. An experimental investigation in the rabbit*. J Bone Joint Surg Am, 1986. **68**(7): p. 1017-35.

49. Hangody, L., et al., *Arthroscopic autogenous osteochondral mosaicplasty for the treatment of femoral condylar articular defects. A preliminary report*. Knee Surg Sports Traumatol Arthrosc, 1997. **5**(4): p. 262-7.

50. Ebrahimi, A. and B.G. Ashford, *Advances in temporomandibular joint reconstruction*. Curr Opin Otolaryngol Head Neck Surg, 2010. **18**(4): p. 255-60.

51. Engroff, S.L., *Fibula flap reconstruction of the condyle in disarticulation resections of the mandible: a case report and review of the technique*. Oral Surg Oral Med Oral Pathol Oral Radiol Endod, 2005. **100**(6): p. 661-5.

52. Brittberg, M., et al., *Rabbit articular cartilage defects treated with autologous cultured chondrocytes*. Clin Orthop, 1996(326): p. 270-83.

53. Ahmad, C.S., et al., *Biomechanical and topographic considerations for autologous osteochondral grafting in the knee*. Am J Sports Med, 2001. **29**(2): p. 201-6.

54. Lee, C.R., et al., *Effects of harvest and selected cartilage repair procedures on the physical and biochemical properties of articular cartilage in the canine knee*. J Orthop Res, 2000. **18**(5): p. 790-9.

55. Lee, D.A., et al., *The influence of mechanical loading on isolated chondrocytes seeded in agarose constructs*. Biorheology, 2000. **37**(1-2): p. 149-61.

56. Wiesmann, H.P., et al., *Bone tissue engineering by primary osteoblast-like cells in a monolayer system and 3-dimensional collagen gel*. J Oral Maxillofac Surg, 2003. **61**(12): p. 1455-62.

57. Alsberg, E., et al., *Cell-interactive alginate hydrogels for bone tissue engineering*. J Dent Res, 2001. **80**(11): p. 2025-9.

58. Ma, P.X., et al., *Engineering new bone tissue in vitro on highly porous poly(alpha-hydroxyl acids)/hydroxyapatite composite scaffolds*. J Biomed Mater Res, 2001. **54**(2): p. 284-93.

59. Mauck, R.L., et al., *The role of cell seeding density and nutrient supply for articular cartilage tissue engineering with deformational loading*. Osteoarthritis Cartilage, 2003. **11**(12): p. 879-90.

60. Haisch, A., et al., *A tissue-engineering model for the manufacture of auricular-shaped cartilage implants*. Eur Arch Otorhinolaryngol, 2002. **259**(6): p. 316-21.

61. Gimble, J.M., A.J. Katz, and B.A. Bunnell, *Adipose-derived stem cells for regenerative medicine*. Circ Res, 2007. **100**(9): p. 1249-60.

62. Monaco, E., et al., *Strategies for regeneration of the bone using porcine adult adipose-derived mesenchymal stem cells*. Theriogenology, 2011. **75**(8): p. 1381-99.

63. Gronthos, S., et al., *Postnatal human dental pulp stem cells (DPSCs) in vitro and in vivo*. Proc Natl Acad Sci U S A, 2000. **97**(25): p. 13625-30.

64. Kern, S., et al., *Comparative analysis of mesenchymal stem cells from bone marrow, umbilical cord blood, or adipose tissue*. Stem Cells, 2006. **24**(5): p. 1294-301.

65. Laino, G., et al., *An approachable human adult stem cell source for hard-tissue engineering*. J Cell Physiol, 2006. **206**(3): p. 693-701.

66. Marolt, D., et al., *Engineering bone tissue from human embryonic stem cells*. Proc Natl Acad Sci U S A, 2012.

67. Takahashi, K., et al., *Induction of pluripotent stem cells from adult human fibroblasts by defined factors*. Cell, 2007. **131**(5): p. 861-72.

68. Illich, D.J., et al., *Concise review: induced pluripotent stem cells and lineage reprogramming: prospects for bone regeneration*. Stem Cells, 2011. **29**(4): p. 555-63.

69. Vunjak-Novakovic, G. and S.A. Goldstein, in *Basic Orthopaedic Biomechanics and Mechano-biology*., V.C. Mow and r. Huiskes, Editors. 2005, Lippincott Williams and Wilkins: Philadelphia. p. 343-408.

70. Mizuno, M., et al., *Osteogenesis by bone marrow stromal cells maintained on type I collagen matrix gels in vivo*. Bone, 1997. **20**(2): p. 101-7.

71. Liu, X. and P.X. Ma, *Polymeric scaffolds for bone tissue engineering*. Ann Biomed Eng, 2004. **32**(3): p. 477-86.

72. Vacanti, C.A., et al., *Replacement of an avulsed phalanx with tissue-engineered bone*. N Engl J Med, 2001. **344**(20): p. 1511-4.

73. Grundel, R.E., et al., *Autogeneic bone marrow and porous biphasic calcium phosphate ceramic for segmental bone defects in the canine ulna*. Clin Orthop Relat Res, 1991(266): p. 244-58.

74. Hutmacher, D.W., et al., *State of the art and future directions of scaffold-based bone engineering from a biomaterials perspective*. J Tissue Eng Regen Med, 2007. **1**(4): p. 245-60.

75. Kofron, M.D. and C.T. Laurencin, *Bone tissue engineering by gene delivery*. Adv Drug Deliv Rev, 2006. **58**(4): p. 555-76.

76. Dimitriou, R. and G.C. Babis, *Biomaterial osseointegration enhancement with biophysical stimulation*. J Musculoskelet Neuronal Interact, 2007. **7**(3): p. 253-65.

77. Vunjak-Novakovic, G. and D.T. Scadden, *Biomimetic platforms for human stem cell research*. Cell Stem Cell, 2011. **8**(3): p. 252-61.

78. Grayson, W.L., et al., *Engineering anatomically shaped human bone grafts*. Proc Natl Acad Sci U S A, 2010. **107**(8): p. 3299-304.

79. Sikavitsas, V.I., et al., *Mineralized matrix deposition by marrow stromal osteoblasts in 3D perfusion culture increases with increasing fluid shear forces*. Proc Natl Acad Sci U S A, 2003. **100**(25): p. 14683-8.

80. Cheng, S.L., et al., *Differentiation of human bone marrow osteogenic stromal cells in vitro: induction of the osteoblast phenotype by dexamethasone*. Endocrinology, 1994. **134**(1): p. 277-86.

81. Hanada, K., J.E. Dennis, and A.I. Caplan, *Stimulatory effects of basic fibroblast growth factor and bone morphogenetic protein-2 on osteogenic differentiation of rat bone marrow-derived mesenchymal stem cells*. J Bone Miner Res, 1997. **12**(10): p. 1606-14.

82. Meinel, L., et al., *Osteogenesis by human mesenchymal stem cells cultured on silk biomaterials: comparison of adenovirus mediated gene transfer and protein delivery of BMP-2*. Biomaterials, 2006. **27**(28): p. 4993-5002.

83. Carter, D.R., et al., *Influences of mechanical stress on prenatal and postnatal skeletal development*. Clin Orthop Relat Res, 1987(219): p. 237-50.

84. Salgado, A.J., O.P. Coutinho, and R.L. Reis, *Bone tissue engineering: state of the art and future trends*. Macromol Biosci, 2004. **4**(8): p. 743-65.

85. Rauh, J., et al., *Bioreactor systems for bone tissue engineering*. Tissue Eng Part B Rev, 2011. **17**(4): p. 263-80.

86. Chao, P.H., W. Grayson, and G. Vunjak-Novakovic, *Engineering cartilage and bone using human mesenchymal stem cells*. J Orthop Sci, 2007. **12**(4): p. 398-404.

87. Grayson, W.L., et al., *Effects of initial seeding density and fluid perfusion rate on formation of tissue-engineered bone*. Tissue Eng Part A, 2008. **14**(11): p. 1809-20.

88. Meinel, L., et al., *Engineering bone-like tissue in vitro using human bone marrow stem cells and silk scaffolds*. J Biomed Mater Res A, 2004. **71**(1): p. 25-34.

89. Bancroft, G.N., et al., *Fluid flow increases mineralized matrix deposition in 3D perfusion culture of marrow stromal osteoblasts in a dose-dependent manner*. Proc Natl Acad Sci U S A, 2002. **99**(20): p. 12600-5.

90. Meinel, L., et al., *Bone tissue engineering using human mesenchymal stem cells: effects of scaffold material and medium flow*. Ann Biomed Eng, 2004. **32**(1): p. 112-22.

91. Hollinger, J.O. and J.C. Kleinschmidt, *The critical size defect as an experimental model to test bone repair materials*. J Craniofac Surg, 1990. **1**(1): p. 60-8.

92. Smetana, K., *Cell biology of hydrogels*. Biomaterials, 1993. **14**(14): p. 1046-1050.

93. Rice, M.A., et al., *Effects of directed gel degradation and collagenase digestion on the integration of neocartilage produced by chondrocytes encapsulated in hydrogel carriers*. J Tissue Eng Regen Med, 2008. **2**(7): p. 418-29.

94. Burdick, J.A., et al., *Controlled degradation and mechanical behavior of photopolymerized hyaluronic acid networks*. Biomacromolecules, 2005. **6**(1): p. 386-91.

95. Chao, P.H., et al., *Silk hydrogel for cartilage tissue engineering*. J Biomed Mater Res B Appl Biomater, 2010. **95**(1): p. 84-90.

96. van Susante, J.L., et al., *Culture of chondrocytes in alginate and collagen carrier gels*. Acta. Orthop. Scand., 1995. **66**(6): p. 549-556.

97. Buschmann, M.D., et al., *Mechanical compression modulates matrix biosynthesis in chondrocyte/agarose culture*. J Cell Sci, 1995. **108 (Pt 4)**: p. 1497-508.

98. Benya, P.D. and J.D. Shaffer, *Dedifferentiated chondrocytes reexpress the differentiated collagen phenotype when cultured in agarose gels*. Cell, 1982. **30**(1): p. 215-24.

99. Buschmann, M.D., et al., *Chondrocytes in agarose culture synthesize a mechanically functional extracellular matrix*. J Orthop Res, 1992. **10**(6): p. 745-58.

100. Lee, D.A. and D.L. Bader, *The development and characterization of an in vitro system to study strain-induced cell deformation in isolated chondrocytes*. In Vitro Cell Dev Biol Anim, 1995. **31**(11): p. 828-35.

101. Lee, D.A. and D.L. Bader, *Compressive strains at physiological frequencies influence the metabolism of chondrocytes seeded in agarose*. J Orthop Res, 1997. **15**(2): p. 181-8.

102. Mauck, R.L., et al., *Influence of seeding density and dynamic deformational loading on the developing structure/function relationships of chondrocyte-seeded agarose hydrogels*. Ann Biomed Eng, 2002. **30**(8): p. 1046-56.

103. Mauck, R.L., et al., *Functional tissue engineering of articular cartilage through dynamic loading of chondrocyte-seeded agarose gels*. J Biomech Eng, 2000. **122**(3): p. 252-60.

104. Rahfoth, B., et al., *Transplantation of allograft chondrocytes embedded in agarose gel into cartilage defects of rabbits*. Osteoarthritis Cartilage, 1998. **6**(1): p. 50-65.

105. Cook, J.L., et al., *Biocompatibility of three-dimensional chondrocyte grafts in large tibial defects of rabbits*. Am J Vet Res, 2003. **64**(1): p. 12-20.

106. Lima, E.G., et al., *The beneficial effect of delayed compressive loading on tissue-engineered cartilage constructs cultured with TGF-beta3*. Osteoarthritis Cartilage, 2007. **15**(9): p. 1025-33.

107. Selmi, T.A., et al., *Autologous chondrocyte transplantation in combination with an alginate-agarose based hydrogel (Cartipatch)*. Tech. Knee Surg., 2007. **6**(4): p. 253-258.

108. Selmi, T.A., et al., *Autologous chondrocyte implantation in a novel alginate-agarose hydrogel: outcome at two years*. J. Bone Jt. Surg., 2008. **90**(5): p. 597-604.

109. Byers, B.A., et al., *Temporal exposure of TGF-B3 under serum-free conditions enhances biomechanical and biochemical maturation of tissue-engineered cartilage*. Trans Orthop Res Soc, 2006. **31**: p. 43.

110. Mauck, R.L., et al., *Synergistic action of growth factors and dynamic loading for articular cartilage tissue engineering*. Tissue Eng, 2003. **9**(4): p. 597-611.

111. Mauck, R.L., et al., *Transforming growth factor B1 increases the mechanical properties and matrix development of chondrocyte-seeded agarose hydrogels*. Adv. Bioeng., 2001. **50**: p. 691-692.

112. Thorp, B.H., I. Anderson, and S.B. Jakowlew, *Transforming growth factor-beta1, -beta2 and -beta3 in cartilage and bone cells during endochondral ossification in the chick*. Development, 1992. **114**(4): p. 907-911.

113. Bian, L., et al., *Effects of dexamethasone on the functional properties of cartilage explants during long-term culture*. Trans Orthop Res Soc, 2009. **34**: p. 329.

114. Awad, H., et al., *Effects of transforming growth factor beta1 and dexamethasone on the growth and chondrogenic differentiation of adipose-derived stromal cells*. Tiss Eng, 2003. **9**(6): p. 1301-1312.

115. Ratcliffe, A., J.A. Tyler, and T.E. Hardingham, *Articular cartilage cultured with interleukin 1. Increased release of link protein, hyaluronate-binding region and other proteoglycan fragments*. Biochem J, 1986. **238**(2): p. 571-80.

116. Aydelotte, M.B., et al., *Influence of interleukin-1 on the morphology and proteoglycan metabolism of cultured bovine articular chondrocytes*. Connect. Tissue Res., 1992. **28**(1-2): p. 143-159.

117. Lima, E.G., et al., *Differences in Interleukin-1 Response between Engineered and Native Cartilage*. Tissue Eng Part A, 2008. **14**(10): p. 1721-1730.

118. Hung, C.T., et al., *A paradigm for functional tissue engineering of articular cartilage via applied physiologic deformational loading*. Ann Biomed Eng, 2004. **32**(1): p. 35-49.

119. Gooch, K.J., et al., *Effects of mixing intensity on tissue-engineered cartilage*. Biotechnol Bioeng, 2001. **72**(4): p. 402-7.

120. Kaysen, J.H., et al., *Select de novo gene and protein expression during renal epithelial cell culture in rotating wall vessels is shear stress dependent*. J Membr Biol, 1999. **168**(1): p. 77-89.

121. Vunjak-Novakovic, G., et al., *Bioreactor cultivation conditions modulate the composition and mechanical properties of tissue-engineered cartilage*. J Orthop Res, 1999. **17**(1): p. 130-8.

122. Freed, L.E., et al., *Tissue engineering of cartilage in space*. Proc Natl Acad Sci U S A, 1997. **94**(25): p. 13885-90.

123. Obradovic, B., et al., *Gas exchange is essential for bioreactor cultivation of tissue engineered cartilage*. Biotechnol Bioeng, 1999. **63**(2): p. 197-205.

124. Ateshian, G.A. and C.T. Hung, *Functional properties of native articular cartilage*, in *Functional tissue engineering: The role of biomechanics*, F. Guilak, et al., Editors. 2003, Springer-Verlag: New York. p. In Press.

125. Carver, S.E. and C.A. Heath, *Increasing extracellular matrix production in regenerating cartilage with intermittent physiological pressure*. Biotechnol Bioeng, 1999. **62**(2): p. 166-74.

126. Mauck, R.L., C.T. Hung, and G.A. Ateshian, *Modeling of neutral solute transport in a dynamically loaded porous permeable gel: implications for articular cartilage biosynthesis and tissue*. J. Biomech. Eng., 2003. **125**(5): p. 602-614.

127. Albro, M.B., et al., *Dynamic loading of deformable porous media can induce active solute transport*. J Biomech, 2008. **41**(15): p. 3152-3157.

128. Elder, S.H., et al., *Chondrocyte differentiation is modulated by frequency and druation of cyclic compressive loading*. Ann. Biomed. Eng., 2001. **29**(6): p. 476-482.

129. Huang, C.Y., et al., *Effects of cyclic compressive loading on chondrogenesis of rabbit bone-marrow derived mesenchymal stem cells*. Stem Cells, 2004. **22**(3): p. 313-323.

130. Miyanishi, K., et al., *Effects of hydrostatic pressure and transforming growth factor-beta 3 on adult human mesenchymal stem cell chondrogenesis in vitro*. Tissue Eng, 2006. **12**(6): p. 1419-28.

131. Kisiday, J.D., et al., *Dynamic compression stimulates proteoglycan synthesis by mesenchymal stem cells in the absence of chondrogenic cytokines*. Tissue Eng Part A, 2009. **15**(10): p. 2817-24.

132. Huang, A.H., M.J. Farrell, and R.L. Mauck, *Mechanics and mechanobiology of mesenchymal stem cell-based engineered cartilage*. J Biomech, 2010. **43**(1): p. 128-36.

133. Grayson, W.L., et al., *Engineering custom-designed osteochondral tissue grafts*. Trends Biotechnol, 2008. **26**(4): p. 181-9.

134. Tuli, R., et al., *Human mesenchymal progenitor cell-based tissue engineering of a single-unit osteochondral construct*. Tissue Eng, 2004. **10**(7-8): p. 1169-79.

135. Alhadlaq, A., et al., *Adult stem cell driven genesis of human-shaped articular condyle*. Ann Biomed Eng, 2004. **32**(7): p. 911-23.

136. Augst, A., et al., *Effects of chondrogenic and osteogenic regulatory factors on composite constructs grown using human mesenchymal stem cells, silk scaffolds and bioreactors*. J R Soc Interface, 2008. **5**(25): p. 929-39.

137. Marolt, D., et al., *Bone and cartilage tissue constructs grown using human bone marrow stromal cells, silk scaffolds and rotating bioreactors*. Biomaterials, 2006. **27**(36): p. 6138-49.

138. Shea, L.D., et al., *Engineered bone development from a pre-osteoblast cell line on three-dimensional scaffolds*. Tissue Eng, 2000. **6**(6): p. 605-17.

139. Rho, J.Y., L. Kuhn-Spearing, and P. Zioupos, *Mechanical properties and the hierarchical structure of bone*. Med Eng Phys, 1998. **20**(2): p. 92-102.

140. Weiner, S. and H.D. Wagner, *The material bone: Structure-mechanical function relations*. annu. rev. mater. sci., 1998. **28**: p. 271-98.

141. Olszta, M.J., et al., *Bone structure and formation: A new perspective*. Materials Science and Engineering: R, 2007. **59**(3-5): p. 77-116.

142. Beck, G.R., Jr., *Inorganic phosphate as a signaling molecule in osteoblast differentiation*. J Cell Biochem, 2003. **90**(2): p. 234-43.

143. Lundquist, P., H. Murer, and J. Biber, *Type II Na+-Pi cotransporters in osteoblast mineral formation: regulation by inorganic phosphate*. Cell Physiol Biochem, 2007. **19**(1-4): p. 43-56.

144. Wang, W., et al., *Role of the progressive ankylosis gene (ank) in cartilage mineralization*. Mol Cell Biol, 2005. **25**(1): p. 312-23.

145. Midura, R.J., et al., *Bone acidic glycoprotein-75 delineates the extracellular sites of future bone sialoprotein accumulation and apatite nucleation in osteoblastic cultures*. J Biol Chem, 2004. **279**(24): p. 25464-73.

146. He, G., et al., *Spatially and temporally controlled biomineralization is facilitated by interaction between self-assembled dentin matrix protein 1 and calcium phosphate nuclei in solution*. Biochemistry, 2005. **44**(49): p. 16140-8.

147. Hunter, G.K., et al., *Induction of collagen mineralization by a bone sialoprotein--decorin chimeric protein*. J Biomed Mater Res, 2001. **55**(4): p. 496-502.

148. Tye, C.E., G.K. Hunter, and H.A. Goldberg, *Identification of the type I collagen-binding domain of bone sialoprotein and characterization of the mechanism of interaction*. J Biol Chem, 2005. **280**(14): p. 13487-92.

149. Tye, C.E., et al., *Delineation of the hydroxyapatite-nucleating domains of bone sialoprotein*. J Biol Chem, 2003. **278**(10): p. 7949-55.

150. Stanford, C.M., et al., *Rapidly forming apatitic mineral in an osteoblastic cell line (UMR 106-01 BSP)*. J Biol Chem, 1995. **270**(16): p. 9420-8.

151. Wang, A., et al., *Reversible suppression of in vitro biomineralization by activation of protein kinase A*. J Biol Chem, 2000. **275**(15): p. 11082-91.

152. Gorski, J.P., et al., *Extracellular bone acidic glycoprotein-75 defines condensed mesenchyme regions to be mineralized and localizes with bone sialoprotein during intramembranous bone formation*. J Biol Chem, 2004. **279**(24): p. 25455-63.

153. Gorski, J.P., et al., *Bone acidic glycoprotein-75 self-associates to form macromolecular complexes in vitro and in vivo with the potential to sequester phosphate ions*. J Cell Biochem, 1997. **64**(4): p. 547-64.

154. Alford, A.I. and K.D. Hankenson, *Matricellular proteins: Extracellular modulators of bone development, remodeling, and regeneration*. Bone, 2006. **38**(6): p. 749-57.

155. Addison, W.N., et al., *Pyrophosphate inhibits mineralization of osteoblast cultures by binding to mineral, up-regulating osteopontin, and inhibiting alkaline phosphatase activity*. J Biol Chem, 2007. **282**(21): p. 15872-83.

156. Gericke, A., et al., *Importance of phosphorylation for osteopontin regulation of biomineralization*. Calcif Tissue Int, 2005. **77**(1): p. 45-54.

157. Shapses, S.A., et al., *Osteopontin facilitates bone resorption, decreasing bone mineral crystallinity and content during calcium deficiency*. Calcif Tissue Int, 2003. **73**(1): p. 86-92.

158. Ducy, P., et al., *Increased bone formation in osteocalcin-deficient mice*. Nature, 1996. **382**(6590): p. 448-52.

159. Rammelt, S., et al., *Osteocalcin enhances bone remodeling around hydroxyapatite/collagen composites*. J Biomed Mater Res A, 2005. **73**(3): p. 284-94.

160. Doi, Y., et al., *Effects of non-collagenous proteins on the formation of apatite in calcium beta-glycerophosphate solutions*. Arch Oral Biol, 1992. **37**(1): p. 15-21.

161. Hunter, G.K. and H.A. Goldberg, *Nucleation of hydroxyapatite by bone sialoprotein*. Proc Natl Acad Sci U S A, 1993. **90**(18): p. 8562-5.

162. van de Lest, C.H. and A.B. Vaandrager, *Mechanism of cell-mediated mineralization*. Current Opinion in Orthopaedics, 2007. **18**(5): p. 434.

163. Rohde, M. and H. Mayer, *Exocytotic process as a novel model for mineralization by osteoblasts in vitro and in vivo determined by electron microscopic analysis*. Calcif Tissue Int, 2007. **80**(5): p. 323-36.

164. Gentleman, E., et al., *Comparative materials differences revealed in engineered bone as a function of cell-specific differentiation*. Nat Mater, 2009. **8**(9): p. 763-70.

165. Deshpande, A.S. and E. Beniash, *Bio-inspired Synthesis of Mineralized Collagen Fibrils*. Cryst Growth Des, 2008. **8**(8): p. 3084-3090.

166. Price, P.A., D. Toroian, and J.E. Lim, *Mineralization by inhibitor exclusion: the calcification of collagen with fetuin*. J Biol Chem, 2009. **284**(25): p. 17092-101.

167. Nudelman, F., et al., *The role of collagen in bone apatite formation in the presence of hydroxyapatite nucleation inhibitors*. Nat Mater, 2010. **9**(12): p. 1004-9.

168. Colfen, H., *Biomineralization: A crystal-clear view*. Nat Mater, 2010. **9**(12): p. 960-1.

169. Gilbert, J.E., *Current treatment options for the restoration of articular cartilage*. Am J Knee Surg, 1998. **11**(1): p. 42-6.

170. Tran-Khanh, N., et al., *Aged bovine chondrocytes display a diminished capacity to produce a collagen-rich, mechanically functional cartilage extracellular matrix*. J Orthop Res, 2005. **23**(6): p. 1354-62.

171. Adkisson, H.D.t., et al., *The potential of human allogeneic juvenile chondrocytes for restoration of articular cartilage*. Am J Sports Med, 2010. **38**(7): p. 1324-33.

172. Martin, I., et al., *Modulation of the mechanical properties of tissue engineered cartilage*. Biorheology, 2000. **37**(1-2): p. 141-7.

173. Wang, J., et al., *Homeostasis of the extracellular matrix of normal and osteoarthritic human articular cartilage chondrocytes in vitro*. Osteoarthritis Cartilage, 2003. **11**(11): p. 801-9.

174. Bulstra, S.K., et al., *Metabolic characteristics of in vitro cultured human chondrocytes in relation to the histopathologic grade of osteoarthritis*. Clin Orthop Relat Res, 1989(242): p. 294-302.

175. Tew, S.R., et al., *Cellular methods in cartilage research: primary human chondrocytes in culture and chondrogenesis in human bone marrow stem cells*. Methods, 2008. **45**(1): p. 2-9.

176. Zuk, P.A., et al., *Multilineage cells from human adipose tissue: implications for cell-based therapies*. Tissue Eng, 2001. **7**(2): p. 211-28.

177. Zuk, P.A., et al., *Human adipose tissue is a source of multipotent stem cells*. Mol Biol Cell, 2002. **13**(12): p. 4279-95.

178. Xu, Y., et al., *In vitro expansion of adipose-derived adult stromal cells in hypoxia enhances early chondrogenesis*. Tissue Eng, 2007. **13**(12): p. 2981-93.

179. Xu, Y., et al., *Analysis of the material properties of early chondrogenic differentiated adipose-derived stromal cells (ASC) using an in vitro three-dimensional micromass culture system*. Biochem Biophys Res Commun, 2007. **359**(2): p. 311-6.

180. Kim, J.H., et al., *Enhanced Proliferation and Chondrogenic Differentiation of Human Synovium-Derived Stem Cells Expanded with Basic Fibroblast Growth Factor*. Tissue Eng Part A, 2010.

181. Arufe, M.C., et al., *Chondrogenic potential of subpopulations of cells expressing mesenchymal stem cell markers derived from human synovial membranes*. J Cell Biochem, 2010. **111**(4): p. 834-45.

182. Li, J. and M. Pei, *Optimization of an in vitro three-dimensional microenvironment to reprogram synovium-derived stem cells for cartilage tissue engineering*. Tissue Eng Part A, 2010.

183. Mauck, R.L., et al., *Regulation of cartilaginous ECM gene transcription by chondrocytes and MSCs in 3D culture in response to dynamic loading*. Biomech Model Mechanobiol, 2007. **6**(1-2): p. 113-25.

184. Hu, J.C. and K.A. Athanasiou, *A self-assembling process in articular cartilage tissue engineering*. Tissue Eng, 2006. **12**(4): p. 969-79.

185. Niyama, K., et al., *Construction of osteochondral-like tissue graft combining beta-tricalcium phosphate block and scaffold-free centrifuged chondrocyte cell sheet*. J Orthop Sci, 2011. **16**(5): p. 613-21.

186. Khan, Y., et al., *Tissue engineering of bone: material and matrix considerations*. J Bone Joint Surg Am, 2008. **90 Suppl 1**: p. 36-42.

187. Griffith, L.G. and G. Naughton, *Tissue engineering--current challenges and expanding opportunities*. Science, 2002. **295**(5557): p. 1009-14.

188. Langer, R. and J.P. Vacanti, *Tissue engineering*. Science, 1993. **260**(5110): p. 920-6.

189. Kim, H.J., et al., *Influence of macroporous protein scaffolds on bone tissue engineering from bone marrow stem cells*. Biomaterials, 2005. **26**(21): p. 4442-52.

190. Martin, I., et al., *Selective differentiation of mammalian bone marrow stromal cells cultured on three-dimensional polymer foams*. J Biomed Mater Res, 2001. **55**(2): p. 229-35.

191. Ishaug, S.L., et al., *Bone formation by three-dimensional stromal osteoblast culture in biodegradable polymer scaffolds*. J Biomed Mater Res, 1997. **36**(1): p. 17-28.

192. Waite, P.D., et al., *Reconstruction of cranial defects with porous hydroxylapatite blocks*. Neurosurgery, 1989. **25**(2): p. 214-7.

193. Rockwood, D.N., et al., *Ingrowth of human mesenchymal stem cells into porous silk particle reinforced silk composite scaffolds: An in vitro study*. Acta Biomater, 2010.

194. Nazarov, R., H.J. Jin, and D.L. Kaplan, *Porous 3-D scaffolds from regenerated silk fibroin*. Biomacromolecules, 2004. **5**(3): p. 718-26.

195. Na, K., et al., *Osteogenic differentiation of rabbit mesenchymal stem cells in thermo-reversible hydrogel constructs containing hydroxyapatite and bone morphogenic protein-2 (BMP-2)*. Biomaterials, 2007. **28**(16): p. 2631-7.

196. Bucholz, R.W., A. Carlton, and R.E. Holmes, *Hydroxyapatite and tricalcium phosphate bone graft substitutes*. Orthop Clin North Am, 1987. **18**(2): p. 323-34.

197. Radin, S.R. and P. Ducheyne, *Effect of bioactive ceramic composition and structure on in vitro behavior. III. Porous versus dense ceramics*. J Biomed Mater Res, 1994. **28**(11): p. 1303-9.

198. Redey, S.A., et al., *Osteoclast adhesion and activity on synthetic hydroxyapatite, carbonated hydroxyapatite, and natural calcium carbonate: relationship to surface energies*. J Biomed Mater Res, 1999. **45**(2): p. 140-7.

199. Friedenstein, A.J., R.K. Chailakhyan, and U.V. Gerasimov, *Bone marrow osteogenic stem cells: in vitro cultivation and transplantation in diffusion chambers*. Cell Tissue Kinet, 1987. **20**(3): p. 263-72.

200. Pittenger, M.F., et al., *Multilineage potential of adult human mesenchymal stem cells*. Science, 1999. **284**(5411): p. 143-7.

201. Mauney, J.R., D.L. Kaplan, and V. Volloch, *Matrix-mediated retention of osteogenic differentiation potential by human adult bone marrow stromal cells during ex vivo expansion*. Biomaterials, 2004. **25**(16): p. 3233-43.

202. Derubeis, A.R. and R. Cancedda, *Bone marrow stromal cells (BMSCs) in bone engineering: limitations and recent advances*. Ann Biomed Eng, 2004. **32**(1): p. 160-5.

203. Cancedda, R., et al., *Cell therapy for bone disease: a review of current status*. Stem Cells, 2003. **21**(5): p. 610-9.

204. Grayson, W.L., et al., *Spatial regulation of human mesenchymal stem cell differentiation in engineered osteochondral constructs: effects of pre-differentiation, soluble factors and medium perfusion*. Osteoarthritis Cartilage, 2010. **18**(5): p. 714-23.

205. Porter, B., et al., *3-D computational modeling of media flow through scaffolds in a perfusion bioreactor*. J Biomech, 2005. **38**(3): p. 543-9.

206. Datta, N., et al., *In vitro generated extracellular matrix and fluid shear stress synergistically enhance 3D osteoblastic differentiation*. Proc Natl Acad Sci U S A, 2006. **103**(8): p. 2488-93.

207. Li, Y.J., et al., *Oscillatory fluid flow affects human marrow stromal cell proliferation and differentiation*. J Orthop Res, 2004. **22**(6): p. 1283-9.

208. Liu, X.S., et al., *Quantification of the roles of trabecular microarchitecture and trabecular type in determining the elastic modulus of human trabecular bone*. J Bone Miner Res, 2006. **21**(10): p. 1608-17.

209. Hofmann, S., et al., *Control of in vitro tissue-engineered bone-like structures using human mesenchymal stem cells and porous silk scaffolds*. Biomaterials, 2007. **28**(6): p. 1152-62.

210. Kim, H.J., et al., *Bone regeneration on macroporous aqueous-derived silk 3-D scaffolds*. Macromol Biosci, 2007. **7**(5): p. 643-55.

211. Jensen, K.S. and L. Mosekilde, *A model of vertebral trabecular bone architecture and its mechanical properties*. Bone, 1990. **11**(6): p. 417-23.

212. Okumura, M., et al., *Osteoblastic phenotype expression on the surface of hydroxyapatite ceramics*. J Biomed Mater Res, 1997. **37**(1): p. 122-9.

213. Cong, Z., et al., *Repairing segmental bone defects with living porous ceramic cylinders: an experimental study in dog femora*. J Biomed Mater Res, 2001. **55**(1): p. 28-32.

214. Norman, M.E., et al., *An in-vitro evaluation of coralline porous hydroxyapatite as a scaffold for osteoblast growth*. Clin Mater, 1994. **17**(2): p. 85-91.

215. Li, C., et al., *Electrospun silk-BMP-2 scaffolds for bone tissue engineering*. Biomaterials, 2006. **27**(16): p. 3115-24.

216. Kim, H.J., et al., *Bone tissue engineering with premineralized silk scaffolds*. Bone, 2008. **42**(6): p. 1226-34.

217. Drosse, I., et al., *Tissue engineering for bone defect healing: an update on a multi-component approach*. Injury, 2008. **39 Suppl 2**: p. S9-20.

218. Marquis, M.E., et al., *Bone cells-biomaterials interactions*. Front Biosci, 2009. **14**: p. 1023-67.

219. Barralet, J., et al., *Angiogenesis in calcium phosphate scaffolds by inorganic copper ion release*. Tissue Eng Part A, 2009. **15**(7): p. 1601-9.

220. Jiang, T., W.I. Abdel-Fattah, and C.T. Laurencin, *In vitro evaluation of chitosan/poly(lactic acid-glycolic acid) sintered microsphere scaffolds for bone tissue engineering*. Biomaterials, 2006. **27**(28): p. 4894-903.

221. Borden, M., et al., *Tissue engineered microsphere-based matrices for bone repair: design and evaluation*. Biomaterials, 2002. **23**(2): p. 551-9.

222. Laurencin, C.T., et al., *Tissue engineering: orthopedic applications*. Annu Rev Biomed Eng, 1999. **1**: p. 19-46.

223. Thelen, S., F. Barthelat, and L.C. Brinson, *Mechanics considerations for microporous titanium as an orthopedic implant material*. J Biomed Mater Res A, 2004. **69**(4): p. 601-10.

224. McIntosh Ambrose, W., et al., *Collagen Vitrigel membranes for the in vitro reconstruction of separate corneal epithelial, stromal, and endothelial cell layers*. J Biomed Mater Res B Appl Biomater, 2009. **90**(2): p. 818-31.

225. Meinel, L., et al., *Silk implants for the healing of critical size bone defects*. Bone, 2005. **37**(5): p. 688-98.

226. Lin, H., et al., *The effect of crosslinking heparin to demineralized bone matrix on mechanical strength and specific binding to human bone morphogenetic protein-2*. Biomaterials, 2008. **29**(9): p. 1189-97.

227. Rezwan, K., et al., *Biodegradable and bioactive porous polymer/inorganic composite scaffolds for bone tissue engineering*. Biomaterials, 2006. **27**(18): p. 3413-31.

228. Zhang, K., Y. Ma, and L.F. Francis, *Porous polymer/bioactive glass composites for soft-to-hard tissue interfaces*. J Biomed Mater Res, 2002. **61**(4): p. 551-63.

229. Khan, Y.M., D.S. Katti, and C.T. Laurencin, *Novel polymer-synthesized ceramic composite-based system for bone repair: an in vitro evaluation*. J Biomed Mater Res A, 2004. **69**(4): p. 728-37.

230. Wei, G. and P.X. Ma, *Structure and properties of nano-hydroxyapatite/polymer composite scaffolds for bone tissue engineering*. Biomaterials, 2004. **25**(19): p. 4749-57.

231. Thein-Han, W.W., J. Shah, and R.D. Misra, *Superior in vitro biological response and mechanical properties of an implantable nanostructured biomaterial: Nanohydroxyapatite-silicone rubber composite*. Acta Biomater, 2009. **5**(7): p. 2668-79.

232. Altman, G.H., et al., *Silk-based biomaterials*. Biomaterials, 2003. **24**(3): p. 401-16.

233. Rajkhowa, R., et al., *Reinforcing silk scaffolds with silk particles*. Macromol Biosci, 2010. **10**(6): p. 599-611.

234. Bhumiratana, S., et al., *Nucleation and growth of mineralized bone matrix on silk-hydroxyapatite composite scaffolds*. Biomaterials, 2011. **32**(11): p. 2812-20.

235. Rockwood, D.N., et al., *Ingrowth of human mesenchymal stem cells into porous silk particle reinforced silk composite scaffolds: An in vitro study*. Acta Biomater, 2011. **7**(1): p. 144-51.

236. Legant, W.R., et al., *Microfabricated tissue gauges to measure and manipulate forces from 3D microtissues*. Proc Natl Acad Sci U S A, 2009. **106**(25): p. 10097-102.

237. Discher, D.E., P. Janmey, and Y.L. Wang, *Tissue cells feel and respond to the stiffness of their substrate*. Science, 2005. **310**(5751): p. 1139-43.

238. Engler, A.J., et al., *Matrix elasticity directs stem cell lineage specification*. Cell, 2006. **126**(4): p. 677-89.

239. Gebauer, D., A. Volkel, and H. Colfen, *Stable prenucleation calcium carbonate clusters*. Science, 2008. **322**(5909): p. 1819-22.

240. Pouget, E.M., et al., *The initial stages of template-controlled CaCO3 formation revealed by cryo-TEM*. Science, 2009. **323**(5920): p. 1455-8.

241. Termine, J.D., et al., *Properties of dissociatively extracted fetal tooth matrix proteins. II. Separation and purification of fetal bovine dentin phosphoprotein*. J Biol Chem, 1980. **255**(20): p. 9769-72.

242. George, A. and A. Veis, *Phosphorylated proteins and control over apatite nucleation, crystal growth, and inhibition*. Chem Rev, 2008. **108**(11): p. 4670-93.

243. Termine, J.D., et al., *Mineral and collagen-binding proteins of fetal calf bone*. J Biol Chem, 1981. **256**(20): p. 10403-8.

244. Termine, J.D., et al., *Osteonectin, a bone-specific protein linking mineral to collagen*. Cell, 1981. **26**(1 Pt 1): p. 99-105.

245. Choi, S.T., et al., *Osteopontin might be involved in bone remodelling rather than in inflammation in ankylosing spondylitis*. Rheumatology (Oxford), 2008. **47**(12): p. 1775-9.

246. Reinholt, F.P., et al., *Osteopontin--a possible anchor of osteoclasts to bone*. Proc Natl Acad Sci U S A, 1990. **87**(12): p. 4473-5.

247. Krishnan, R., E.N. Mariner, and G.A. Ateshian, *Effect of dynamic loading on the frictional response of bovine articular cartilage*. J Biomech, 2005. **38**(8): p. 1665-73.

248. Murdoch, A.D., et al., *Chondrogenic differentiation of human bone marrow stem cells in transwell cultures: generation of scaffold-free cartilage*. Stem Cells, 2007. **25**(11): p. 2786-96.

249. Carter, M.J., I.M. Basalo, and G.A. Ateshian, *The temporal response of the friction coefficient of articular cartilage depends on the contact area*. J Biomech, 2007. **40**(14): p. 3257-60.

250. Hangody, L., et al., *Autologous osteochondral grafting--technique and long-term results*. Injury, 2008. **39 Suppl 1**: p. S32-9.

251. Alhadlaq, A. and J.J. Mao, *Tissue-engineered neogenesis of human-shaped mandibular condyle from rat mesenchymal stem cells*. J Dent Res, 2003. **82**(12): p. 951-6.

252. Alhadlaq, A. and J.J. Mao, *Tissue-engineered osteochondral constructs in the shape of an articular condyle*. J Bone Joint Surg Am, 2005. **87**(5): p. 936-44.

253. Holtorf, H.L., J.A. Jansen, and A.G. Mikos, *Flow perfusion culture induces the osteoblastic differentiation of marrow stroma cell-scaffold constructs in the absence of dexamethasone*. J Biomed Mater Res A, 2005. **72**(3): p. 326-34.

254. Meinel, L., et al., *Engineering cartilage-like tissue using human mesenchymal stem cells and silk protein scaffolds*. Biotechnol Bioeng, 2004. **88**(3): p. 379-91.

255. Mauney, J.R., et al., *In vitro and in vivo evaluation of differentially demineralized cancellous bone scaffolds combined with human bone marrow stromal cells for tissue engineering*. Biomaterials, 2005. **26**(16): p. 3173-85.

256. Lima, E.G., et al., *Functional tissue engineering of chondral and osteochondral constructs*. Biorheology, 2004. **41**(3-4): p. 577-90.

257. Lima, E.G., et al., *The effect of devitalized trabecular bone on the formation of osteochondral tissue-engineered constructs*. Biomaterials, 2008. **29**(32): p. 4292-9.

258. Lennon, D.P. and A.I. Caplan, *Isolation of human marrow-derived mesenchymal stem cells*. Exp Hematol, 2006. **34**(11): p. 1604-5.

259. Chao, P.G., et al., *Dynamic osmotic loading of chondrocytes using a novel microfluidic device*. J Biomech, 2005. **38**(6): p. 1273-81.

260. Chao, P.H., A.C. West, and C.T. Hung, *Chondrocyte intracellular calcium, cytoskeletal organization, and gene expression responses to dynamic osmotic loading*. Am J Physiol Cell Physiol, 2006. **291**(4): p. C718-25.

261. Schaefer, D., et al., *Tissue-engineered composites for the repair of large osteochondral defects*. Arthritis Rheum, 2002. **46**(9): p. 2524-34.

262. Schaefer, D., et al., *In vitro generation of osteochondral composites*. Biomaterials, 2000. **21**(24): p. 2599-606.

263. Wendt, D., M. Jakob, and I. Martin, *Bioreactor-based engineering of osteochondral grafts: from model systems to tissue manufacturing*. J Biosci Bioeng, 2005. **100**(5): p. 489-94.

264. Martin, I., D. Wendt, and M. Heberer, *The role of bioreactors in tissue engineering*. Trends Biotechnol, 2004. **22**(2): p. 80-6.

265. Helms, J.A. and R.A. Schneider, *Cranial skeletal biology*. Nature, 2003. **423**(6937): p. 326-31.

266. Herring, S.W. and P. Ochareon, *Bone--special problems of the craniofacial region*. Orthod Craniofac Res, 2005. **8**(3): p. 174-82.

267. Taylor, J.A., *Bilateral orbitozygomatic reconstruction with tissue-engineered bone*. J Craniofac Surg, 2010. **21**(5): p. 1612-4.

268. Zizelmann, C., et al., *Bone formation after sinus augmentation with engineered bone*. Clin Oral Implants Res, 2007. **18**(1): p. 69-73.

269. *U.S. Trauma Fixation Markets*, 2008, Frost and Sullivan.

270. Bauer, T.W. and G.F. Muschler, *Bone graft materials. An overview of the basic science*. Clin Orthop Relat Res, 2000(371): p. 10-27.

271. Zins, J.E., C.J. Langevin, and S. Nasir, *Controversies in skull reconstruction*. J Craniofac Surg, 2010. **21**(6): p. 1755-60.

272. Zins, J.E. and L.A. Whitaker, *Membranous versus endochondral bone: implications for craniofacial reconstruction*. Plast Reconstr Surg, 1983. **72**(6): p. 778-85.

273. Stevenson, S., *Biology of bone grafts*. Orthop Clin North Am, 1999. **30**(4): p. 543-52.

274. Eppley, B.L., W.S. Pietrzak, and M.W. Blanton, *Allograft and alloplastic bone substitutes: a review of science and technology for the craniomaxillofacial surgeon*. J Craniofac Surg, 2005. **16**(6): p. 981-9.

275. Davy, D.T., *Biomechanical issues in bone transplantation*. Orthop Clin North Am, 1999. **30**(4): p. 553-63.

276. Rudman, K., C. Hoekzema, and J. Rhee, *Computer-assisted innovations in craniofacial surgery*. Facial Plast Surg, 2011. **27**(4): p. 358-65.

277. Hanasono, M.M., et al., *Correction of the soft tissue pollybeak using triamcinolone injection*. Arch Facial Plast Surg, 2002. **4**(1): p. 26-30; discussion 31.

278. Hollister, S.J., *Porous scaffold design for tissue engineering*. Nat Mater, 2005. **4**(7): p. 518-24.

279. Singare, S., et al., *Design and fabrication of custom mandible titanium tray based on rapid prototyping*. Med Eng Phys, 2004. **26**(8): p. 671-6.

280. Vats, A., et al., *Scaffolds and biomaterials for tissue engineering: a review of clinical applications*. Clin Otolaryngol Allied Sci, 2003. **28**(3): p. 165-72.

281. Giesen, E.B., et al., *Mechanical properties of cancellous bone in the human mandibular condyle are anisotropic*. J Biomech, 2001. **34**(6): p. 799-803.

282. Giesen, E.B. and T.M. van Eijden, *The three-dimensional cancellous bone architecture of the human mandibular condyle*. J Dent Res, 2000. **79**(4): p. 957-63.

283. Kato, Y., et al., *Internal structure of zygomatic bone related to zygomatic fixture*. J Oral Maxillofac Surg, 2005. **63**(9): p. 1325-9.

284. Peterson, J. and P.C. Dechow, *Material properties of the human cranial vault and zygoma*. Anat Rec A Discov Mol Cell Evol Biol, 2003. **274**(1): p. 785-97.

285. Rafferty, K.L., S.W. Herring, and F. Artese, *Three-dimensional loading and growth of the zygomatic arch*. J Exp Biol, 2000. **203**(Pt 14): p. 2093-104.

286. Teng, S., et al., *Stereological analysis of bone architecture in the pig zygomatic arch*. Anat Rec, 1997. **248**(2): p. 205-13.

287. Hutmacher, D.W., M. Sittinger, and M.V. Risbud, *Scaffold-based tissue engineering: rationale for computer-aided design and solid free-form fabrication systems*. Trends Biotechnol, 2004. **22**(7): p. 354-62.

288. Sinha, V.R. and A. Trehan, *Biodegradable microspheres for parenteral delivery*. Crit Rev Ther Drug Carrier Syst, 2005. **22**(6): p. 535-602.

289. Pritchard, E.M. and D.L. Kaplan, *Silk fibroin biomaterials for controlled release drug delivery*. Expert Opin Drug Deliv, 2011. **8**(6): p. 797-811.

290. Lieberman, J.R., A. Daluiski, and T.A. Einhorn, *The role of growth factors in the repair of bone. Biology and clinical applications*. J Bone Joint Surg Am, 2002. **84-A**(6): p. 1032-44.

291. Marx, R.E., *Platelet-rich plasma: evidence to support its use*. J Oral Maxillofac Surg, 2004. **62**(4): p. 489-96.

292. Caplan, A.I., *Review: mesenchymal stem cells: cell-based reconstructive therapy in orthopedics*. Tissue Eng, 2005. **11**(7-8): p. 1198-211.

293. Mendonca, J.J. and P. Juiz-Lopez, *Regenerative facial reconstruction of terminal stage osteoradionecrosis and other advanced craniofacial diseases with adult cultured stem and progenitor cells*. Plast Reconstr Surg, 2010. **126**(5): p. 1699-709.

294. Boo, J.S., et al., *Tissue-engineered bone using mesenchymal stem cells and a biodegradable scaffold*. J Craniofac Surg, 2002. **13**(2): p. 231-9; discussion 240-3.

295. Yamada, Y., et al., *Autogenous injectable bone for regeneration with mesenchymal stem cells and platelet-rich plasma: tissue-engineered bone regeneration*. Tissue Eng, 2004. **10**(5-6): p. 955-64.

296. Frohlich, M., et al., *Bone grafts engineered from human adipose-derived stem cells in perfusion bioreactor culture*. Tissue Eng Part A, 2010. **16**(1): p. 179-89.

297. Grayson, W.L., et al., *Optimizing the medium perfusion rate in bone tissue engineering bioreactors*. Biotechnol Bioeng, 2011. **108**(5): p. 1159-70.

298. Williams, K.J., et al., *Isolation and characterization of porcine adipose tissue-derived adult stem cells*. Cells Tissues Organs, 2008. **188**(3): p. 251-8.